THE EFFECT OF NUCLEUS REUNIENS INACTIVATION ON NEOCORTICAL K-COMPLEX AND HIPPOCAMPAL SHARP WAVE-RIPPLE CORRELATIONS

MITCHELL T. KESLER
Bachelor of Science, University of Lethbridge, 2016

A Thesis
Submitted to the School of Graduate Studies
of the University of Lethbridge
in Partial Fulfilment of the
Requirement for the Degree

MASTER OF SCIENCE

Department of Neuroscience

University of Lethbridge

LETHBRIDGE, ALBERTA, CANADA

THE EFFECT OF NUCLEUS REUNIENS INACTIVATION ON NEOCORTICAL
K-COMPLEX AND HIPPOCAMPAL SHARP WAVE-RIPPLE CORRELATIONS

MITCHELL T. KESLER

Date of Defence: December 14, 2016

Dr. Bruce McNaughton   Professor   Ph.D.
Thesis Supervisor

Dr. Robert J. Sutherland   Professor   Ph.D.
Thesis Examination Committee Member

Dr. David Euston   Associate Professor   Ph.D.
Thesis Examination Committee Member

Dr. Sergio Pellis   Professor   Ph.D.
Chair, Thesis Examination Committee

Dedication

This work is dedicated to my wife and my family and friends.

Abstract

Cortico-hippocampal communication is critical for cognitive processes including behavioural flexibility, and memory formation, consolidation, and retrieval. Nucleus reuniens of the thalamus has been implicated in memory consolidation. Consolidation involves the reactivation of hippocampal ensembles with neocortical memory traces to convert episodic memories to semantic knowledge and is believed to rely on coordinated interactions between sharp wave-ripples (SPWRs) and K-complexes (KCs). The aim of my study was to investigate whether inactivation of reuniens affects SPWR and KC coordination. I found that dialysis of lidocaine into reuniens did not affect the coordination of KCs and SPWRs. While previous studies have demonstrated effective local neural inactivation using lidocaine dialysis, I did not observe any effects that could be used to positively verify a drug effect. The data thus tentatively provide evidence that reuniens does not coordinate KSs and SPWRs. Future studies will be needed using methods for which inactivation can be positively identified.

Preface

This dissertation is original, unpublished, independent work by the author, M. T. Kesler.

Acknowledgement

Table of Contents

List of Tables

List of Figures

List of Abbreviations

%NREM	Percent non-rapid eye movement
Ach	Acetylcholine
AP	Anterior-posterior
CI	Confidence interval
dCA1	Dorsal CA1
DV	Dorsal-ventral
HF	Hippocampal formation
HPC	Hippocampus
IRI	Inter-ripple-interval
KC	K-complex
LTP	Long-term potentiation
M	Mean
ML	Medial-lateral
mPFC	Medial prefrontal cortex
NAc	Nucleus accumbens
NACh	Nicotinic acetylcholine
NRe	Nucleus reuniens
NREM	Non-rapid eye movement
Rh	Rhomboid nucleus
SD	Standard deviation
SPWR	Sharp-wave ripple
VSub	Ventral subiculum
VTA	Ventral tegmental area

Chapter One - *Introduction*

1.1 Background information

1.1.1 Framing the problem

Cortico-hippocampal communication is crucial to higher-order cognitive processes including behavioural flexibility, information processing, and memory formation, consolidation, and retrieval. It is well established that the hippocampus is critically involved in declarative memory processes (Eichenbaum, 2000), and damage to the hippocampus and associated temporal lobe structures can cause complete anterograde amnesia and temporally graded retrograde amnesia (Zola-Morgan et al., 1986). In addition, diencephalic lesions of the thalamus can induce deficits in declarative memory formation and persistence that are comparable to those produced by hippocampal damage (Aggleton & Brown, 1999; Louriero et al., 2012). Furthermore, nucleus reuniens of the ventral midline thalamus has recently been implicated in long-term memory consolidation (Louriero et al., 2012). It is thought that nucleus reuniens plays some critical role facilitating the consolidation of information into neocortical networks due to its dense reciprocal connectivity with the hippocampus and prefrontal cortex, and because reuniens lesions induce memory deficits.

Consolidation is a process by which a recent episodic memory eventually becomes a remote semantic memory. During waking experience the hippocampus, a cortical structure critical to learning and memory, encodes an associative index for an episodic memory as a pattern of neural activity. This pattern of activity, if reactivated, can be used to retrieve a memory trace encoded by the neocortex. Overtime, as the hippocampus and neocortex are repeatedly reactivated together, the original episodic memory eventually becomes a remote semantic memory. Consolidation occurs during quiet wakefulness, light-sleep and stage 2 non-rapid eye movement sleep (NREM sleep), and is believed to rely on coordinated interactions between sharp wave-ripples (SPWRs) and K-complexes (KCs). The sharp wave-ripple is a high-frequency discharge of many hippocampal neurons (O'keefe & Nadel, 1978), and has been found to encode a neural representation of waking experiences which are reactivated during subsequent sleep epochs (Wilson & McNaughton, 1994). The K-complex, which occurs in the neocortex and represents an isolated cortical down-state (Cash et al., 2009; Johnson et al, 2010), and it is during the down-to-upstate transition of the K-complex when a weakly biased attractor in the neocortical network is thought to be susceptible to

hippocampal inputs, whereby the hippocampus retrieves a memory trace stored within the neocortical network and slowly over many repeated retrievals synapses within the neocortical network are potentiated (Mclelland et al., 1995) and a semantic memory is formed. Though the exact coordinating mechanism is as of yet unknown nucleus reuniens of the ventral midline thalamus has been suggested to facilitate the coordination of hippocampal ripples and cortical spindles (Varela and Wilson, 2014) which are often preceded by K-complexes (Amzica & Steriade, 1997, 2002).

Hence, I elected to study the effect of nucleus reuniens inactivation on the correlations of hippocampal sharp-wave ripples and mPFC K-complexes in a naturally sleeping animal.

1.1.2 The thalamus

The word thalamus derives from the Greek word *thalamos* meaning inner room or bridal chamber. Its attribution to the brain structure is often believed to have been inspired by Galen's dissection of an Ox brain in the 2nd century AD. Galen traced the optic tract back to what we now refer to as the lateral geniculate nucleus which he and others after him believed to be chambers where the soul intersected with the

brain. Later in the 17th century Thomas Willis referred to the thalamus as a "chamber for the Optick nerves", an expression originally attributed to Galen. Despite never observing these "chambers" Willis did observe fiber tracts that projected from the thalamus into the cerebral cortex and hence it was believed to be here that the "spirit" entered the cerebrum.

While the original description of the thalamus may be attributed to Galen it wasn't until the 19th century that Karl Friedrich Burdach described nuclear subdivisions of the thalamus by studying alcohol-hardened slices of human brain tissue. Burdach catalogued clear divisions in the thalamus: the anterior, medial, and lateral nuclei among others including what he called the "*stratum corneum*" which may have been early descriptions of the reticular nucleus. Later in the 19th century Jules Bernard Luys proposed that the thalamus was subdivided into four nuclei. (1) The *anterior nuclei* which he believed to be olfactory in nature. (2) The *internal (medial) nuclei*, believed to relay visual information. (3) The *central medial nuclei,* including the medial dorsal nucleus which he believed to be the "terminus" for somatosensory information. (4) The *central posterior nuclei* which he believed relayed auditory information. Luys

concluded that the thalamic nuclei were "*the sole and unique open gates by which all stimuli […] pass.*" And so as early as the 19nd century the thalamus has been suggested to be a relay hub routing information from the environment to the cerebral cortex.

1.1.3 Subdivisions of the thalamus

Despite its original four-part categorization, the thalamus has more recently, and more accurately, been divided into three parts. (1) The epithalamus which generally does not send or receive fibers from the cerebral cortex. (2) The dorsal thalamus which has extensive thalamocortical and corticothalamic connectivity. (3) The ventral thalamus (prethalamus) which routes information from the brain stem and other subcortical structures to the neocortex, but does not receive cortical afferents in return (Jones, 1985). A brief overview of the three subdivisions will be provided, but I will focus on the dorsal thalamus, in particular the medioventral nucleus (reuniens), for the remainder of this work.
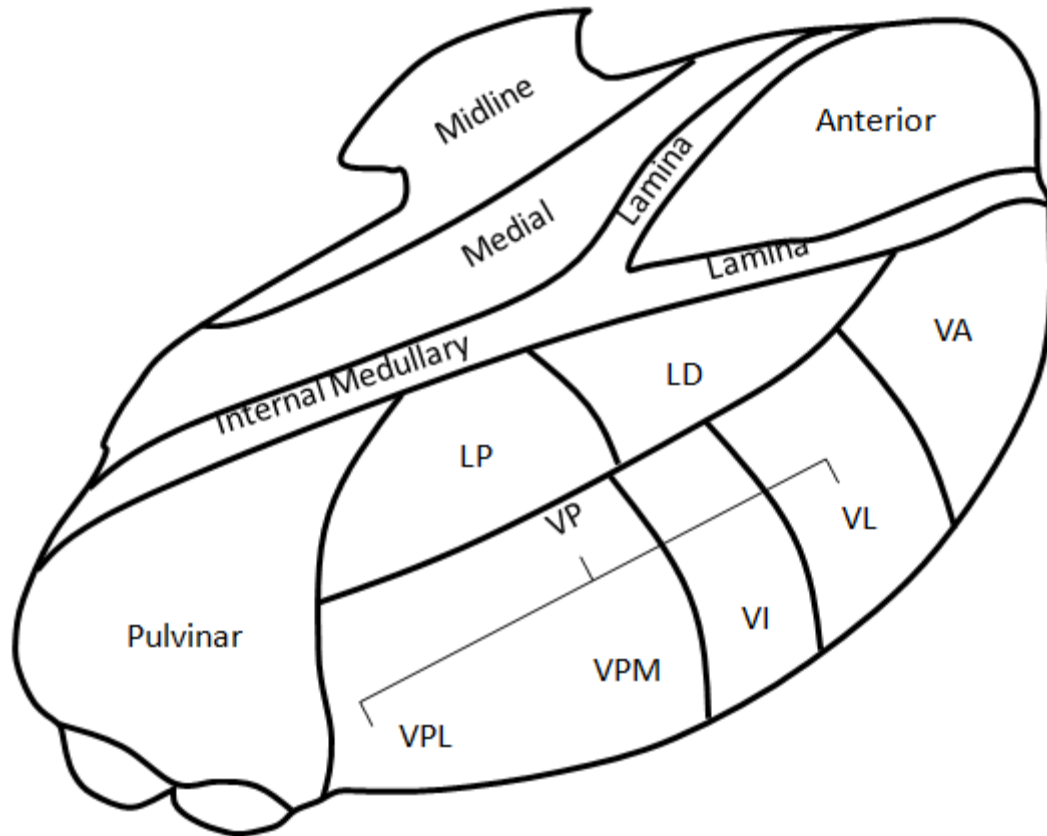
Figure 1. Thalamic subdivisions. The above figure illustrates the thalamus and the various subdivisions and constituent nuclei. Reuniens and rhomboid are a part of the midline group.

1.1.4 Epithalamus

The Epithalamus is a portion of the diencephalon located dorsally and posteriorly. It is subdivided into distinct substructures including the habenula and its associated fibres, the pineal body, which secretes melatonin; a hormonal sleep-wake cycle regulator (Guilding et al., 2010), and the stria medullaris. The main function of the

epithalamus is to connect the limbic system to other regions in the brain (Nieuwenhuys, 1998).

1.1.5 Ventral thalamus

The ventral thalamus, now referred to as the prethalamus, includes the ventral posterior, ventral lateral, and ventral anterior nuclei, and is largely believed to be responsible for relaying information from subcortical sites such as the brainstem to primary sensory cortices (Jones, 1985).

1.1.6 Dorsal thalamus

Thalamocortical reciprocal connectivity is characteristic of dorsal thalamic nuclei: every dorsal thalamic nucleus projects to some region of the cerebral cortex, some more specifically than others, and almost the entire cerebral cortex receives input from dorsal thalamic nuclei (Jones, 1985). Most importantly however, the dorsal subdivision has access to nearly the entire cerebral hemisphere including the neocortex and subcortical structures such as the striatum, hippocampus, and basal ganglia making it a principal hub to bidirectionally route information between cortical and subcortical sites.

Thalamocortical connectivity can be further subdivided by termination specificity. Some dorsal thalamic nuclei project densely and specifically to one or more cortical fields, while others project non-specifically to diffuse cortical fields leading some to inaccurately group dorsal thalamic nuclei as being exclusively "specific" or "non-specific". However, this sweeping categorization cannot be used as the sole basis to delineate the parent nuclei of the thalamocortical projections, as some parent nuclei project both specifically and non-specifically (Macchi et al., 1983).

1.1.7 Nonspecific thalamus

The nonspecific thalamus has traditionally included the intralaminar group and the ventral midline nuclei. The *intralaminar group* includes the central medial, central lateral, paracentral, centre median, and parafasicular nuclei. Whereas the ventral midline nuclei include the medioventral nucleus, also known as nucleus reuniens (NRe), and the rhomboid nucleus (Rh).

The intralaminar group and the ventral midline nuclei are so named the "nonspecific thalamus" because of their effect on

cortical targets following electrical stimulation. When stimulated, the intralaminar and ventral midline nuclei generate diffuse and widespread non-specific neocortical responses and were thus categorized as non-specific nuclei (Morison and Dempsey, 1942; Jasper et al., 1949, 1960). Recently however, projection studies have suggested that grouping *both* the intralaminar group and the ventral midline thalamus into the nonspecific category is not entirely accurate (Macchi, 1983; Cassel et al., 2013). Tracing studies have shown that the intralaminar nuclei are most certainly nonspecific nuclei as they project neither densely nor specifically to cortical layer I fields, though they do exhibit some regional projection dominance, namely to the striatum (Jones, 1975; Macchi et al., 1975, 1977), and as previously described electrical stimulation elicits generalized and non-specific neocortical responses. However, the ventral midline group has properties of both specific and nonspecific nuclei as its projection specificity can be at once diffuse and very light, similar to the intralaminar group, and also densely confined to discrete layers of single cortical fields. But, the ventral midline thalamus differs from typical specific relay nuclei as their projections terminate largely in cortical layer I

(Cruikshank et al., 2012) and V/VI (Vertes et al., 2006) instead of the middle cortical layers common to specific relay nuclei (Jones and Burton, 1975).

Of particular recent interest (Vertes et al., 2006, 2007; Hembrook and Mair, 2010; Eleore et al., 2011; Hembrook et al., 2012; Varela et al., 2013; Xu and Sudhof, 2013; Ito et al., 2013; Linley et al., 2016; Zimmerman & Grace, 2016) is the projection density and specificity of the ventral midline thalamus to the medial prefrontal cortex, including prelimbic and infralimbic cortices, and the hippocampal formation including the subiculum, fornix, and dorsal and ventral CA1 (Herkenham, 1978; Vertes et al., 2006, Varela and Wilson, 2013) for which I will now turn.

1.2 The ventral midline thalamus: reuniens and rhomboid nuclei

1.2.1 Reuniens and rhomboid anatomy

In the rat brain, nucleus reuniens and rhomboid nucleus are among the largest thalamic nuclei and occupy approximately one-third of the anterior thalamus. Their size and thalamic occupation show relative heterogeneity amongst other mammalian species. In bats the reuniens is almost absent; perhaps related to reuniens' direct retinal connection

(Calvacante et al., 2005). Conversely, in human and non-human primates it is quite prominent but not to the same degree as in rats or mice, and in dogs it is very prominent (Jones, 1985). It is likely that the reuniens' prominence as a thalamic nucleus may depend on its relative importance to the fitness and survivability of the organism, as would be expected. For instance, the general absence of reuniens in bats may be related to their heavy reliance on echolocation for navigation purposes as opposed to vision, as reuniens receives direct retinal projections. For the remainder of this work I will focus on reuniens in the rat.

In rat, nucleus reuniens spans a region of the medioventral thalamus from approximately -1.0 AP, where it is bilateral and bilobed, to -4.0 where it is bilateral and unilobed. Rhomboid nucleus sits immediately dorsal to nucleus reuniens and is bilateral and unilobed throughout its AP axis from approximately -1.0AP to -4.0AP (Paxinos and Watson, 2007) as illustrated in figure 2 below.
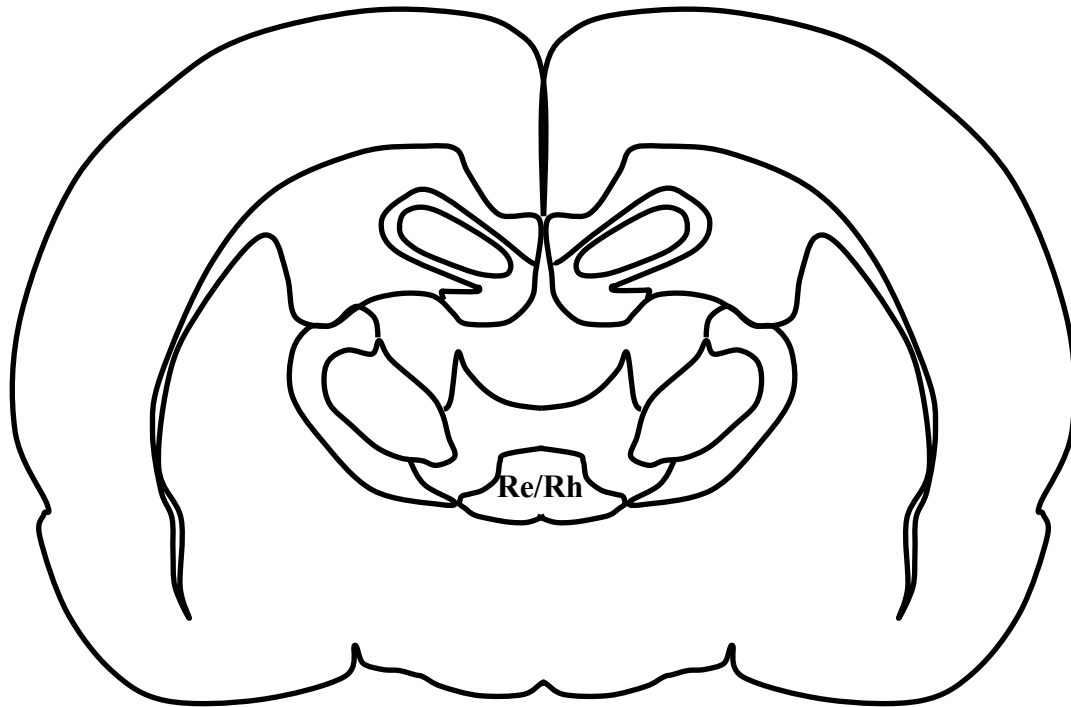
Figure 2. Illustration of nucleus reuniens and rhomboid nucleus in rat. The above figure demonstrates the location of nucleus reuniens and rhomboid nucleus in the rat brain. Figure adapted from Paxinos & Watson (2007).

Reuniens also shows some degree of topographical organization to its projection density. The most rostral regions project primarily to the hippocampal stratum lacunosum moleculare where it makes asymmetric contacts on apical dendrites, while the more caudal regions project primarily to the ventromedial prefrontal cortex (Eleore et al., 2011; Hoover & Vertes, 2012; Varela et al., 2013). Such significant projection density would suggest some inherent utility in facilitating communication between the two

regions. Furthermore, there are neurons found in nucleus reuniens which send axon collateral projections to both the mPFC and hippocampus simultaneously and are thought to serve some key function synchronizing activity in the two regions (Varela and Wilson, 2013; Hallock et al., 2016).

1.2.2 Reuniens efferent connectivity

Nucleus reuniens sends inputs to over 90 cortical and subcortical regions. Some projections to subcortical and cortical fields are diffuse and very sparse, while other projections are very dense and highly specific, such as its projections to the medial prefrontal cortex (Di Prisco et al., 2006), and hippocampal formation (Herkenham, 1978; Vertes et al., 2006, Hoover and Vertes, 2007; Dolleman Van-der Weel, et al 1996, 1997, 2000; Cavdar et al., 2008; Varela et al., 2013).

In the cortex, reuniens sends very dense projections to layer II of the medial and lateral entorhinal cortices as well as to the medial frontal polar cortex, the infralimbic cortex, the medial and ventral orbital cortices, the anterior piriform cortex, prelimbic cortex, and the retrosplenial cortex, as well as moderate projections to

14

anterior cingulate cortex (Vertes et al., 2006). Reuniens also projects very densely to the hippocampal formation including the dorsal and ventral stratum lacunosum moleculare of hippocampal CA1, dorsal and ventral subiculum, and select subcortical sites including the claustrum and the dorsal tania tecta. All other cortical and subcortical efferent projections of nucleus reuniens are either moderate or light in projection density (Vertes et al., 2006). Interestingly, reuniens projections to the hippocampus are asymmetric, and therefore excitatory, and they synapse on the apical dendrites of CA1 pyramidal neurons in the stratum lacunosum molecular, as well as on inhibitory interneurons (Bokor et al, 2002). Furthermore it was found by stimulating reuniens in various locations and recording evoked responses in the hippocampus that reuniens exerts a dual influence over hippocampal activity: a subthreshold depolarization on pyramidal neurons and a suprathreshold depolarization on inhibitory interneurons (Dolleman-van der Weel et al., 1997). Generally speaking, nucleus reuniens projects densely and specifically to the medial prefrontal cortex and the hippocampal formation and is likely an important conduit in the exchange of limbic associated information important for processes which are thought to depend on communication

between the medial prefrontal cortex and the hippocampus such as behavioural flexibility, strategy shifting, and learning and memory (Vertes et al., 2006; Vertes et al., 2007; Cassel et al., 2013; Varela et al., 2013; Xu and Sudhof, 2013; Ito et al., 2013; Hallock et al., 2016; Linley et al., 2016).

1.2.3 Reuniens afferent connectivity

Nucleus reuniens receives projections from many cortical and subcortical sites (Herkenham, 1978; McKenna and Vertes, 2004). From the cortex, reuniens receives the densest projections from the infralimbic, prelimbic, medial orbital cortex and to a lesser extent the dorsal and ventral anterior cingulate regions of the medial prefrontal cortex. Particularly layer V/VI of the prelimbic and infralimbic cortices (McKenna and Vertes, 2004) as well as the dorsal and ventral subiculum of the hippocampal formation. Subcortical inputs to reuniens include the anterior nucleus, lateral hypothalamus, posterior hypothalamus, supramammillary nucleus, ventromedial nucleus, zona incerta and reticular nucleus which are thought to provide inhibitory modulation to reuniens (Zimmerman & Grace, 2016; Lara-Vasquez et al., 2016), and various brainstem nuclei

including the central gray mesencephalon, the commissural nucleus, the laterodorsal tegmental nucleus, parabrachial nucleus, pedunculopontine tegmental nucleus, precommisural nucleus, and the pretectum. Reuniens also receives direct retinal projections (Cavalcante et al., 2005) that bypass traditional preprocessing and are thought to play some role in the modulation of wakefulness and arousal processes.

Of interest to our study are the projections to reuniens from the medial prefrontal cortex and the hippocampal formation. In particular it was shown that the reuniens-projecting mPFC neurons synapse asymmetrically on the distal dendrites of hippocampally projecting reuniens neurons likely forming a critical link between the mPFC and hippocampus (Vertes et al., 2007). Furthermore, the hippocampal projection to nucleus reuniens arising from the dorsal and ventral subiculum is thought to be excitatory in nature, and interestingly the hippocampal inputs to reuniens synapse primarily in caudal reuniens which then exerts excitatory influences on rostral reuniens (Bokor et al., 2002). It is in this way that reuniens has been suggested to be capable of modulating hippocampal activity depending on the output of the hippocampus (Bokor et al., 2002).

In short, nucleus reuniens receives substantial cortical and subcortical inputs with the densest inputs arising from the mPFC and hippocampal formation (McKenna and Vertes, 2004), and they are believed to be largely excitatory in nature (Bokor et al., 2002; Vertes et al., 2007); Cassel et al., 2013).

1.2.4 Reuniens neurotransmitter systems

Nucleus reuniens is believed to be largely excitatory in nature, containing calretinin and calbindin positive glutamatergic/aspartatergic neurons (Lara-Vásquez et al., 2016), as well as cholinergic and serotonergic receptor expressing cells (Clarke et al., 1985; Varela, 2014). Reuniens also does not have any intrinsic interneuron activity and instead is thought to receive inhibitory modulation from the reticular nucleus or the zona incerta although this is merely speculative (Zimmerman & Grace, 2016; Lara-Vásquez et al., 2016).

Nucleus reuniens expresses primarily glutamatergic and aspartatergic receptors (Bokor et al., 2002), and a high density of ionotropic nicotinic ACh receptors (Clarke et al., 1985). When activated, nACh receptor channels allow an

influx of Na$^+$ and Ca^{2+}, and an efflux of K$^+$ with the net effect being a fast acting depolarization of the post-synaptic neuron. Furthermore, nACh receptors are believed to be primarily thalamic *drivers* (Sherman, 2007; Varela, 2014). Thalamic drivers are believed to transmit a reliable and accurate spike message to their targets as the input-out relationship between EPSPs and the firing rate of thalamic driver nuclei show a nearly linear relationship (Sherman, 2001); in other words input approximately equals output. Additionally, reuniens expresses metabotropic muscarinic ACh receptors which have mixed responses but are generally excitatory and much slower to action than nACh expressing cells and largely neuromodulatory in function (Varela, 2014). Neuromodulators are thought to modify incoming spike messages enroute to their targets (Sherman, 2001). Moreover, the presence of cholinergic receptors in nucleus reuniens may suggest a possible role in attention as high acetylcholine is often associated with wakefulness (Hasselmo, 2004, 2006; Varela, 2014), and unilateral and bilateral lesions of the pedunculopontine tegmentum (PPT), a major source of cholinergic input to the cortex, induces severe deficits in a 5-choice serial reaction time task (5CSRT) compared to pre-surgical performance in rats. Recent

evidence, however, suggests that reuniens role in attention may be less prominent, as rats with reuniens lesions exhibited less perseveration than control animals on a 5CSRT while exhibiting what even appeared to have been enhanced performance, suggesting reuniens may play some role in response inhibition rather than attention per-se (Prasad et al., 2013; Cassel et al., 2013). Interestingly, reuniens receives direct projections from the PPT and the laterodorsal tegemental nucleus (LDT), so while reuniens lesions do not cause clear deficits in attention based tasks, reuniens mode of activation may still be influenced by cholinergic inputs (McKenna and Vertes, 2004; Varela, 2014) which are typically associated with wakefulness and arousal, and given that reuniens receives direct retinal projections it may be that reuniens' activity is modulated by light-dark cycles (Cassel et al., 2013).

Generally speaking, the thalamus has two modes of activation: burst and tonic (Steriade et al., 1993; McCormick and Bal, 1997; Kim and McCormick, 1998; Sherman et al., 2001). Burst mode is most often associated with sleep-wake cycles and the generation and propagation of slow-waves (Steriade et al., 1993) as illustrated in figure 3 below.
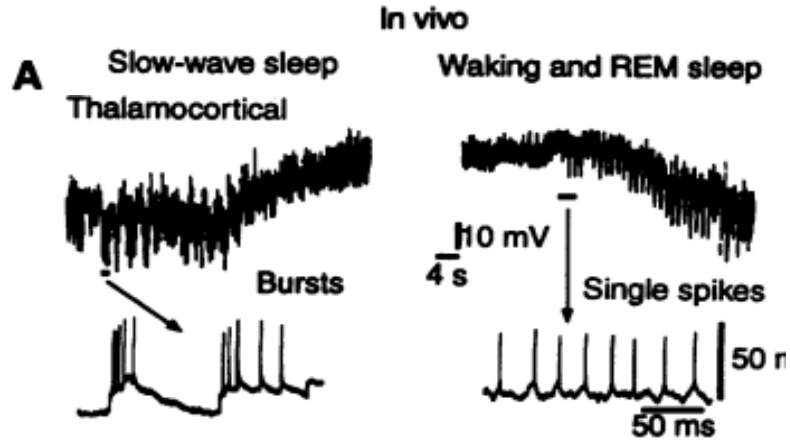
Figure 3. Illustration of thalamocortical burst and tonic mode and their effect of sleep-wake cycle. The left subfigure demonstrates the effect of thalamocortical bursting on slow-wave sleep generation. The right subfigure depicts tonic firing activity during waking and REM sleep. Figure adapted from Steriade et al. (1993).

However, evidence (Sherman, 2001) suggests the burst mode also occurs during wake-states and may play a role in modulating information as it passes through thalamic nuclei. Sherman (2001) hypothesized that in addition to generating and maintaining the slow-wave sleep state the thalamic burst mode is also related to attention and arousal processes in that thalamocortical bursting allows for rapid shifting of attention; much like a spotlight shifting from one locus of attention to another as described by Francis Crick (Crick, 1984; Sherman et al., 2001). Sherman (2001) claimed that increased EPSPs arriving at thalamic relay nuclei do not

necessarily generate larger low-threshold spikes (LTSs) and corresponding rebound bursts. Thus the input-output curves of bursting cells are more of an all-or-none function whereby the bursting of a cell is driven by a large EPSP sufficient to activate the IT current and thus create a burst. Sherman (2001) surmised that the burst function of thalamic relay cells during wakefulness may be for rapidly shifting attention to a specific stimulus, rather than to encode information per-se. Tonic mode on the other hand is classically associated with wakefulness and attention, as the input-output curves of thalamic relay cells is nearly linear during tonic mode and as such the tonic mode facilitates greater detail encoded in spike-trains to be reliably transferred to exothalamic targets (Sherman, 2001).

Recently, Hay and colleagues (2015) reported the presence of orexinergic afferents projecting to rhomboid nucleus. Orexin is a key neurotransmitter in the sleep-wake cycle (Fadel and Frederick-Duss, 2008; Schwartz et al., 2008) and orexinergic afferents of rhomboid nucleus may play a key role regulating sleep-wake cycles, attention and arousal mechanisms, and potentially information relay as it has been previously shown that stimulating orexinergic cells in rhomboid nucleus

shifts the nucleus from burst mode to tonic mode (Bayer et al., 2002).

In addition to glutamatergic and cholinergic inputs reuniens cells also express serotonergic 5-HT$_7$ receptors which are thought to play important roles in cognition (Gasbarri & Pompili. 2014) and sleep wake-cycles (Portis et al., 2000). 5-HT$_7$ receptor agonists block the K$^+_{Ih}$ current slow after-hyperpolarization inducing *tonic* activation in affected neurons (Goaillard and Vincent, 2002; Guseva, et al. 2014; Varela, 2014). Thus, serotonergic inputs to reuniens may shift the nucleus from burst to tonic mode and play a key role in mechanisms underpinning information processing and transfer.

In all, it would seem that reuniens is not strictly a relay nucleus faithfully relaying information between targets, but likely also has intrinsic neuromodulatory functionality and a possible role maintaining arousal, or perhaps its relay functionality is driven by innervation by cholinergic, orexinergic, and serotonergic inputs. Furthermore, given its dense reciprocal connectivity between the medial prefrontal cortex and hippocampus reuniens is strongly implicated in higher-order cognitive processes relying on cortico-hippocampal communication.

1.2.5 The role of nucleus reuniens in higher-order cognitive processes

It has been demonstrated through a combination of retrograde, anterograde, and viral transfection studies that nucleus reuniens exhibits dense *reciprocal* connectivity with the hippocampus and medial prefrontal cortex (Vertes, et al 2011; Varela et al., 2014) depicted in figure 4 below. It is estimated that approximately 8-10% of reuniens neurons exhibit this collateral projection to prefrontal and hippocampal networks in the rat brain (Varela et al., 2014).
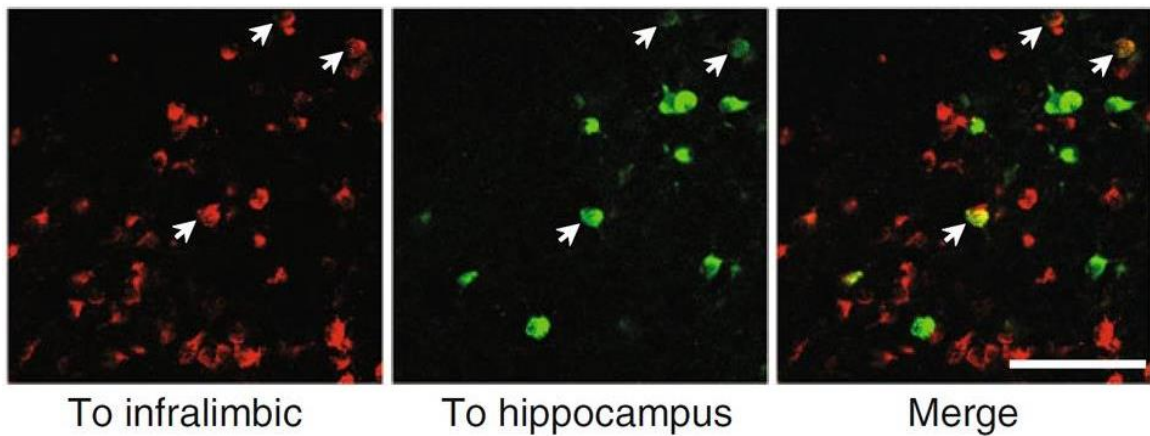
Figure 4. Illustration of infralimbic and dorsal hippocampal projecting reuniens cells. The left panel depicts reuniens neurons (labelled red) which projecting to the infralimbic cortex in the rat brain. The center panel illustrates reuniens neurons (labelled green) projecting to the dorsal hippocampus. The right-most panel illustrates double labelled reuniens neurons (white arrows) depicting collateral projections to both prefrontal and hippocampal networks from reuniens nucleus. Figure adapted from Varela et al. (2014).

It is believed that this reciprocal connectivity is paramount to higher-order cognitive processes such as behavioural flexibility (Hembrook and Mair, 2010; Hembrook et al., 2012; Prasad et al., 2012; Linley et al., 2016), and learning and memory processes (Dolleman Van-der Weel, 2008; Loureiro et al., 2012; Cassel et al., 2013; Xu and Sudhof, 2013). Additionally, dysfunction of nucleus reuniens has been implicated in Alzheimer's disease (German, 1987; Braak and Braak, 1991), schizophrenia (Duan et al., 2015; Zimmerman et al., 2016), seizures (Hirayasu et al., 1992; Drexel et al., 2011; Sloan et al., 2011), and disorders of consciousness (Saalmann et al., 2014).

The exact influence neocortical and hippocampal afferents have on reuniens cells remains to be explored but it is hypothesized that the afferents to reuniens may have varied effects on reuniens' ability to facilitate information flow. On the one hand by reliably transmitting spike information between targets via tonic activation (thalamic drivers), and on the other by modifying and modulating spike information via burst firing (thalamic modulator) as it passes through reuniens (Sherman, 2001). Xu and Sudhof demonstrated that depending on the firing mode of nucleus reuniens cells

(burst or tonic) they could affect the specificity of an encoded fear memory as represented in figure 5 below.
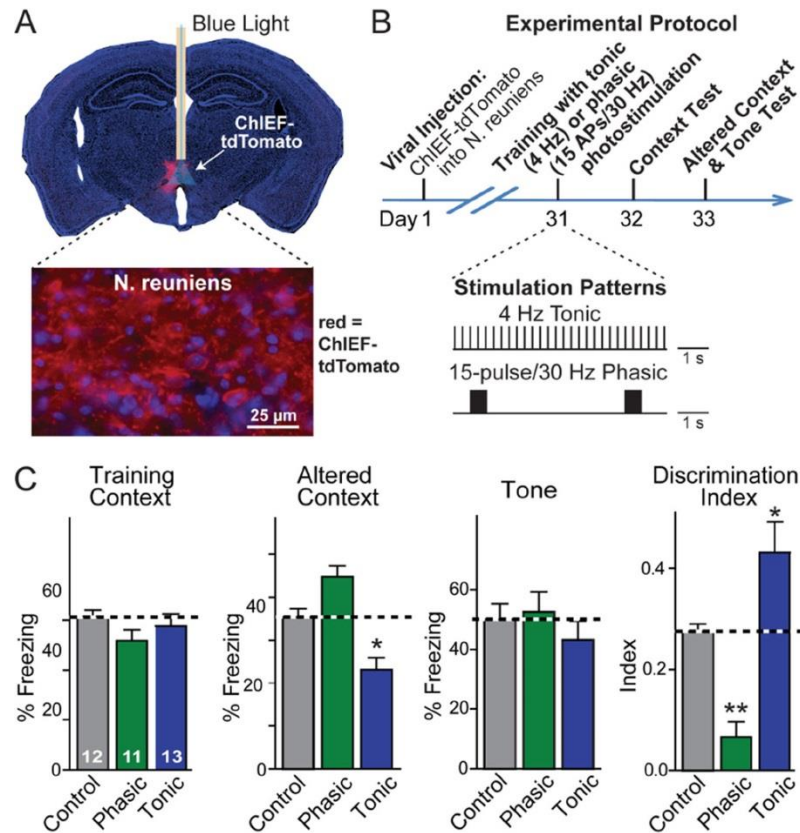
Figure 5. Effect of phasic vs. tonic activation of reuniens neurons on fear memory representation. In the above figure (**A**) illustrates the optogenetic implant into nucleus reuniens. Panel (**B**) represents the experimental stimulation protocol. Panel (**C**) represents the effect of phasic vs. tonic activation of reuniens neurons on measures of fear memory. Note the decreased freezing response as a result of tonic activation, indicating fear memory specificity. Likewise, note the significant increase in discrimination ability of mice receiving tonic stimulation, compared to mice receiving phasic activation of reuniens neurons. Taken together these results indicate that nucleus reuniens facilitates the encoding of fear memory as a function of firing mode; tonic mode encodes greater detail than phasic. The above figure was taken from Xu & Sudhof (2013).

Presumably then, depending on the firing mode, nucleus reuniens can modulate the accuracy of a spike message transmitted between the neocortex and the hippocampus which could ultimately affect the degree to which information is accurately encoded and consolidated.

Recently it was found that lesioning nucleus reuniens impedes the transfer of trajectory dependent information from the mPFC to the hippocampus in freely moving rats as illustrated in figure 6 below, (Ito et al., 2013). The lesions caused CA1 cells to behave more like CA3 cells, showing no trajectory dependent firing rate selectivity. Taken together it would seem to be the case that nucleus reuniens is a principal hub for the accurate relay of information from neocortical to hippocampal targets and perhaps from the hippocampus to the neocortex as well.
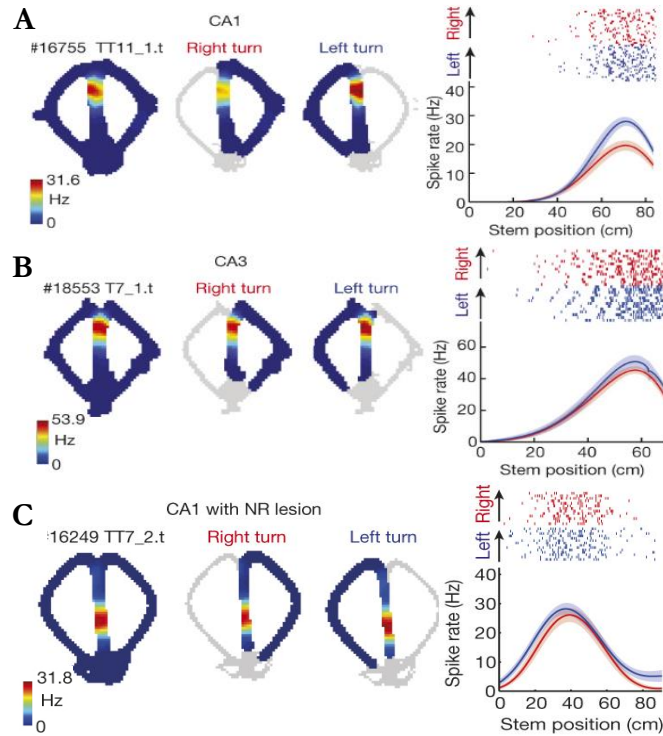
Figure 6. Effect of reuniens inactivation on trajectory dependent firing activity of CA1 neurons. The top figure (**A**) represents the trajectory dependent firing of CA1 neurons indicating a preference for left turns as depicted by the higher firing rate immediately preceding a left turn. Note in panel (**B**), CA3 neurons exhibit no trajectory dependent firing rate activity; the CA3 neurons fire with equal rate before the choice point whether the mouse makes a right turn or a left turn. In panel (**C**) it should be noted that with reuniens lesion, the CA1 neurons exhibit no trajectory dependent firing rate activity, namely they fire with equal rate before the choice point whether the animal makes a right turn or a left turn, this suggested to the authors that reuniens gates information flow to the hippocampus from prefrontal cortical networks. Figure adapted from Ito et al. (2013).

Furthermore, in a groundbreaking study it was shown that lesioning nucleus reuniens affected remote memory retrieval

on a spatial memory task (Loureiro et al., 2012). Rats received fiber-sparing excitotoxic NDMA lesions to nucleus reuniens prior to training on a water maze. The lesioned animals exhibited normal learning curves and acquisition no different from sham controls as well as normal task retention at a five day post-training delay. However, at a twenty-five day post training delay animals showed no evidence of having learned the task at all as depicted in figure 7 below. The authors concluded that nucleus reuniens is not needed to learn a spatial navigation task, as that process is largely dependent on the hippocampus (Morris et al., 1982), but nucleus reuniens does appear to play some important role in long-term memory formation and/or retrieval such that interfering with reuniens affects performance on spatial memory task at a remote time-point.
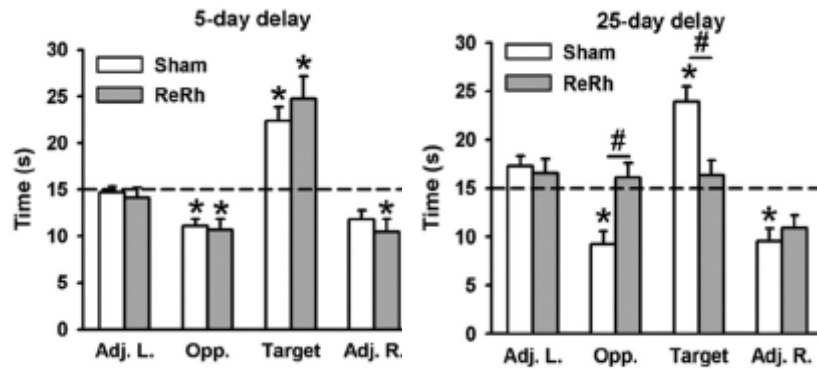
Figure 7. Effect of reuniens lesions on total time spent in target quadrant on a Morris Water Maze. The above figure depicts the amount of time rats spent in each of the four quadrants on the water maze. The subfigure on the left illustrates the effect of reuniens lesions on time spent in the target quadrant after a 5 day delay compared to those who were unlesioned. Likewise, the subfigure on the right depicts the effect of reuniens lesions on time spent in the target quadrant after a 25 day delay. Note, at a 25 day post-acquisition delay lesioned animals show no evidence of having learned the task and perform at chance levels. Figure adapted from Louriero et al. (2012).

They also observed that at a twenty five day delay *intact* animals showed enhanced c-Fos expression in reuniens which was not observed at the five day delay, suggesting a potential role in retrieval processes, as illustrated in figure 8 below, though they only reported the 5-day and 25-day post-acquisition delay time-points, it would be pertinent to investigate at exactly what point in time reuniens damage interferes with spatial memory retrieval.

30
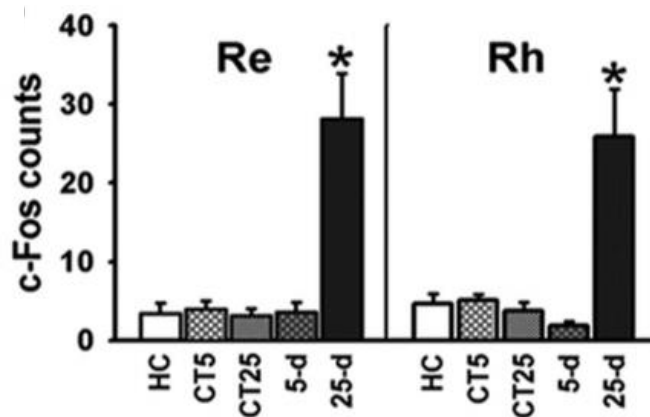
Figure 8. Reuniens and Rhomboid c-Fos expression. The above figure illustrates elevated c-Fos expression in reuniens (Re) and rhomboid (Rh) nuclei at a 25-day post-acquisition delay but not at a 5-day post-acquisition delay. These results indicate that reuniens and rhomboid nuclei are preferentially active during retrieval of a memory trace from long-term storage. The above figure was adapted from Louriero et al. (2012).

Furthermore, the authors subjected intact animals to transient inactivation of reuniens prior to retention tests at both five and twenty five day delays using microinjections of 74mM lidocaine, and observed no difference in recall ability or task performance (figure 9). They concluded that nucleus reuniens plays an important and as of yet unexplored role in facilitating long-term memory consolidation (Loureiro et al., 2012), though due to the lack of appropriate positive control in their lidocaine study the authors were unable to rule out the role of reuniens in remote spatial memory retrieval.

31
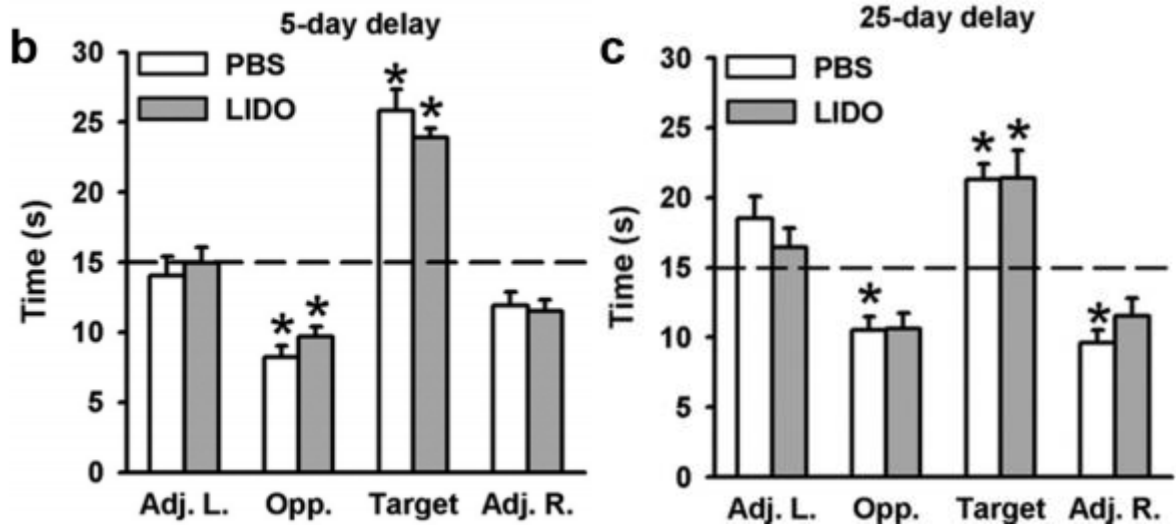
Figure 9. Effect of lidocaine inactivation on Morris Water Maze performance. The above figure illustrates that lidocaine inactivation of nucleus reuniens prior to retention tests at 5 day and 25 day post-acquisition delays has no effect on task performance. These results indicate that the memory deficits observed by Loureiro et al. (2012) are likely the result reuniens lesions affecting long-term consolidation. Figure adapted from Louriero et al. (2012).

Thus it seems to be the case that nucleus reuniens may serve a dual function: on the one hand reuniens is involved in "online" information processing by transferring information between mPFC and hippocampal networks and likely as a function of its mode of activation, namely tonic mode, and on the other hand by facilitating the "offline" consolidation of spatial information within neocortical networks, a process thought to involve coordinated activity between hippocampal sharp wave-ripples and neocortical K-

complexes (Sirota et al., 2009; Johnson et al., 2010; Peyrache et al., 2011) during sleep.

1.3 Hippocampal sharp wave-ripples

1.3.1 Anatomical etiology

Hippocampal sharp wave-ripples (SPWRs) are large amplitude local events occurring primarily during slow-wave sleep (SWS). SPWRs can also occur during quiet wakefulness and consummatory drive-reduction behaviours (O'keefe & Nadel, 1978; Buszaki, G., 1986; McNaughton, B. L., et al., 2003). Sharp wave-ripples are the result of large scale depolarization of approximately 50,000-100,000 hippocampal neurons in the CA3-CA1-subicular complex, or approximately 5-15% of the local population. Beginning in the CA3 region and then spreading throughout the hippocampal formation to the CA1 region via the Schaffer collaterals; spreading neural activation from CA3 results in synchronous bursts in CA1 which are then terminated by feed-forward inhibition from GABAergic interneurons (Buszaki, 1986; Buszaki, 2015).

The sharp wave-ripple oscillation is a complex of two simultaneous events: a high-frequency 100-300 Hz oscillation generated by a local burst depolarization of many pyramidal

neurons in the CA1 stratum pyramidale called a *ripple*, and a lower frequency negative going deflection in the record of the stratum lacunosum moleculare local field called a *sharp wave* (Chrobak & Buszaki, 1994, 1998) which is the result of strong depolarizing inputs from bursting CA3 neurons via the Schaffer collaterals (Buszaki, 2006).
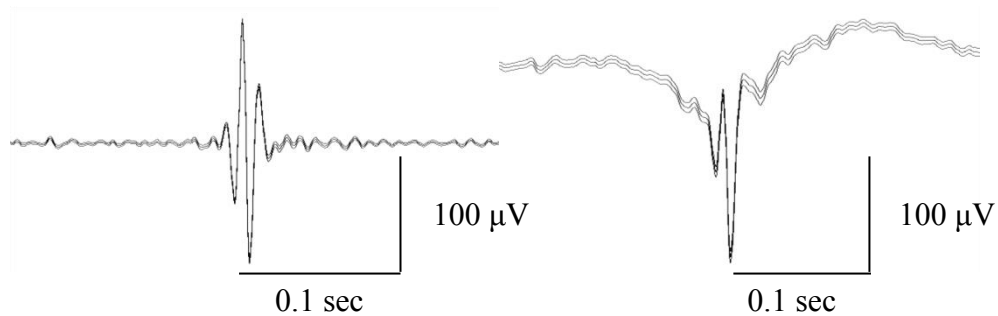
Figure 10. Sample sharp-wave ripples. The left panel illustrates a 100-300Hz filtered SPWR. The panel on the right illustrates a raw unfiltered SPWR. Note, in the panel on the right there is a negative deflection that is characteristic of the sharp wave component of the SPWR.

1.3.2 Functional Significance

Due to the large number of neurons recruited, the SPWR is a good candidate to facilitate memory consolidation via synaptic plasticity in downstream targets. The relatively short duration 50-100ms activity roughly corresponds with NDMA receptor activity (Kandel, 2001). Furthermore, the

ripple's high-frequency 100-300 Hz oscillations are ideal for long-term potentiation (LTP) mechanisms of synaptic plasticity (Douglas and Goddard, 1975; Buszaki et al., 1987; Ben-Ari & Gho, 1988; King et al., 1999). Thus, it seems probable that SPWRs are a candidate mechanism for facilitating synaptic potentiation in neocortical networks and thus consolidation.

Additionally, it has been demonstrated that patterns of neural activity recorded while animals traverse an open field, or move on a maze, are reactivated during SPWRs during post-task stage 2 of NREM sleep, and quiet wakefulness regardless of whether the task is well-learned or novel (Wilson & McNaughton, 1994; Kudrimoti et al., 1999; Zoltan et al., 1999; Lee and Wilson, 2002). Also, it has been demonstrated that SPWR density increases during post-task sleep following a learning epoch (Eschenko et al., 2008). Recently, it was found that the increased ripple density associated with learning can be later blocked using amyloid beta oligomers with concomitant learning deficits (Nicole et al., 2016). Though the results of Nicole and colleagues (Nicole et al., 2016) are more related to the pathology of Alzheimer's they do provide support to the notion that ripples are important to memory consolidation.

Thus, the hippocampal SPWRs play a critical role in learning and memory processes and will be one focus of this thesis

1.4 Neocortical K-complexes

1.4.1 Anatomical Etiology

The K-complex (KC) is the largest observable electrophysiological phenomenon in the human electroencephalogram (EEG). It occurs predominately during stage 2 of Non-REM sleep but is also observable during deeper stages of slow-wave sleep (SWS) only much less frequently (Colrain, 2005). The KC was originally described by Alfred Lee Loomis in 1935 (Loomis et al., 1935). He observed a large *triphasic* deflection in the surface EEG potential of a sleeping subject when the subject was presented with an auditory stimulus. Loomis described the KC as having two distinct components, a slow component which we now refer to as the KC, and a fast component characterized by a high-frequency discharge which persisted for a second or more and was likely an alpha burst or sleep spindle.

The KC is now generally described as a large *biphasic* deflection which does not include the spindle oscillation and lasts approximately a half-second or less. The KC is

characterized by a large negative-going hyperpolarizing phase followed by a strong positive-going depolarizing phase but can also include a smaller depolarizing vertex sharp wave that precedes the early slow phase. Sirota and Buszaki (2005) classified the K-complex as a sharp down-to-upstate transition in the slow oscillation. This down-to-upstate transition is thought to be the result of a shift from an absence of local neuronal activity to a fast synchronous discharge of local neurons (Johnson et al., 2010). Furthermore, the KC and delta-wave are now believed to be substructures of the slow oscillation (Steriade & Amzica, 1998); with the KC manifesting as a sharp down-to-upstate transition, and the delta wave as a slower oscillation encompassing the entire downstate. See figure 11 below for an illustration of the K-complex.

A   B

200 µV

0.5 sec
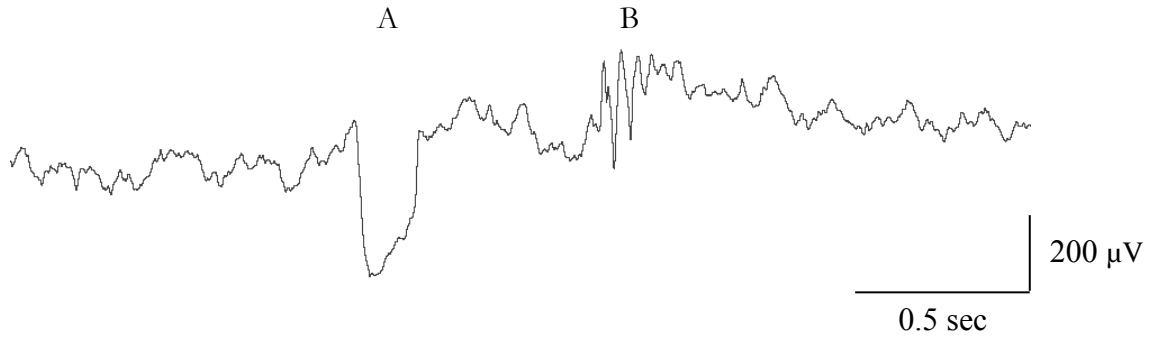
Figure 11. Sample K-complex and spindle oscillation. The figure above illustrates a raw unfiltered sample K-complex (A) and associated spindle oscillation (**B**). As previously noted, the original description of a KC included a spindle oscillation though this is no longer the case.

1.4.2 The K-complex and information processing

The large biphasic deflection of the KC is believed, by some, to be a transient and rapid processing of external information, such as a knock, and if judged by the sleeping and vulnerable brain to be *non*-threatening, neural activity is suppressed to prevent the brain from rousing further; as a form of sleep preservation (Colrain, I. 2005). In fact, if one claps their hands or snaps their fingers while recording local field potential activity under anaesthesia or sleep a K-complex can be elicited. While the evoked KC has classically been associated with auditory and somatosensory stimuli the KC can also, and frequently does, occur spontaneously during natural sleep and anaesthesia and tends to precede transitions from stage 2 NREM sleep to stages 3

38

and 4 NREM sleep. Additionally, the KC does not tend to occur during transitions from stage 2 to paradoxical sleep; further reinforcing its supposed role in sleep preservation (Forget et al., 2011).

Evoked KC's are typically thought to suppress brain arousal to *external* stimuli without a graded response related to stimulus intensity: higher *intensity* does not make it easier to evoke a KC (Bastien & Campbell, 1989). But, it is spontaneously generated KC's that are of particular interest to us as they may represent *internal* information processing. In a ground breaking study, researchers (Oswald et al., 1960) found that significantly more KC's were elicited from sleeping patients when *their* names were spoken to them as opposed to neutral names carrying no intrinsic significance. This suggested to the researchers that while some KC's may be important for keeping an individual asleep, other KC's may be important to sleep related information processing. Although it is possible the salient information merely roused the subjects closer to wakefulness and thus a KC was more likely to be generated to maintain sleep. Furthermore, because fewer K-complexes were elicited when researchers addressed subjects with neutral names, they inferred that the information saliency was insufficient to rouse

significant neocortical activity. However when stimuli carrying sufficiently salient information was presented to subjects, the subject's name in this case, the neocortex was roused suggesting to the researchers that KC's respond selectively, to some degree, to the information content of such stimuli. Thus, since the evoked K-complex density is correlated with information salience it may be the case that *spontaneously* generated KC's are related to *internally* salient information such as the excitatory input of the hippocampus on the medial prefrontal cortex.

More recently, the K-complex has been implicated in learning and memory processes (McDonald et al., 1975; Wilson & Ji, 2007; Cash et al., 2009). The down-to-upstate transition, which defines the K-complex, is a temporary period of quiescence in the neocortical network whereby weakly biased attractors may be reactivated during the following upstate in conjunction with hippocampal networks potentially facilitating consolidation (Johnson et al., 2010). In fact, it has been demonstrated that hippocampal ripples actually lead KC's in some cases (Peyrache et al., 2011), though there are substantially more ripples than KC's, but some KC's are correlated with ripple activity in the hippocampus. Thus, it would seem, that if ripples occasionally lead KC's,

and if neocortical replay occurring during the vertex sharp-wave, and again during the spindle, coincides with hippocampal reactivation, then the down-to-upstate transition may be an important substrate for memory consolidation.

1.5.0 Hippocampal-cortical communication

1.5.1 Hippocampal-cortical communication and consolidation

Previous studies (Wilson and McNaughton, 1994; Kudrimoti et al., 1999; Eichenbaum, 2000; Lee and Wilson, 2002; Buzsaki, 1998; Benchenane et al., 2010; Born and Wilhelm, 2012) have demonstrated the importance of the hippocampus in learning and memory but an important question remains:

How are memories encoded by the hippocampus then stored in neocortical networks for later recall? And what circuit elements are crucial to this process?

One prevailing hypothesis is that recent experiences encoded by the hippocampus and the neocortex are reactivated during sleep consolidating the episodic memory into a semantic memory (Jay et al., 1991, 1992, 1995; Parent et al., 2012). This process involves coordinated interactions between hippocampal sharp wave-ripples and neocortical down-to-

upstate transitions (Johnson et al., 2010; Peyrache et al., 2011), including K-complexes, delta waves, and sleep spindles. In fact, a previous study (Peyrache et al., 2011) demonstrated that hippocampal sharp wave-ripples tend to precede neocortical K-complex and spindle activity by approximately 100-200ms. Furthermore, Johnson et al (2010) showed that neocortical reactivation strength is correlated with down-to-upstate fluctuation density, or K-complex density. In other words, as K-complex density increases, neocortical replay *strength* increases concomitantly.

So, since we know that sharp wave-ripples represent reactivation of previously encoded experiences, and because K-complexes are correlated with neocortical ensemble reactivation, and since ripples precede neocortical K-complexes and spindles it stands to reason that the coordinated interaction of hippocampal sharp wave-ripple complexes and neocortical K-complexes may provide the requisite oscillatory coupling necessary for long-range information transfer from hippocampal to neocortical targets. In other words, the coordinated interaction of hippocampal ripples and neocortical K-complexes may represent a principal opportunity for the consolidation of hippocampally encoded memory traces into neocortical

42

targets. And, since we know from previous studies that nucleus reuniens facilitates bidirectional communication between the mPFC and hippocampus and because nucleus reuniens has been implicated in facilitating long-term memory consolidation (Loureiro et al., 2012), it is possible that reuniens may play some role in facilitating the coordination of hippocampal sharp wave-ripples and neocortical K-complexes in a naturally sleeping animal. And so, the aim of this work was to investigate the degree to which transient inactivation of nucleus reuniens affects the coordination of hippocampal sharp wave-ripples and neocortical K-complexes during natural sleep. I hypothesized that transiently inactivating nucleus reuniens would adversely affect the coordination of neocortical K-complexes and hippocampal sharp wave-ripples in naïve animals. This will be the principal focus for the remainder of this thesis.

Chapter Two – *Methods and Materials*

2.1 Animals

Female Fisher Brown-Norway hybrid rats (N=5; mean weight=224.6 + 7.4g) housed on a 12 hour reverse light-dark cycle were used for freely behaving experiments; 4 were used for analysis. All procedures were conducted in accordance with the Canadian Council for Animal Care and approved by the University of Lethbridge Animal Welfare Committee.

2.2 Surgical procedures

Animals were anaesthetized with isoflurane and mounted in a stereotaxic frame (Kopf Instruments, #962). Their scalps were shaved and then scrubbed with alternating stanhexidine and 70% ethanol solutions. The animals then received a 5mg/kg subcutaneous injection of Metacam® for anti-inflammation and a 1mg/kg subcutaneous injection of a 2% lidocaine hydrochloride and epinephrine solution to provide local analgesia and minimize bleeding at the incision site.

Using a #10 blade, the scalp was incised and retracted and the overlying periosteum scraped away. The skull was then cleaned with a sterile 0.9% saline solution and allowed to air dry. Once the skull was dry, bregma and lambda were marked, the skull was leveled, and locations for craniotomies were stereotaxically marked using bregma as the

point of reference. The craniotomy locations were as follows: mPFC (AP= +3.00mm, ML= -1.60mm, DV= -3.70mm, θ=9.5°), HPC (AP= -4.40mm, ML= -3.40mm, DV= -2.42mm, θ=9.5°), NRe (AP= -1.92mm, ML= +2.00mm, DV= -7.0mm, θ=16.0°). I then drilled a hole over the left cerebellum for placement of a ground-screw. To provide additional structural support, 3-4 holes were drilled for stainless steel screw placement contralateral to each implant. The surface of the skull was then coated with a thin layer of low viscosity ethyl-cyanoacrylate glue (Krazy Glue® Advanced) and allowed to air dry.

The HPC local field potential electrode was lowered slowly in 100μm steps until negative-going sharp waves were recorded on the deepest electrode and ripples detected on the upper electrode. Tip separation was critical to this process and is described in detail in the following *Electrophysiology* section of this work. Once electrodes were in place, Kwik-Sil was applied around the electrode. Once the Kwik-Sil had polymerized a small drop of dental acrylic (Lang Dental®, Jet Denture Repair Package) was applied to affix the implant to the surface of the skull and to nearby support screws. The mPFC electrodes were implanted in 100μm

steps until the electrodes reached an approximate depth of 3.7mm in prelimbic cortex.

The NRe dialysis guide cannulae (CMA 11 Guide Cannula, #8309018) were implanted in 100μm incremental steps until reaching a depth of 7.1mm. Neck electromyogram (EMG) electrodes were implanted unilaterally into the left nuchal muscle and left trapezius muscle as described in Steenland et al., (2009). Once the implants were completed all electrodes were connected to a custom-made linear electrode interface board, and the implants were affixed with dental acrylic.

Following surgical procedures the animals were given one injection of 1mg/kg of buprenorphine for analgesia and daily injections of 1mg/kg Baytril® antibiotic for 3-5 days. Animals were allowed 1-2 weeks for recovery.

2.3 Electrophysiology

2.3.1 Electrode fabrication

Recordings were performed using Teflon-coated stainless steel bipolar twisted-pair electrodes. Raw stainless steel material (MedWire, #316-SS-3T) was cut to length and twisted 80 revolutions in the clockwise direction and 20 revolutions

in the anti-clockwise direction to reduce torsional strain. 250μm of Teflon coating was then removed from the electrode tips to increase the sampling volume. The electrode tips were then separated by 300-500μm depending on the target region. For HPC recordings the electrodes had a vertical tip-offset of ~300μm to allow recording from both the dorsal CA1 pyramidal layer, and the stratum lacunosum moleculare. In the mPFC the tips were separated vertically by ~500μm, similarly for NRe electrodes. The ends of the electrodes were then stripped and connected to gold-plated pins.

2.3.2 Electrophysiology recordings

Signals were acquired with a Neuralynx Headstage-27 preamplifier and Neuralynx Digital Lynx 16SX data acquisition system, through a NeuroTek commutator (CMTR-96-NT). All signals were acquired with a sampling rate of 32,000Hz and band-passed filtered 0.1-600.0Hz. The mPFC electrodes were referenced to their respective pair to acquire bipolar signals. The HPC electrodes were referenced to the cerebellar electrode to facilitate greater sharp wave-ripple detection; these signals were later subtracted, offline, from their bipolar pair if necessary. EMG signals

were referenced to each other and bandpass filtered at 1.0-2000Hz.

2.4 Pharmacology

2.4.1 Microdialysis

Drug delivery was conducted using the reverse microdialysis technique (Crochet et al., 1996; Crochet et al., 2006; Hocht et al., 2004; Hocht et al., 2007; Darvesh, et al., 2011). Perfusate is dialyzed at a constant fluid volume flow rate typically ranging between 0.1-10µL/min. The perfusate is pumped from a 1mL syringe via a syringe pump (Basi Worker Bee MD-1000, MD-1001) through a zero-volume fluid switch (Basi UniSwitch® MD-1508) and a fluid swivel (Instech®, 375/22PS) to a dialysis probe with an outside diameter of 240µm (CMA Microdialysis, CMA 11 MD Probe #8309581). The perfusate then diffuses passively across a 1mm semi-permeable membrane into the brain area of interest. Fluid called the dialysate passes from the brain into the probe along a concentration gradient and can be collected for later analysis if required. Over time, the concentration of perfusate inside the probe establishes a dynamic equilibrium with the concentration of perfusate outside the probe thereby establishing a constant concentration of perfusate

at the probe site. Most drugs, if not lipophilic or strongly polar, will not dialyze further than 1.5mm. In fact most drugs, even those capable of passing through the blood brain barrier, will only have an effect radius of approximately 1.0-1.5mm (Van Duuren, E. 2007). Therefore in-vivo reverse microdialysis is an effective means of delivering drugs both acutely and chronically with good spatial and temporal acuity without much concern for diffuse and erroneous drug spread. Figure 34 depicts the hypothetical drug spread given pre-existing studies utilizing lidocaine inactivation and the same dialysis probe the we used for our studies.

To prevent dialysate from dripping on the animal and disturbing its behavioural state a modified 1mL Eppendorf tube was secured to the outlet tubing to collect dialysate. A small hole was bored in the lid of the Eppendorf tube with a 20 gauge needle and the outlet tubing was threaded through this hole. The collecting tube was emptied or replaced as needed.

2.4.2 Reversible inactivation
74mM lidocaine hydrochloride (Sigma Aldrich, #L5647) was used for reversible inactivation. Lidocaine hydrochloride is a hydrophilic non-selective sodium channel blocker that has

been used to good effect in other studies of reversible inactivation of nucleus reuniens in-vivo (Loureiro, et al. 2012; Davoodi, et al. 2011; Davoodi et al. 2009). Lidocaine was delivered via reverse microdialysis at a volume flow rate of 2.5µL/min for 60 minute intervals. The lidocaine was mixed fresh before every experiment. A 2% concentration was used, as it is within the bounds of acceptable physiological osmolality, and has been electrophysiologically verified to have an effective radius of spread of 1.0mm with ~80% local block which is washed out in less than 30 minutes with aCSF (Van Duuren, E. 2007).

2.5 Habituation

Prior to surgery, animals were handled regularly to habituate them to each other and the experimenter. Approximately 1-2 weeks post-surgery animals were placed into a flower pot with a towel for bedding and allowed 1 night of habituation with no outside intervention to acclimate to the new environment. The animals were not plugged into the data acquisition system at this time. Following the 1 night "offline" habituation period the animals were given an additional 1-2 nights "online" habituation period where they were connected to the data

acquisition system and allowed to sleep freely. This second habituation period allowed the animal to habituate to the recording system. I qualitatively assessed this habituation protocol to be best for optimizing quality sleep bouts as animals exhibited fewer signs of distress and discomfort.

2.6 Microdialysis implant

Following the "offline" and "online" habituation periods the animals were lightly anaesthetized with isoflurane and the "dummy" probe was removed from the microdialysis cannula. A sterile microdialysis probe was then carefully inserted into the guide cannula until fully seated in the guide with the 1mm probe membrane protruding from the bottom of the guide cannula. This placement allowed the dialysis probe membrane to span the diagonal width of nucleus reuniens to enhance pharmacological manipulation of the region. The inlet and outlets of the dialysis probe were connected via 2 tubing adaptors (CMA FEP tubing adaptors, #3409500) and a small length of FEP tubing (FEP Tubing #3409501) forming a continuous fluid loop which prevented the dialysis probe from drying out and foreign material from entering. After implantation the probe was secured in place with dental acrylic and ethyl cyanoacrylate glue, and the animal was

allowed 1 day of recovery to prevent carry-over effects from the anaesthesia.

2.7 Experimental Protocol

Following the recovery period the animals were taken into the experimental room approximately 30 minutes before their "lights on" time and connected to the dialysis and data acquisition systems. A small dab of hot-glue (Mastercraft®, #054-0154-6) was added to the anterior and posterior portions of the interface between the electrode interface board and the headstage connector to ensure a sturdy connection. The animals were given 30 minutes to settle down while aCSF (Tocris Biosciences, #3525) was dialyzed at a rate of 2.5μL/min. Following this short habituation the baseline period began. 2-4 trials were conducted per recording session.

During baseline periods aCSF was delivered to nucleus reuniens via reverse microdialysis at a volume flow rate of 2.5μL/min for 60 minutes. I chose 60 minute epochs as rats' NREM bouts last, on average, 2 minutes (Stephenson, et al. 2012) and I wanted to maximize the number of NREM bouts per epoch. During drug interventions the selected

pharmacological agent was also dialyzed into nucleus reuniens at a volume flow-rate of 2.5µL/min for 60 minutes. Following the drug interventions I conducted a 60 minute washout period with aCSF at a volume flow rate of 2.5µL/min. Lidocaine hydrochloride has an effect washout of approximately 30 minutes however I chose to use 60 minute washout periods to ensure that local neuronal activity would have adequate time to return to baseline levels. The experimental protocol is summarized in table 1 below.

Table 1.1

Baseline	Drug	Washout
aCSF	74mM lidocaine HCl	aCSF
Time = 60 minutes	Time = 60 minutes	Time = 60 minutes

Table 1.1 – Tabulated Experimental protocol. The table above depicts the interventions and the duration of each intervention. Baseline periods were conducted using dialysis of aCSF to approximate the electrolyte concentrations of the extracellular fluid, or cerebrospinal fluid. Drug interventions were conducted using 74mM (2%) lidocaine hydrochloride salts dissolved in aCSF. Washout periods were also 60 minutes in length and were conducted using aCSF.

2.8 Data analysis

2.8.1 Preprocessing

Data were cut into distinct baseline, drug, and washout epochs with Neuraview Data Analysis Software (Neuralynx)

using event timestamps logged during experimental procedures. Each 60 minute epoch was then down-sampled from 32,000Hz to 2000Hz.

2.8.2 Sleep detection

1. EMG signals were band-pass filtered 10-50Hz using a 4th order Chebyshev type I filter, squared, and smoothed using a Gaussian smoothing function with a 2 second smoothing window. This was used to detect motionless epochs.

2. Motion epochs were determined by finding periods when the processed EMG signal exceeds the signal median. The median was used in place of the mean because the signal can have high amplitude rapid deflections that are, in effect, outliers to the true signal mean whereas the median is not subject to this variability. Motionless periods were determined by finding periods when the processed EMG signal was less than 50% of the signal median. Motionless epochs less than 30 seconds were discarded as these periods may have simply represented periods of quiet wakefulness and not true sleep (Steenland et al., 2009, 2012).

2.8.3 K-complex detection

1. The mPFC local field potential signal was band-pass filtered 2-6Hz using a 4th order Chebyshev type I filter. The filtered signal was then smoothed using a Gaussian smoothing function with a 100ms sliding window.

2. K-complexes reflect a rapid local field depolarization and so slope differences were used to detect rapid deflections in the signal. Start and end time-stamps for KC's were detected when the slope crossed zero going downward indicating a shift to a downstate. The signals were thresholded to 3 standard deviations above the mean and threshold crossings were detected and logged as K-complex events as illustrated in figure 12 below.

Filtered a)
2-6Hz

Raw   b)
Unfiltered

400μV
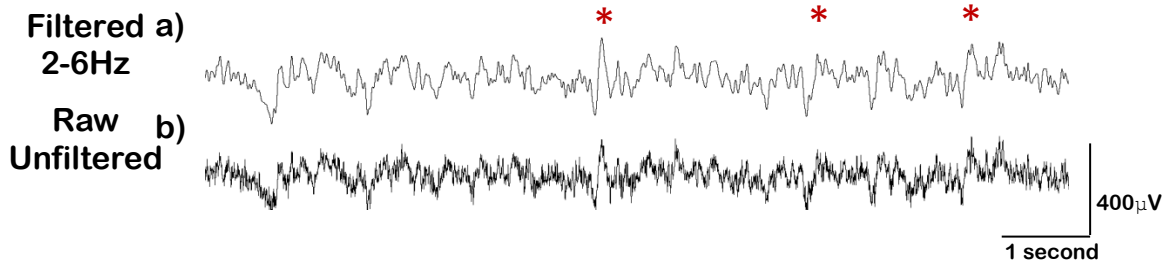
1 second

Figure 12. 10-second raw and filtered mPFC local field potential traces.   a) Filtered mPFC LFP trace in the K-complex band, 2-6Hz. The red asterisks depict detected and time-stamped mPFC KCs. **b)** Raw unfiltered mPFC LFP trace.

2.8.4 Sharp wave-ripple detection

Hippocampal sharp wave-ripple detection was conducted using a common thresholding algorithm as described in (Eschenko et al., 2008) and the steps are outlined as follows.

1. The hippocampal LFP signal was first band pass filtered 100-300Hz using a 4th order Chebyshev Type I filter. Then the filtered HPC data was squared, and smoothed using a Gaussian smoothing function with a 40ms window, and converted to z-scores.

2. A detection threshold was set at 3 standard deviations above the mean (z=3), and a "limit threshold" to detect start and end times of the ripples was set at 1 standard deviation above the mean (z=1). Then peaks were detected using MATLAB's peak detection algorithm, and any peak above the "detect threshold" was logged as a ripple. The start and end times were timestamped when then events crossed the "limit threshold". An example is illustrated in figure 13 below.
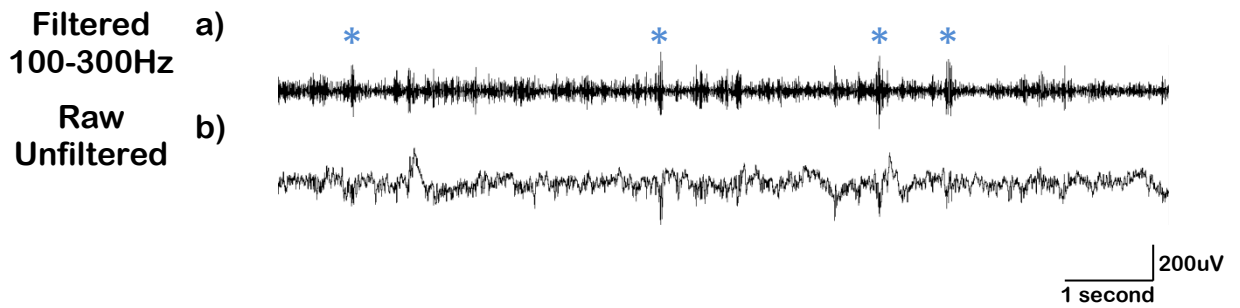
Figure 13. 10-second Raw, and Filtered Hippocampal Local Field Potential Traces. **a)** Filtered Hippocampal LFP trace in the ripple-band, 100-300Hz. The blue asterisks depict detected and time-stamped hippocampal ripples that surpassed the detection of 3-standard deviations above the mean. **b)** Raw unfiltered Hippocampal LFP trace, illustrating sharp wave-ripple complexes coinciding with the detection of ripples in trace **(a)**.

2.8.5 Sharp wave-ripple envelope

The ripple-envelope is a continuously sampled time-series dataset derived from the hippocampal local field. First, the raw local field is bandpass filtered in the ripple-band (100-300Hz), then the signal is Hilbert transformed and squared, low-pass filtered (1-20Hz), and smoothed. This continuously sampled time-series data can then be used for the continuous signal cross-correlation analyses as outlined below in *Section 2.8.7.*

2.8.6 Discrete Cross-correlation analysis

Cross-correlogram's were computed for each trial to compare hippocampal sharp wave-ripple activity with cortical K-complex activity. K-complex timestamps were selected as the reference event because K-complexes occur, approximately, $1/10^{th}$ as frequently as sharp wave-ripples. Hence, if there is a correlation between the two discrete events it will be better captured binning ripples relative to K-complexes as is common practice (Peyrache et al., 2011). The cross-correlogram was constructed by selecting a K-complex timestamp and designating that time as t=0ms. All timestamped ripple events occurring within 1000ms before or after the K-complex were binned into 10ms bins as illustrated in figure 3 below. If there was no correlation between the two events one would expect a flat line or a bar graph with no obvious peaks or valleys. A prominent peak in the ripple histogram represented a correlation between ripple events and K-complexes at the time-lag corresponding to the peak. See equation 1.1, and figure 3 below for mathematical and graphical representations of the stochastic cross-correlation.

$$\langle f * g \rangle(n) \overset{\text{def}}{=} \sum_{i=1}^{n} f(t_i)g\langle f(t_i \pm \tau)\rangle \qquad \text{Equation 1.1}$$

Equation 1.1 – Cross-correlogram calculation. In the above equation, let "i" represent the iteration index, let "**τ**" represent the time-lag in milliseconds, let n represent the number of events "f", let "$f(t_i)$" represent the timestamp for event f(n), let "$g\langle f(t_i \pm \tau)\rangle$" represent the timestamps for event "g(n)" occurring within window $f(t_i \pm \tau)$. The function computes the sum of event "g" proximal to event "f" plus or minus some time-lag **τ** as described in figure 14 below. Function described in Diggle (1990).
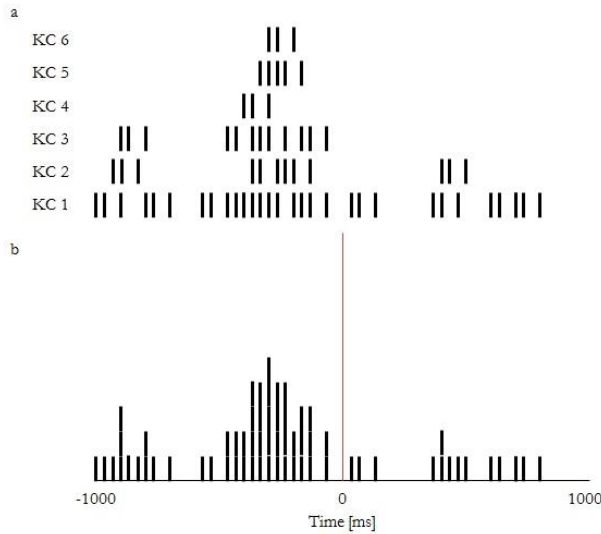
Figure 14. Sample Cross-correlogram illustration with simulated data. a) KC 1-6 represents 6 sequential K-complex events. Each black vertical line represents a single ripple event 1 second before and after the K-complex. **b)** Binned histogram of data in **a)** showing a peak that precedes the K-complex.

60

2.8.7 Local field potential event-triggered average

Event triggered averages were calculated by acquiring 2-second traces of mPFC and CA1 LFP activity triggered off previously detected K-Complex events (1 second before a KC and 1 second after a KC) for each data set. The signals were then populated into a matrix, averaged, and plotted. The event triggered average provides insight into the gross electrophysiological activity temporally proximal to a particular event.

$$C(\tau) = \langle \frac{1}{n} \sum_{i=1}^{n} s(t_i \pm \tau) \rangle \approx \frac{1}{\langle n \rangle} \langle \sum_{i=1}^{n} s(t_i \pm \tau) \rangle \quad \text{Equation 1.2}$$

Equation 1.2 – Event triggered average. In the above equation let "C(τ)" represent the event-triggered average of continuously sampled signal data "s" within time-window "$(t_i \pm \tau)$" around event "t_i". Function described by De Boer & Kuyper (1968).

2.8.8 Ripple envelope cross-correlation analysis

Ripple envelope cross-correlations were calculated by acquiring 2-second traces of mPFC LFP and hippocampal ripple envelope activity, triggered off previously detected K-Complex events (1 second before a KC and 1 second after a KC) for each data set. Cross-correlations were then

calculated for each pair of signals and the cross-correlations were then populated into a matrix, averaged and plotted. The signal cross-correlation provides insight into how two continuously sampled signals are correlated in time, such as whether the signals are in phase, anti-phase, uncorrelated, or whether one signal is leading or lagging. See equation 1.4, below.

$$\langle f * g \rangle (n) \overset{\text{def}}{=} \int_{-\infty}^{\infty} f(t)g(t \pm \tau)dt \qquad \text{Equation 1.4}$$

Equation 1.4 – Continuous signal cross-correlation. In the above formula let "f" represent continuously sampled signal 1, let "g" represent continuously sampled signal 2, let "t" represent some time, and let "**τ**" represent some time-lag. The function calculates the integral of two signals (f, g) as "g" slides relative to "f". If the integral sliding dot-product is positive at some time "t", and positive at some time-lag "**τ**", the two continuously sampled signals can be said to be positively correlated. Function described in Diggle, P (1990).

2.8.9 Continuous time-series statistics

Tests of significance were conducted using 95% confidence intervals, such that overlapping confidence intervals, namely the upper bound of one confidence interval is *lower* than the lower bound of another confidence interval and vice

versa, indicate significance (Knezevic, 2008), though overlapping confidence intervals do not always indicate non-significance (Austin, P., Hux, J. 2002). Each confidence interval was calculated according to equation 1.5 below.

$$ci = \bar{X} \pm Z_{\alpha/2} * \frac{\sigma}{\sqrt{N}}$$ Equation 1.5

Equation 1.5 – Confidence Interval Calculation. In the above formula let "ci" represent the upper and lower bound confidence intervals, let $\bar{X}$ represent the sample mean, let Z represent the z-score for the interval, and let σ represent the standard deviation, and N the sample size. Reinhart, A (2015).

2.8.10 Sharp wave-ripple density and K-complex density

Sharp wave-ripple density is the number of sharp wave-ripple events occurring in some interval of time (t). Often, one second, or one minute intervals are chosen, but I chose one minute intervals as I felt this would provide a clearer picture of ripple density as a function of sleep state and sleep bouts were categorized as being no less than 30 seconds in duration. Ripple density was calculated by dividing the total number of ripples within a given trial by the total time, in minutes, of that trial. The same was done for K-complexes.

2.8.11 Cross-Correlation peak-integration ratio analysis

Because overlapping confidence intervals are not *necessarily* non-significant I used a peak-integration ratio analysis to assess the degree to which transient inactivation of nucleus reuniens affects the peak correlation of KC's and SPWR's. For this analysis I calculated the integral of the peak region in the cross-correlogram (± 200ms relative to time zero) as well as a trial-shuffled average region of the same time interval and calculated the ratio between the two integrals; the closer the ratio to 1.0 the lower the correlation between KC's and SPWR's. I predicted that inactivation of reuniens would decrease the ratio close to one indicating a decreased correlation relative to washout and baseline data.

2.9 Histology

Following experimentation, rats were deeply anaesthetized with 150mg/kg Euthansol® via intraperitoneal injection, and transcardially perfused with 0.9% phosphate buffered saline and 4% formalin solution, and the brains were extracted. Following extraction, brains were placed in a 4% formalin solution for a period of 3-7 days, and then into a 30% sucrose solution for an additional week for cryoprotection.

Following fixation, the brains were frozen and sectioned on a cryostat (Leica CM3050) in 40µm sections and mounted. Sections were allowed to air dry for approximately one week before being Nissl stained and cover-slipped.

2.10 Statistical Analyses

All data sets were first tested for normality using the Anderson-Darling normality test. If the data sets passed the Anderson-Darling test One-Way Repeated Measures ANOVAs were used for tests of significance, and 95% confidence intervals were calculated to assess effect size and direction. If the data were found to be significant via the One-Way Repeated Measures ANOVA I then performed a Two-Way ANOVA to investigate whether the source of significance originated in only one animal or across animals and treatments. If data were found to be non-normally distributed the Friedman test was used for tests of significance, and a Bias Corrected and Accelerated Bootstrap confidence interval was used to test for effect size and direction. The Friedman test is a non-parametric statistic used to assess significant differences between two or more non-normal, paired datasets. It is particularly useful in assessing the efficacy of a drug intervention in cross-over studies (McDonald, J.H., 2014),

and is analogous to the One-Way ANOVA. The Bias Corrected and Accelerated Bootstrap confidence interval is a confidence interval applied to a non-normal or skewed distribution, as the classical definition of a confidence interval can only be used on normally distributed data sets (DiCiccio & Efron, 1996). P-values are useful for statistical significance, but confidence intervals provide additional information over and above that of the p-value (Reinhart, 2015). All statistical analyses were conducted using MATLAB® and GraphPad Prism6®.

Chapter Three - *Results*

3.0 Results

The objective of this study was to test the effect of transiently inactivating nucleus reuniens on the correlation and coordination of hippocampal sharp wave-ripples and neocortical K-complexes. All animals were naïve at the time of experimentation and their only exposures to novel environments and stimuli were in the first days of habituation. The following sections describe the results of the metrics used to assess the degree to which transient inactivation of nucleus reuniens affects the coordination of sharp wave-ripples and K-complexes in-vivo.

3.1 K-complex and Sharp wave-ripple detection

In order to assess the effect of transiently inactivating nucleus reuniens on hippocampo-cortical communication, I first detected and timestamped cortical K-complexes and hippocampal sharp wave-ripples using an automated thresholding detection algorithm as described in *Methods 2.8.3 & 2.8.4*. Figure 15 (a-d) below illustrates a 10 second trace of raw and filtered mPFC and hippocampal local field potential activity and the corresponding KCs (red asterisks) and SPWRs (blue asterisks) respectively.
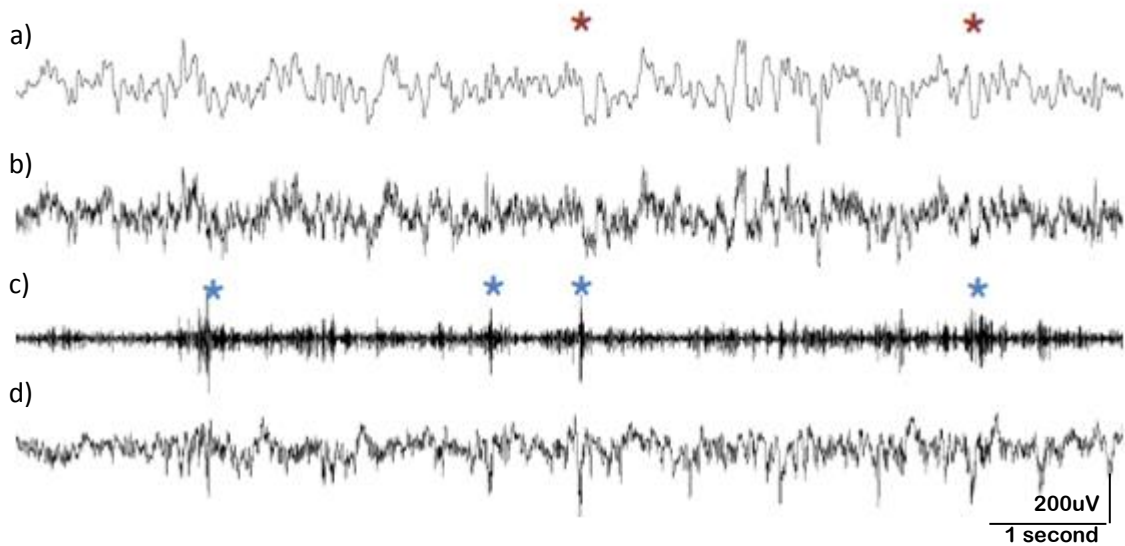
Figure 15. Ten second raw and filtered mPFC and hippocampal local field potential traces depicting detected K-complexes and sharp wave-ripples. In the figure above **(a)** represents the mPFC local field potential filtered for K-complexes (2-6Hz), and **(b)** represents the raw unfiltered mPFC trace. **(c)** Represents the hippocampal local field potential filtered for ripples (100-300Hz), and **(d)** represents the unfiltered hippocampal trace. Note, the red star represents K-Complex/Delta wave events, whilst the blue stars represent detected sharp wave-ripple events. Also of note, one can see in the above figures that SPWRs tend to precede KCs.

3.2 Sharp wave-ripple vs. K-complex cross-correlation

Once I had collected and time-stamped K-complexes and sharp wave-ripples for baseline, drug, and washout trials I then used the discrete cross-correlation to determine whether the two stochastic events, KCs and SPWRs, were correlated with one another in time. The cross-correlation is typically used to study the temporal dynamics of ensemble action potential

69

activity but can also be used to study the temporal dynamics of other discrete electrophysiological phenomena such as K-complexes and sharpwave ripples. In a previous study (Peyrache et al., 2011) it was found that hippocampal sharpwave ripples tended to precede cortical K-complex activity, and I observed the same phenonmenon; hippocampal sharpwave ripples tended to precede neocortical K-complexes by approximately 100-200ms, as illustrated in figure 16 below.

a)   aCSF Baseline: SPWR vs. KC Cross-correlogram
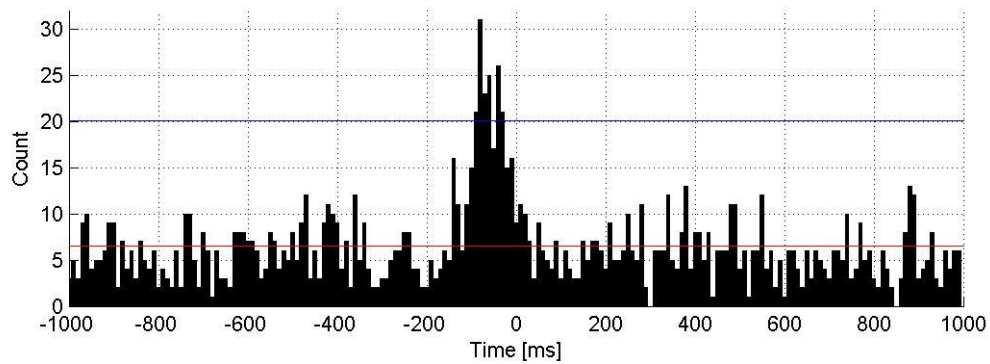
b)   Gaussian Smoothed SPWR vs. KC Cross-correlogram
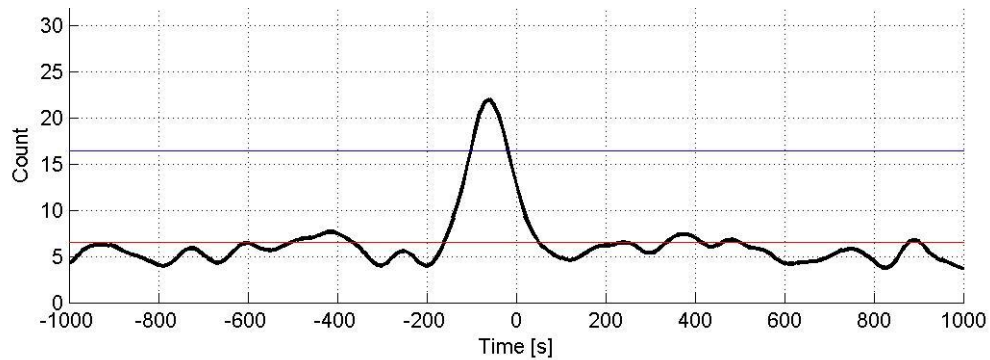
Figure 16. Sample hippocampal sharp wave-ripple vs. Neocortical K-complex cross-correlogram. a) Sample cross-correlogram between K-complexes and sharp wave-ripple events under aCSF baseline conditions. **b)** Gaussian kernel smoothed plot of the graph in **(a).** The blue horizontal lines in a & b represents 3-standard deviations above the mean, and the red horizontal lines in a & b represents the mean of the dataset.

Note, the peak in figure 16 a&b is 3 standard deviations above the expected mean value from the trial shuffled average indicating a significant correlation between K-complexes and sharp wave-ripples. Following aCSF baseline trials I dialyzed 74mM lidocaine hydrochloride into nucleus

reuniens. The results of those inactivation studies are described below.

I found that dialyzing 74mM lidocaine into nucleus reuniens did not affect the cross-correlation of KCs and SPWRs in any of the four animals as depicted in supplementary figures S1-4. To assess differences between baseline and lidocaine interventions I calculated 95% confidence intervals for each data point in the cross-correlogram for each trial. *Non-overlapping* confidence intervals between interventions indicate the population mean for each data point is significantly different whereas overlapping confidence intervals indicate no significant difference. It can be seen in figure 17 that there are overlapping confidence intervals for each data point *indicating* no effect of transient inactivation of nucleus reuniens on K-complex and sharp wave-ripple correlations. In figure 17 the blue dots indicate the aggregate mean of the aCSF baseline trials for each bin and, likewise, the red dots indicate the aggregate mean of each bin for lidocaine interventions. The dashed lines represent 95% confidence intervals. The baseline and lidocaine cross-correlograms calculated for each animal are summarized below.

a) Animal# 150223: Baseline vs. Lidocaine
K-Complex vs. SPWR Cross-correlogram

b) Animal# 150224 Baseline vs. Lidocaine
K-Complex vs. SPWR Cross-correlogram

c) Animal# 150225 Baseline vs. Lidocaine
K-Complex vs. SPWR Cross-correlogram

d) Animal# 150740 Baseline vs. Lidocaine
K-Complex vs. SPWR Cross-correlogram
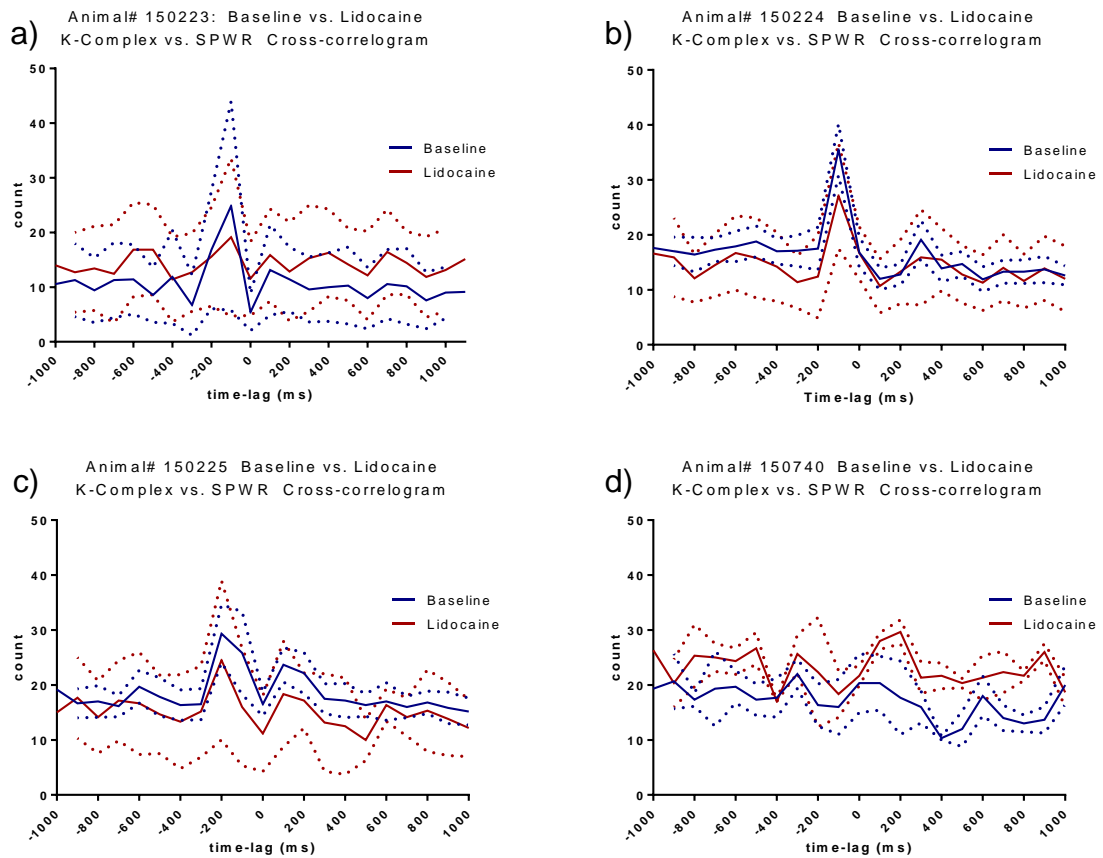
Figure 17. Baseline vs. Lidocaine: KC vs. SPWR Cross-Correlogram Animal summary. The blue solid lines in each sub-figure represent the baseline mean value, whereas the red solid lines represent the mean of the lidocaine data. The dotted lines for each subfigure represent 95% confidence intervals. Note, for each animal the confidence intervals for the baseline and lidocaine data are overlapping. The data for animal# 150223 (a) were derived from 7 trials, the data for animal #150224 (b) were derived from 10 trials, the data for animal #150225 (c) were derived from 6 trials, and the data for animal #150740 (d) were derived from 3 trials. The washout data were not included in these figures for clarity.

Because overlapping confidence intervals do not necessarily indicate non-significance, I performed a Two-Way Repeated

Measures ANOVA on each data point, illustrated in figure 21, between -1000ms and +1000ms, with a Sidak multiple-comparisons family-wise error rate correction. Between Baseline and Lidocaine interventions, significant differences were only observed in Animal# 150225 at a time-lag of -100ms, which is also the time-lag for peak correlations between KC's and SPWR's (mean-difference = -9.833; CI=[-19.41 -0.2564]; p=0.0388. The significant effect of lidocaine on the KC vs. SPWR cross correlations in Animal# 150225 was likely due to a lapse of time rather than intervention because the effect did not wash-out, and the largest and most significant difference was observed between Baseline and Washout trials. The results of these tests for all animals are summarized in figure 18.
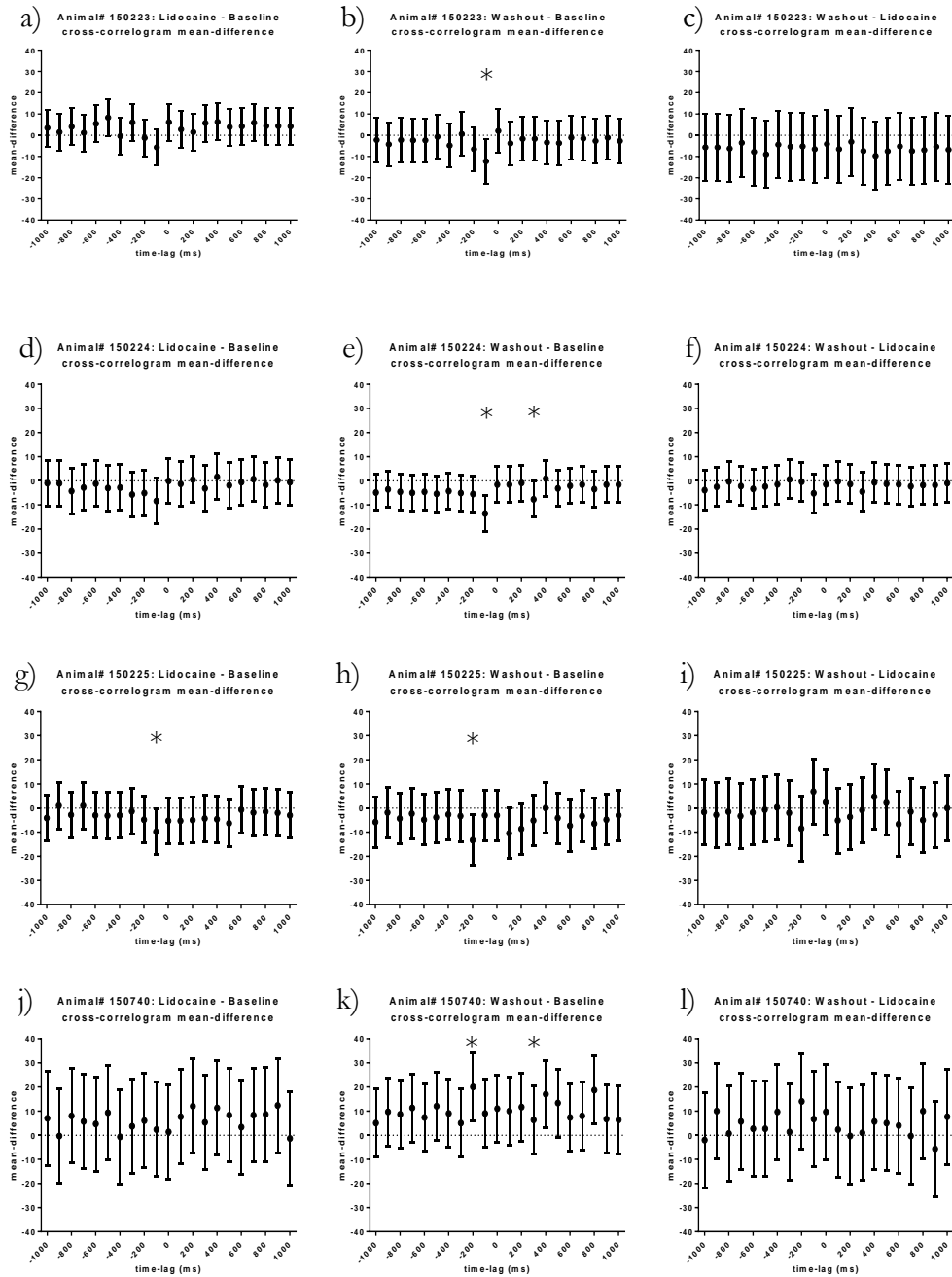
Figure 18. K-Complex vs. Sharp Wave-ripple Cross-correlation mean-difference summary. The above figure illustrates animal summaries for the KC vs. SPWP cross-correlogram mean-difference. Error bars are 95% confidence intervals. Graphs a-c correspond to animal# 150223, graphs d-f correspond to animal# 150224, graphs g-i correspond to animal# 150225, and graphs j-l correspond to animal# 150740. Confidence intervals not overlapping zero are necessarily significant.

Additionally, I performed a cross-correlation peak integration ratio analysis as described in section 2.8.11. The results are summarized in figure 19. Generally, I found no significant effect of intervention on the peak-integral ratios $F(2,44)=0.9841$; $p=0.3819$. Though, upon closer analysis I discovered that animal# 150223 showed a significant difference between baseline and washout interventions in the peak-integral ratio analysis using a Two-Way repeated measures ANOVA with a Tukey multiple-comparisons correction (Mean-diff. = -.4681; CI = [-8.959 - 0.04029]), $p=0.0291$; N=6 trials. For the remaining three animals none showed any significant effect of drug on the peak-integral ratio using the Two-Way repeated measures ANOVA. Animal# 150224 showed no significant differences between each intervention at the $p<.05$ level [$F(1.323, 7.938) = 1.224$, $p=0.3201$]; N=7 trials. Animal# 150740 also showed no significant differences between each intervention at the $p<.05$ level [$F(1.262,2.524)=0.2517$, $p=0.2517$]. N=3 trials. Animal# 150224 showed a trending but non-significant effect between each intervention at the $p<.05$ level [$F(1.430, 12.87)=1.620$, $p=0.233$]; N=10 trials. These results are illustrated in figure 19.
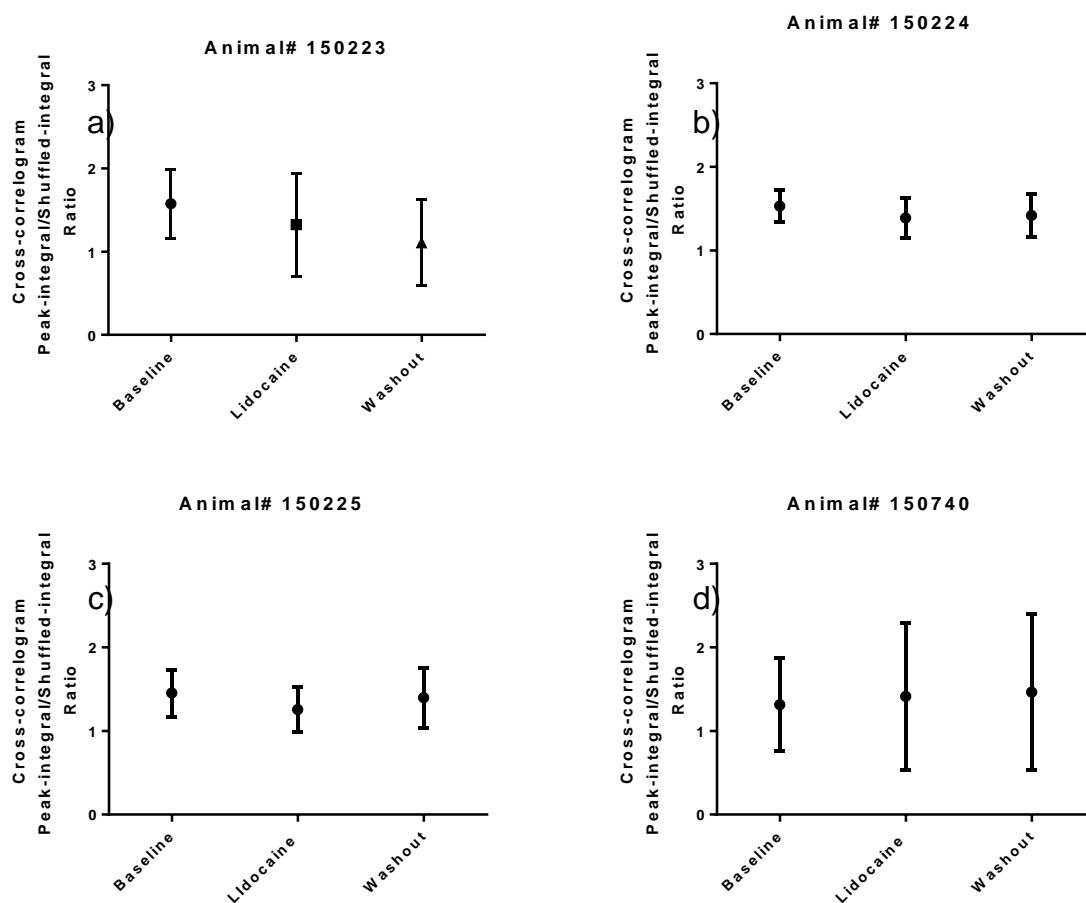
Figure 19. Animal Summary for the peak-integral/shuffled-integral ratio. The above figure depicts the effect of reuniens inactivation on the peak-integral/shuffled-integral ratio calculated for each animal. For animal# 150223 $F_{(1.323, 7.938)} = 1.224$, p=0.3201. N=7 trials. For animal# 150224 $F_{(1.430, 12.87)} = 1.620$, p=0.2333; N=10 trials. For animal# 150225 a significant difference was observed at $\alpha=0.05$ such that $F_{(1.951, 9.753)} = 5.217$, p=0.0294; N=6 trials. For animal# 150740 $F_{(1.262, 2.524)} = 0.2517$, p=0.7067; N=3 trials. All data were assessed at $\alpha=0.05$ significance level. Error bars represent 95% confidence intervals.

Following analysis of the peak-integral ratios using the One-Way repeated measures ANOVA I assessed significance using a Two-Way repeated measures ANOVA and found the only significant result to be from Animal# 150223 between the baseline and washout periods (Mean-diff. = -.4681; CI = [-8.959 -0.04029] p=0.0291; N=6 trials. These data are summarized in figure 20 below.

Peak-integral cross-correlation ratio mean-difference
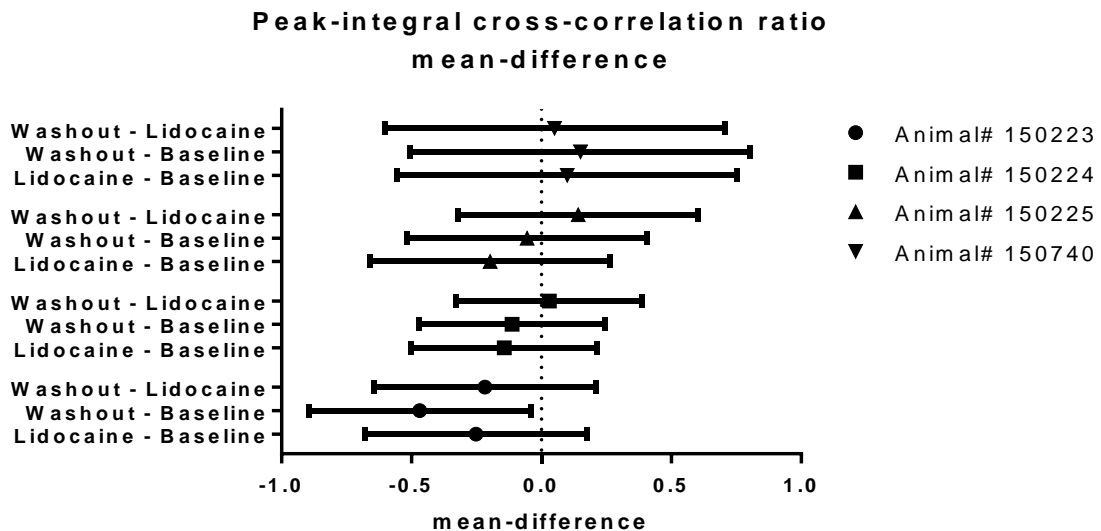
Figure 20. Peak-integral cross-correlation ratio mean-difference animal summary. The above figure depicts the animal summary for the mean-difference cross-correlation peak integral ratio analysis. Note, the only significant result was observed in animal# 150223 between the baseline and washout periods (Mean-diff. = -.4681; CI = [-8.959 - 0.04029]), p=0.0291; N=6 trials. All data were assessed at α=0.05 significance level. Error bars are 95% confidence intervals. Any confidence interval not overlapping a mean-difference of zero is necessarily significant.

3.3 Ripple envelope vs. mPFC signal cross-correlation

Because the discrete cross correlation relies on discrete time-stamped data points with which to calculate correlations, some events can be missed with an automatic detection algorithm if the discrete signals don't meet certain criteria. So I then sought to investigate whether there was an effect of nucleus reuniens inactivation on the correlation between the hippocampal ripple envelope and the mPFC local field potential signal. I utilized a continuously sampled cross-correlation analysis between mPFC local field potential activity and the ripple envelope of the hippocampus. The sharp wave-ripple envelope is a continuously sampled time-series data set derived from the hippocampal local field potential as describe in *Methods: Section 2.8.7.* Signal cross-correlations provide insight into the gross temporal coordination of continuously sampled time-series data. In other words, the signal cross-correlation allows one to examine the degree to which two signals are correlated over time, rather than stochastic events which only provide information about time-lags. Figure 21 illustrates the signal cross-correlations calculated from mPFC local field potential and hippocampal ripple activity. The continuously sampled signals are triggered off of the K-complex at time t=0.
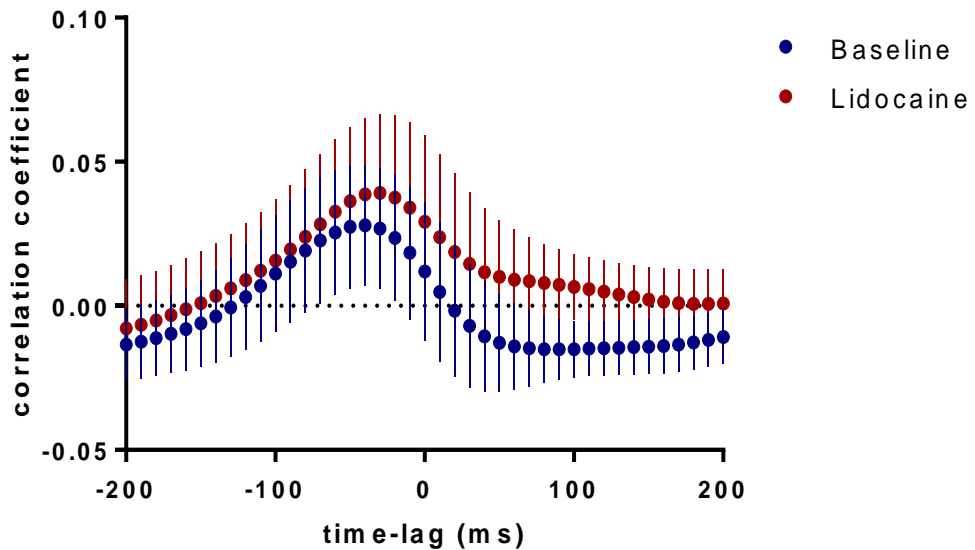
Figure 21. Group Data: mPFC local field vs. hippocampal ripple-envelope cross-correlation. The above figure illustrates the continuous cross-correlation between the mPFC local field and the hippocampal ripple-envelope. The blue dots and vertical lines represent the aCSF baseline average cross-correlation, and 95% confidence intervals respectively. The red dots and vertical lines represent 74mM lidocaine intervention average cross-correlation, and 95% confidence intervals respectively. Of note is the peak correlation coefficient immediately preceding the onset of K-complex activity. Notice there are no periods of non-overlapping 95% confidence intervals indicating to us the lack of any significant effect of drug on the cross correlation between mPFC K-complexes and the hippocampal ripple envelope. $\alpha=.05$; N=4 animals.

The peak of the cross-correlation function precedes the onset of K-complex activity by approximately 100ms, in agreement with our observation from the discrete cross-correlation. Furthermore, within 200ms before or after a K-

complex there were no points of significant difference between aCSF baseline and 74mM lidocaine trials as assessed by overlapping 95% confidence intervals. However, as previously stated, non-overlapping confidence intervals are necessarily significant but overlapping confidence intervals are not necessarily non-significant. To assess significance with a greater degree of accuracy I used the One-Way repeated measures ANOVA with a Sidak correction for the family-wise error-rate. For the lidocaine-baseline mean-difference continuous cross-correlation analysis there were no animals that showed any significant effect of lidocaine dialysis in nucleus reuniens at any time-lag. The data are summarized below in figure 22.

a) **Animal# 150223: Lidocaine - Baseline continuous cross-correlation mean-difference**
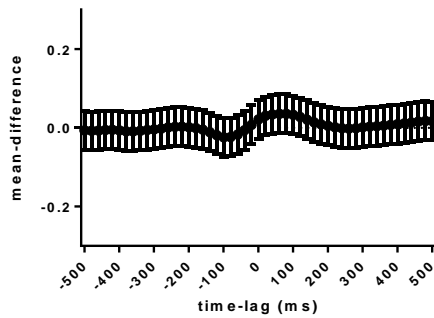
b) **Animal# 150224: Lidocaine - Baseline continuous cross-correlation mean-difference**
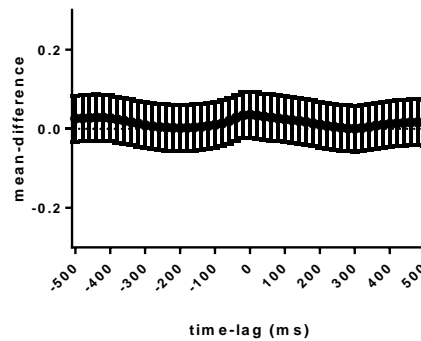
c) **Animal# 150225: Lidocaine - Baseline continuous cross-correlation mean-difference**
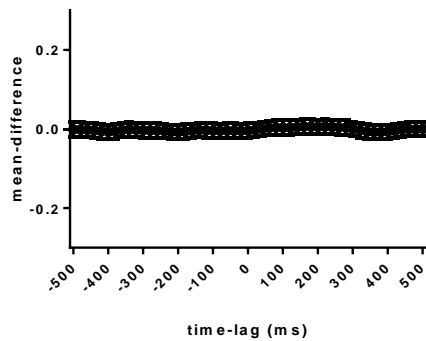
d) **Animal# 150740: Lidocaine - Baseline continuous cross-correlation mean-difference**
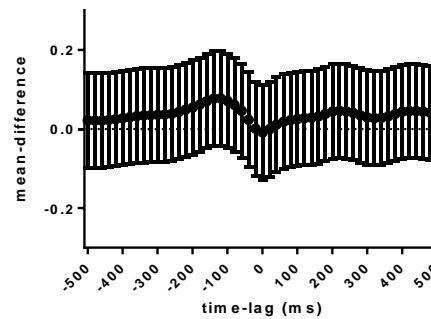
Figure 22. Effect of reuniens inactivation on ripple envelope vs. mPFC LFP continuous cross-correlation mean-difference. The above figure depicts the mean-difference effect of lidocaine dialysis in reuniens on the continuous cross-correlation of the hippocampal ripple envelope with the mPFC LFP. All error bars indicate 95% confidence intervals. Non-zero-overlapping confidence intervals are necessarily significant. Subfigure a) represents the mean-difference cross-correlation for animal# 150223; N=7 trials. Subfigure b) represents the mean-difference cross-correlation for animal# 150224; N=10 trials. Subfigure c) represents the mean-difference cross-correlation for animal# 150225; N=6 trials. Subfigure d) represents the mean-difference cross-correlation for animal# 150740; N=3 trials. Note there are no time-lags for any animal where confidence intervals are not overlapping zero indicating the lack of a significant effect of intervention in any case. Significance was assessed at α=.05 level.

3.4 Effect of reuniens inactivation on percent Non-REM sleep

During experimentation, upon entering the recording room often the animal would briefly stir before returning to sleep. During reuniens inactivation trials however I occasionally observed fewer stirrings from sleep, and given the non-specific thalamus' supposed role in mediating attentive and arousal processes I hypothesized that transiently inactivating nucleus reuniens may be affecting the animal's arousal level. To evaluate this, I calculated the percent of NREM sleep (%NREM) for each trial and for each animal, and assessed the degree to which transient inactivation of nucleus reuniens affects the percent of total sleep time the animal is in NREM sleep.

I first performed an Anderson-Darling test for normality on all %NREM sleep data sets and found that our aCSF baseline measurements were not normally distributed (AD=1.15; p=.004), as well as the 74mM lidocaine data (AD=1.83; p=5.00×10^{-4}), and our aCSF washout data (AD=8.59×10^{-1}; p=.023).

Because our data were non-normally distributed I selected the Friedman non-parametric test to assess significance and did not find any significant effect of nucleus reuniens inactivation on %NREM sleep for any animal. The only

significant result was obtained from animal# 150223 between the lidocaine interventions and the washout interventions (M=40.68 ± 2.131 SEM), p=0.0227. These results are illustrated in figure 23 below.
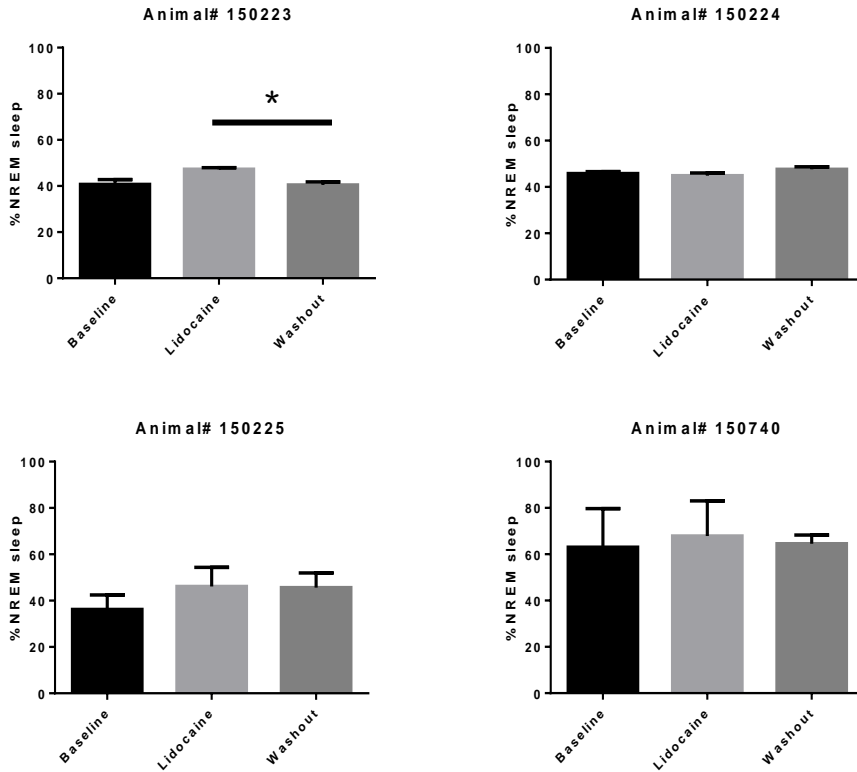
Figure 23. Effect of nucleus reuniens inactivation on %NREM sleep. The above figure illustrates the effect of nucleus reuniens inactivation on %NREM sleep. Error bars represent standard error of the mean. There is a small but significant decrease in %NREM sleep during washout in animal# 150223 compared to the lidocaine interventions (p<.05). Significance was assessed at α=.05.

3.5 Effect of reuniens inactivation on SPWR density

I first performed an Anderson-Darling test for normality on all SPWR density data sets and found that our aCSF baseline SPWR density measurements were normally distributed (AD = 6.32×10^{-2}; p=.887), as were our drug intervention data (AD = 1.84×10^{-1}; p=.913), and aCSF washout data (AD = 2.12×10^{-1}; p=.844). I then applied a mean-difference cross-over confidence interval analysis and found there was a significant effect of intervention on ripple density for animal# 150223 (M=2.931 ripples/min; CI= [0.7479, 5.113] ripples/min) as confidence intervals did not overlap zero for the 74mM lidocaine vs. aCSF baseline comparison group, p=0.0059. Furthermore, the aCSF Baseline vs. aCSF Washout comparison had confidence intervals overlapping zero indicating no significance, and the 74mM Lidocaine vs. aCSF Washout comparison group had confidence intervals that did not overlap with zero (M=-4.256 ripples/min; CI= [-6.439 - 2.073], thus indicating a significant effect of washout p<0.0001. All other animals exhibited non-significant effects of intervention. These data are illustrated in figure 24 below.
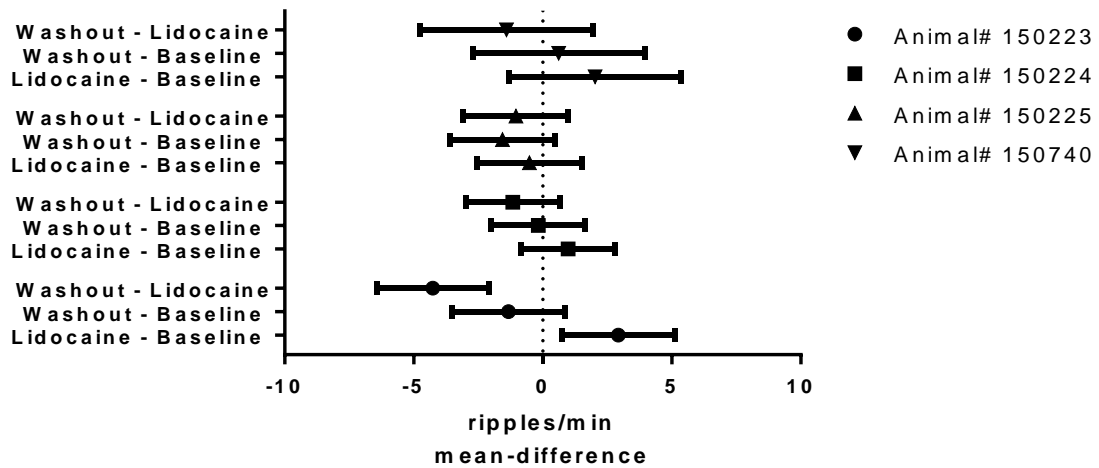
Figure 24. 74mM lidocaine vs. aCSF baseline SPWR density mean-difference. The above figure illustrates the SPWR density mean-difference for each intervention for each animal. Error bars represent 95% confidence intervals. Note the confidence intervals that do not overlap zero indicate a significant effect of intervention. The only interventions that yielded significant results were from animal# 150223 between baseline and lidocaine interventions (p=0.0059), and between washout and lidocaine interventions (p<0.0001), as depicted by the non-zero-overlapping confidence intervals. Significance was assessed at α=.05 for all animals.

I then applied a Two-Way repeated measure ANOVA to test for significant differences between each group because the mean-difference cross-over analysis indicated a significant positive effect of lidocaine on SPWR density for animal# 150223. For animal# 150223 the baseline ripple density was 18.02±0.67 ripples/minute. Following delivery of 74mM lidocaine hydrochloride the average ripple density increased

to 20.59±0.73 ripples/minute, and then subsequently dropped

to 16.70±0.46 ripples/minute during aCSF washout. A

significant p-value was calculated between treatment

conditions $F(1.442, 8.651) = 9.371$; $p=0.0098$. All other

animals showed non-significant effects of intervention. The

results are illustrated in figure 25.
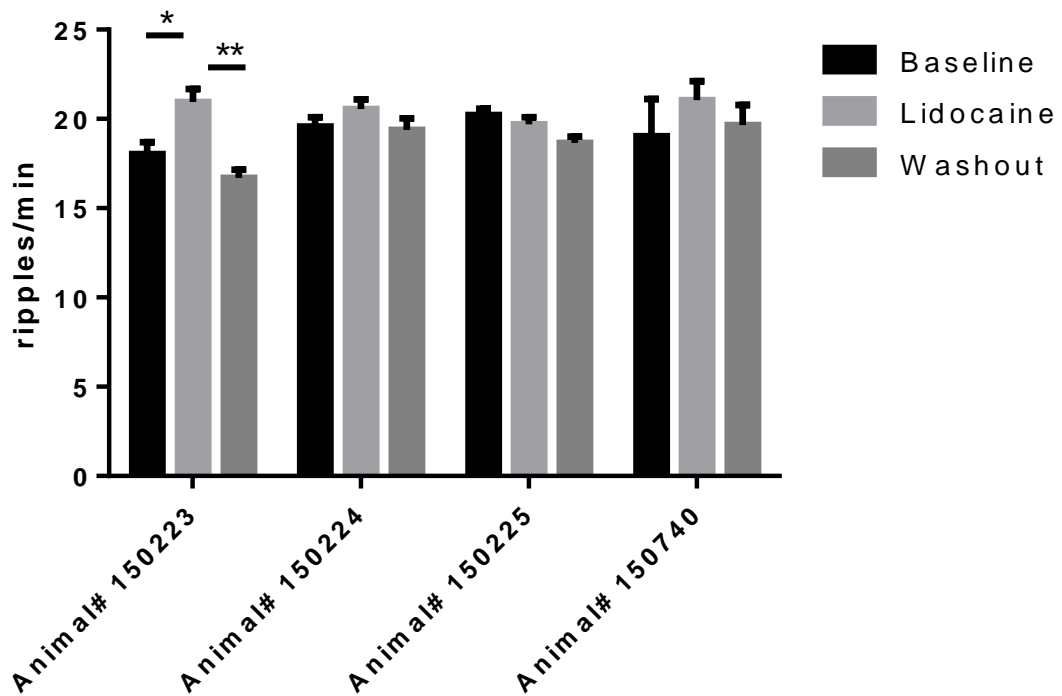
Figure 29. Effect of transient inactivation of nucleus reuniens on sharp wave-ripple density. The above figure represents the effect of transient nucleus reuniens inactivation on hippocampal sharp wave-ripple density. Note the significant increase in ripple density during 74mm lidocaine inactivation compared to aCSF baseline for animal# 150223, $p=.0059$; N=7 trials. Also, note the return of ripple-density, in animal# 150223, below baseline levels during washout $p<0.0001$. $\alpha=.05$.

3.6 Inter-ripple-interval

I measured the inter-ripple-interval for each trial to provide insight into the temporal dynamics of ripple activity. First I applied an Anderson-Darling test for normality to all data sets and found that our aCSF Baseline (AD=4.07; $p=5.0x10^{-4}$), 74mM lidocaine (AD=$5.89x10^{-1}$; p=.114), and aCSF washout data (AD=2.26; $p=5.00x10^{-4}$) were non-normally distributed, so I selected the Two-Sample Kolmogorov-Smirnov test to assess statistical significance. Figure 26 below illustrates a sample inter-ripple-interval plot for a single trial. To run the Kolmogorov-Smirnov test I log-transformed the inter-ripple-interval data to which I then applied the test.

a)

b)
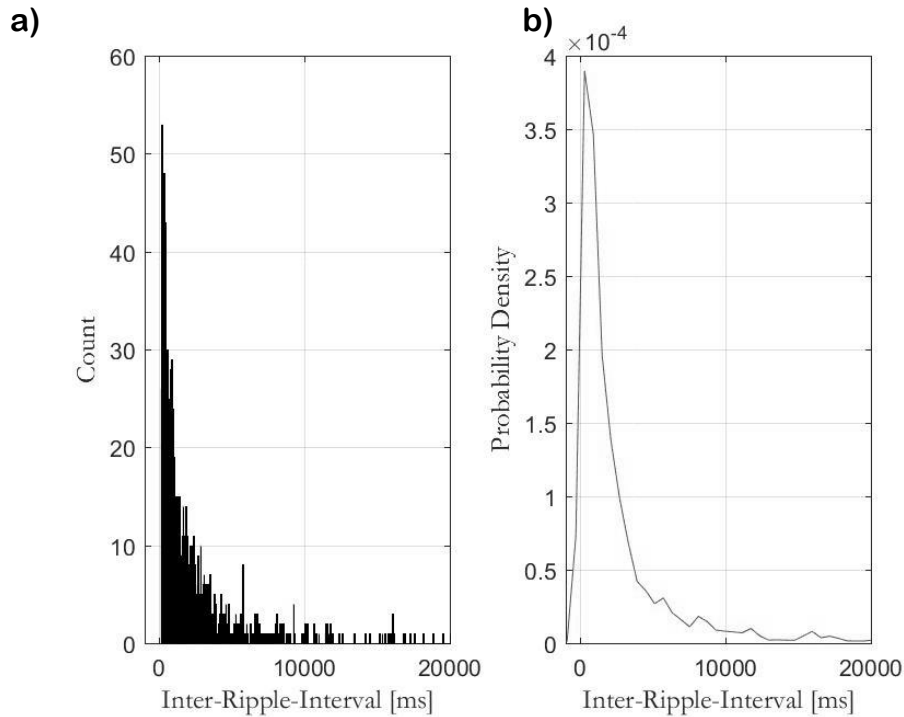
Figure 26. Inter-ripple-interval and Probability density plots. The figure above illustrates **a)** a sample inter-ripple-interval plot and the corresponding **b)** Kernel Smoothed probability density function. Note, the peak IRI probability density indicates that most ripples have an IRI that ranges between 100-2000ms.

The Two-Sample Kolmogorov Smirnov test revealed non-significant increase in the inter-ripple-interval between aCSF baseline and 74mM lidocaine trials in animal# 150223 (K-S=0.017, p=0.9987) and between aCSF baseline and aCSF washout trials (K-S=0.017; p=.9995), and between washout and lidocaine trials (K-S=0.011; p=.999). A total of seven trials were conducted for animal# 150223. For animal# 150224 there were non-significant differences calculated when

89

comparing baseline and lidocaine conditions (K-S=0.009; p=0.999), as well as for comparisons between baseline and washout conditions (K-S=0.009; p=0.999), and also for the comparisons of lidocaine and washout interventions (K-S=0.01; p=0.999). A total of 10 trials were conducted for animal# 150224. For animal# 150225, non-significant differences were calculated for baseline and lidocaine comparisons (K-S=0.013; p=0.999), as well as for the baseline and washout comparisons (K-S=0.010; p=0.999), and for the lidocaine and washout comparisons (K-S=0.020; p=0.9882). A total of 6 trials were conducted for animal# 150225. For animal# 150740, non-significant differences were calculated for all comparisons. For the baseline and lidocaine comparison (K-S=0.009; p=0.999), for the baseline and washout comparisons (K-S=0.0210; p=0.9801), and finally for the lidocaine and washout comparisons (K-S=0.0220; p=0.969). A total of 3 trials were conducted for animal# 150740. These data are illustrated in figure 27 below.
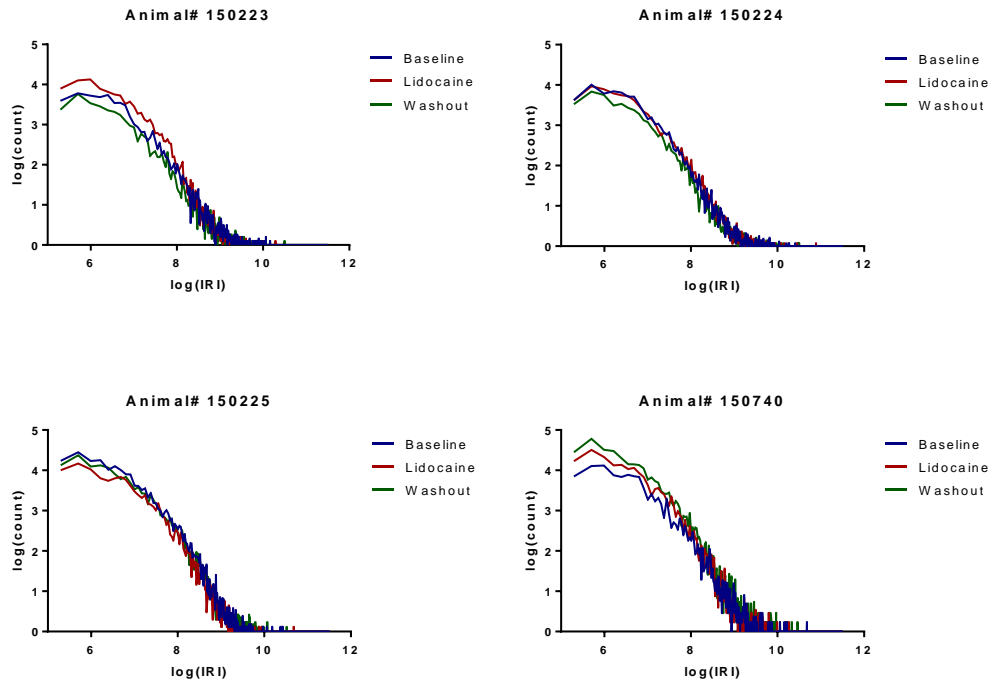
Figure 27. Effect of nucleus reuniens inactivation on inter-ripple-intervals (IRI). The above figure illustrates the effect of nucleus reuniens inactivation on peak IRI. Animal# 150223 was the only animal to exhibit changes in ripple density, and an increase in the log(count) during the lidocaine interventions is clearly visible but statistically non-significant. Significance was assessed at α=.05.

3.7 Effect of reuniens inactivation on K-complex density

I first performed an Anderson-Darling test for normality on all KC density data sets, and found our aCSF baseline KC density measurements were normally distributed (AD = 6.96×10^{-1}; p=.061), as were our 74mM lidocaine intervention data (AD = 5.18×10^{-1}; p=.175), however our aCSF washout data (AD = 1.63; p=.00050) was found to be non-normally

distributed. I then applied a mean-difference cross-over confidence interval analysis and found there was a significant effect of intervention on KC density in animal# 150223 between lidocaine and washout interventions as confidence intervals did not overlap zero (M=-1.201; CI=[-1.903 -0.499]; p=0.0004). All other animals showed no significant effect of intervention. These data are illustrated in figures 27 and 28 below.
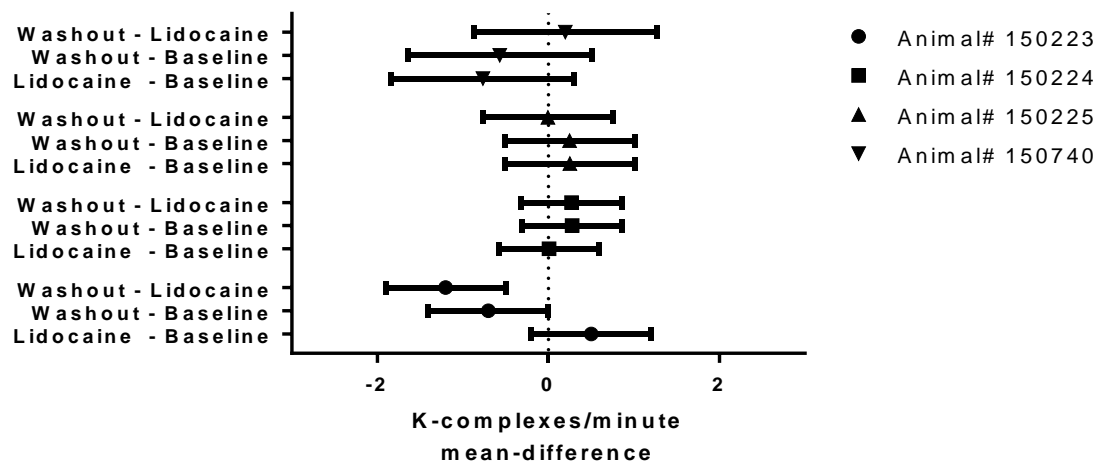
Figure 28. 74mM lidocaine vs. aCSF baseline KC density mean-difference. The above figure illustrates the K-complex density mean-difference. Note, the only significant effect was observed in animal# 150223 between lidocaine and washout interventions (M=-1.201; CI= [-1.903 -0.499]; p=0.0004). The horizontal bars represent 95% confidence intervals. Significance was assessed at α=.05.

I then applied a Two-Way repeated measures ANOVA to test for significant differences between each group. During baseline

aCSF trials the average KC density was 3.80±0.30 KC/minute. Following transient inactivation of nucleus reuniens with 74mM lidocaine hydrochloride the average KC density increased to 3.91±0.26 KC/minute, and then subsequently dropped to 3.71±0.36 KC/minute during aCSF washout. Using the Wilcoxon Signed-Rank test, no significant differences were found between aCSF baseline and 74mM lidocaine inactivation trials, z=-1.41; p=.159, nor between 74mM Lidocaine and aCSF Washout trials, z=.546, p=.585, or between aCSF Baseline and aCSF Washout trials, z=-.191; p=.849 The results are illustrated in figure 29 below.
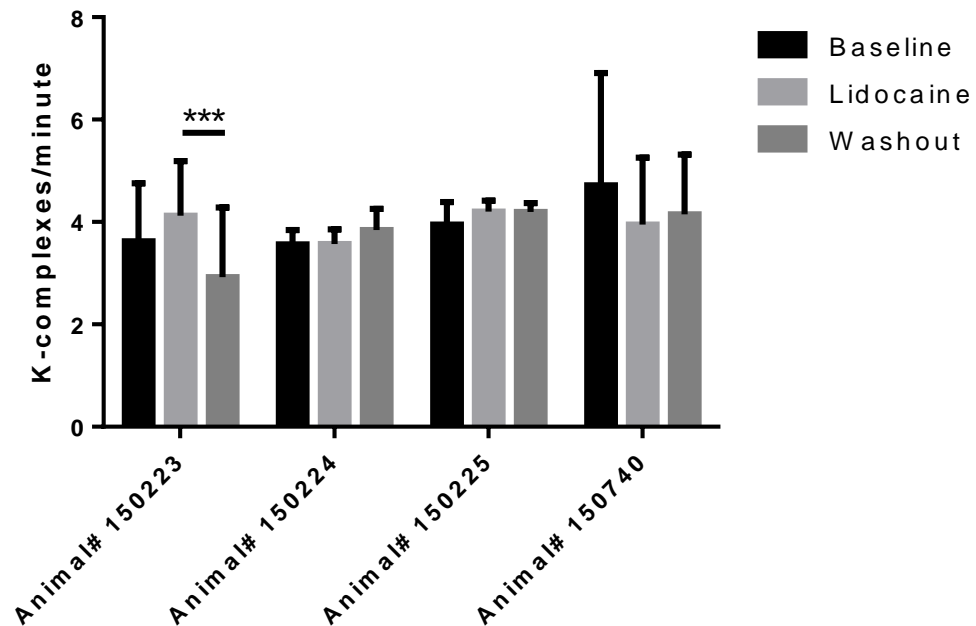
Figure 29. Effect of transient inactivation of nucleus reuniens on KC density in-vivo. The above figure graphically represents the effect of transient nucleus reuniens inactivation on neocortical KC density. Note, no group comparisons were found to be significant (p>.05). α=.05, N=4.

3.8 Histology

Figure 28 a thru c illustrates an example of electrode tip locations in the mPFC (a) and hippocampus (c), and probe location in nucleus reuniens (b). The tissue analyzed from each animal consisted of sections collected from +3.5 and -5.0mm relative to bregma according to the atlas of Paxinos and Watson (2007). The aforementioned range encompasses the lesion sites for the mPFC, NRe, and the hippocampus.

Histological verifications of electrode tip sites were performed using light microscopy. Electrolytic lesions made small holes at the location of the tip and can be visually located during post processing. The electrode and probe tracks can occasionally be visualized if the brain is sectioned exactly in the place of the electrode or probe locations.
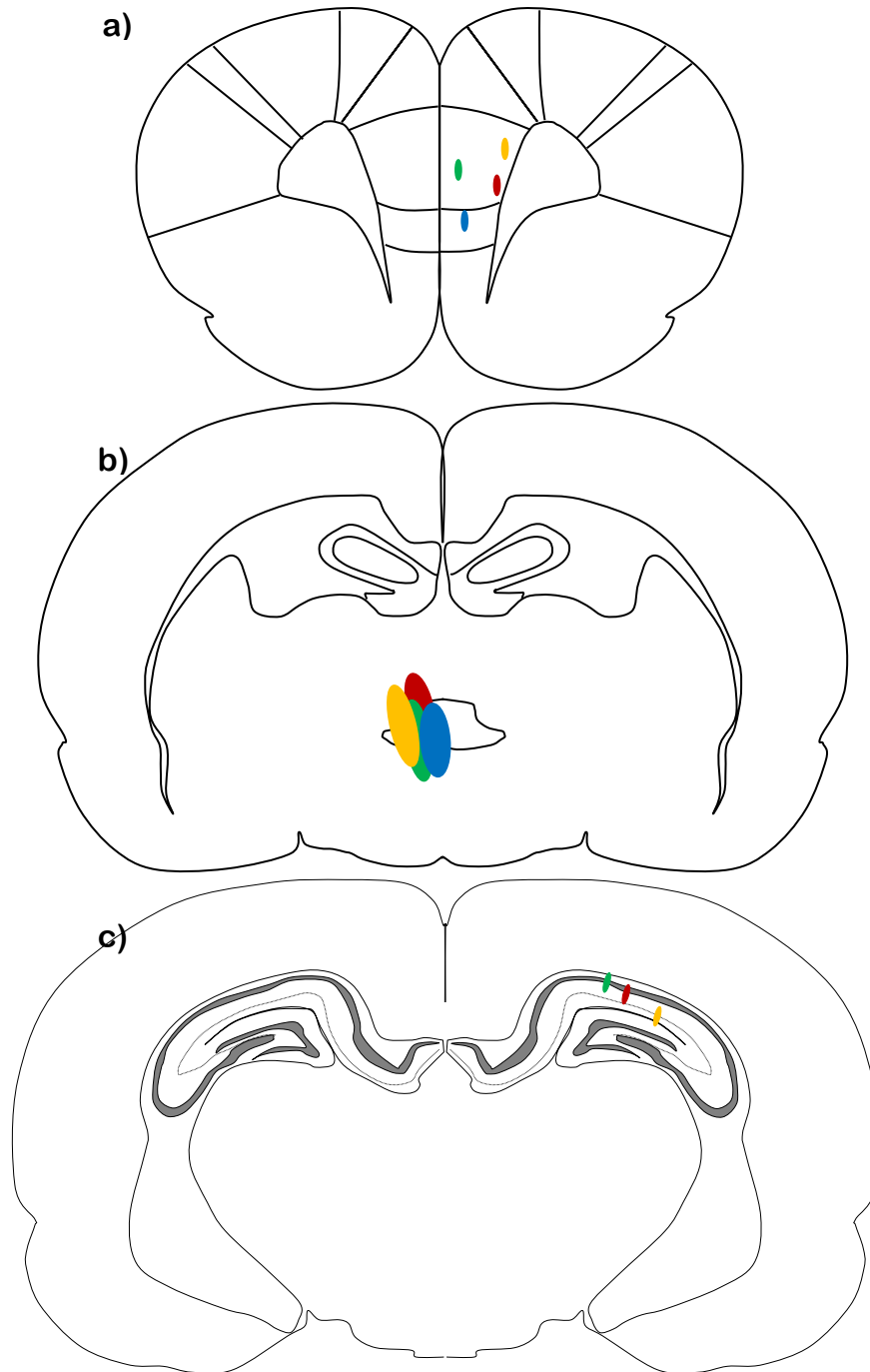
Figure 30. Illustrated histology depicting electrode and probe locations. The figures above depict the electrode locations for mPFC **(a)** and hippocampus **(c)**, as well as probe locations for nucleus reuniens **(b)**. Note, the electrode placement for animal# 150224 in the hippocampus was lost due to a slide defect which caused loss of sections during staining.

The mPFC electrode location varied somewhat from animal to animal but was most often located in the prelimbic cortex. In hippocampus (c) because the lateral electrode tip separation is very minimal it is difficult to distinguish individual tip locations, but generally the lesions indicate accurate placement in the pyramidal layer. Additionally, the probe location in nucleus reuniens (b) indicates accurate placement to successfully inactivate the nucleus. The hypothetical drug spread radius is illustrated in figure 29 below. A previous study (Van Duuren et al., 2007) demonstrated an effective spread of lidocaine using CMA-11 dialysis probes to be approximately 1mm. The grey bar represents the dialysis probe and the blue transparent regions represent 1mm radius of spread. The drug does not spread below the tip because the tip is impermeable.
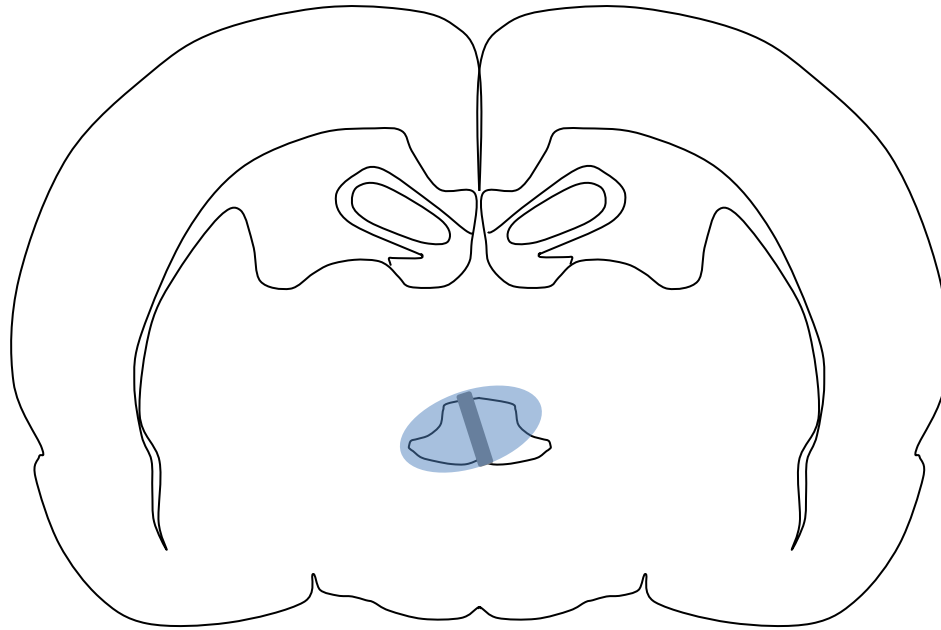
Figure 31. Hypothetical radius of lidocaine spread from CMA-11 microdialysis probe. The above figure illustrates the hypothetical spread of 74mM lidocaine from a CMA-11 dialysis probe. This depiction is based on a previous study (Van Duuren et al., 2007) which demonstrated an effective lidocaine spread of approximately 1mm at its most distal. This indicates that while the drug could potentially spread out of the nucleus its effects would be minimal, affecting reuniens, rhomboid, and peri-reuniens.

This 1mm radius of spread would also inactive most of reuniens as the nucleus spans a A-P distance in rats from approximately -1mm to -4mm. We placed our probe at -1.92mm and so most of reuniens should have been successfully inactivated except for perhaps the most anterior and posterior regions. Additionally, any inter-reuniens connectivity between rostral and caudal regions would likely have been disrupted by the lidocaine infusions.

Chapter Four – *Discussion & Concluding Remarks*

4.0 Discussion

The aim of the current study was to investigate to what extent, if any, transient inactivation of nucleus reuniens affects the correlation of hippocampal sharp wave-ripples and neocortical K-complexes in naïve rats.

We found that:

1. Dialysis of 74mM lidocaine into nucleus reuniens does not seem to affect the correlation of K-complexes and sharp wave-ripples.

2. Dialysis of 74mM lidocaine into nucleus reuniens does not seem to affect sharp wave-ripple density other than a single animal which showed significant effect of lidocaine dialysis with significant washout. However this could have been due to uncontrollable variables.

3. Dialysis of 74mM lidocaine into nucleus reuniens does not seem to affect inter-ripple-intervals. Again the only animal which appeared to show an effect was animal# 105223. Though not significant, the inter-ripple-interval log-transformed curves seem to suggest more ripples occurring with a smaller IRI.

4. Dialysis of 74mM lidocaine into nucleus reuniens does not seem to affect %NREM sleep. Though there was a significant effect observed in the group data this was later found to be due to variability between animals.

5. K-complex density also does not appear to be affected by dialysis of lidocaine into nucleus reuniens.

6. We cannot safely conclude that reuniens was effectively inactivated using 74mM lidocaine. The lack of positive drug effects in all animals leaves the above conclusions exclusively speculative.

Several seminal studies implicating reuniens/rhomboid in learning and memory processes, particularly with respect to consolidation provided the impetus for our study. Memory consolidation is classically regarded as a process involving communication between the hippocampus and mPFC during an offline state like sleep or quiet wakefulness. Consolidation is thought to involve the coordinated interaction of hippocampal sharp wave-ripples and neocortical K-complexes, delta-waves, and spindle oscillations (Siapas et al., 1998; Stickgold, 2001; Johnson et al., 2010; Peyrache et al., 2011; Cox et al., 2012; Backus et al., 2016). Generally

speaking the down-to-upstate transition of the K-complex is believed to allow the neocortex to encode incoming information from hippocampal afferents. The down-state is a short period of time wherein there is no local neocortical neural activity and is thought to provide the neocortex with an opportunity to reactivate "weakly biased attractors" (Johnson et al., 2010). Put another way: the downstate of the K-complex may be a time when the most salient of neocortical attractors, namely those most recently potentiated, will be reactivated. Furthermore, the upstate is believed to be, in part, an excitatory response to the ripple whereby previously active ensembles of neocortical neurons can be reactivated in conjunction with hippocampal inputs. However, it is not yet known how these two oscillations are temporally synchronized. It may be the case that occasionally a SPWR triggers the K-complex; however many KC's are not correlated with ripples. Additionally, nucleus reuniens of the ventral midline thalamus has been suggested to play some key role synchronizing hippocampal ripples and neocortical spindles (Varela, 2014). Though there have not yet been any studies investigating the role of thalamic lesion or inactivation on K-complex generation, it has been suggested that the K-complex may be triggered in

part by disrupted thalamocortical spindling (Mak-McCully et al., 2014) and hence, given reuniens' connectivity with the mPFC a disruption in its ability to generate thalamocortical spindles may also affect K-complex generation in the mPFC.

A previous study (Davoodi et al., 2011) demonstrated that associative learning processes driven by the medial prefrontal cortex are dependent on reuniens activity within a critical window of time immediately post-task. Furthermore, while pre-learning inactivation of nucleus reuniens did not affect task acquisition on a passive avoidance task it did affect memory retention at a 24-hour delay, suggesting some role in memory consolidation processes. Additionally, a 5-minute post-learning inactivation of nucleus reuniens also induced memory deficits at a 24-hour delay. However, deficits were not observed after either 90 or 360 minute post-task inactivations. These results suggested reuniens plays a fundamental role in the initial consolidation of an associative memory. Incidentally, it would seem that this transfer is not *necessarily* an "online" process occurring *while* the animal is performing the task, but occurs between 5 and 90 minutes post-task potentially during sleep or quiet

wakefulness. This suggests a critical window of time between 5 and 90 minutes post-task whereby newly acquired memories are presumably consolidated. This is in line with previous studies demonstrating hippocampal reactivation during post-task sleep (Wilson and McNaughton, 1994).

Additionally, a recent study (Loureiro et al., 2012) investigated how fiber-sparing excitotoxic NMDA lesions of reuniens and rhomboid nucleus affected performance on spatial-memory acquisition and retention on a water maze task in rats. The authors found that lesioning reuniens/rhomboid did not affect task acquisition, in agreement with previous findings (Davoodi et al., 2011), but the lesions did induce significant memory deficits in probe trials at a 25 day delay; as if the animals had never learned the task. The authors hypothesized that reuniens either plays some critical role in long-term memory consolidation by facilitating hippocampo-prefrontal communication, *or* that reuniens in some way facilitates spatial memory retrieval from long-term storage; this was suggested from elevated c-Fos activity during retention tests in unlesioned animals (Louriero et al., 2012). It is

prudent to note that these findings have been replicated but have yet to be fully explained (Cassel et al., 2013).

Hence, I elected to study reuniens during "offline" states when the hippocampal-prefrontal communication believed to underpin memory consolidation occurs.

To study the role of nucleus reuniens inactivation on the correlation of hippocampal sharp wave-ripples and prefrontal K-complexes I utilized a combined reverse microdialysis and in-vivo electrophysiology approach. Reuniens received dialysis of either artificial cerebral spinal fluid or 74mM lidocaine hydrochloride, while I simultaneously recorded hippocampal and mPFC local field potential activity in a naturally sleeping animal.

I time-stamped and binned SPWRs relative to KCs and compiled the data into a cross-correlogram which allowed us to visualize and quantify differences in time-lag and peak correlation between the different treatment groups. I found that SPWRs tended to precede KCs by approximately 100-200ms under aCSF baseline conditions, as has been previously demonstrated (Peyrache et al., 2011). Upon inactivation of

nucleus reuniens with 74mM lidocaine hydrochloride we found that the correlations between SPWRs and KCs did not appear to be affected. For each data point I calculated 95% confidence intervals. I observed overlapping confidence intervals for each data point. Additionally, I used a cross-correlation integral ratio analysis to further assess the degree to which cross-correlogram's were affected by lidocaine dialysis into nucleus reuniens. We observed one positive effect in animal# 150225 however, the lack of an effective positive control to verify reuniens inactivation prevents us from positively concluding that reuniens plays no role in facilitating the coordination of K-complexes and sharp-wave ripples. I then correlated the hippocampal ripple envelope with the mPFC local field potential and found the continuously sampled local field potential cross-correlations were also unaffected by nucleus reuniens inactivation.

Occasionally, I observed fewer stirrings from sleep when I entered the recording room during the lidocaine inactivation trials. I hypothesized that reuniens/rhomboid may have some role in attention and arousal processes and so I chose to investigate this further. I found that lidocaine dialysis of

nucleus reuniens did not seem to definitively affect the percentage of time spent in NREM sleep in all cases but animal# 150223 did seem to exhibit some effect of lidocaine dialysis on %NREM sleep. I believe the lack of effect across animals could be due simply to passage of time rather than strictly intervention, though reuniens is connected to the entire ascending arousal system including the raphe nucleus, the locus coeruleus, among others (Vertes et al., 2006). Furthermore, any effect that reuniens inactivation may have on sleep architecture is likely secondary to passage of time, homeostatic sleep drive, and/or natural variations in the animals' sleep.

In addition to the lack of definitive effect on %NREM sleep I also was not able to definitively conclude that lidocaine dialysis into reuniens affects SPWR density. As was the case with %NREM sleep, animal# 150223 did seem to exhibit some indication of a positive effect, however the increase in ripple density was not definitively correlated with an increase in shorter inter-ripple-intervals, though it does seem to trend in that direction.

A previous dialysis study using 74mM lidocaine and the same type of probe as I used have demonstrated an effective radius of spread of up to 1mm that is comparable to muscimol or TTX (Van Duuren et al., 2007), and so it is reasonable to assume that reuniens was affected by the lidocaine. However, because the lidocaine dialysis did not seem to elicit any definitive effects across animals and metrics, and because there are no known effects of reuniens inactivation on animal behavior or cortical electrophysiological hallmarks, I cannot definitively conclude that reuniens was inactivated, however I also cannot conclude that it was not inactivated, and as such I also cannot conclude that dialysis of 74mM lidocaine into nucleus reuniens affects the correlation of K-complexes and sharp-wave ripples. However, a very recent study has demonstrated that glutamatergic calretinin positive neurons in nucleus reuniens, and in fact across the midline thalamus, are effectively inactivated during the sharp-wave ripple, presumably due to inhibitory innervations from the zona incerta (Lara-Vasquez et al., 2016). Additionally, these glutamatergic calretinin positive neurons were found to increase their firing rate activity immediately after the ripple. These results would suggest that during the ripple reuniens may be specifically

inhibited to prevent the nucleus from interfering with hippocampal projections to cortex, however immediately afterward perhaps reuniens plays a role in generating the upstate.

In light of the results of the current work, and the work of others on nucleus reuniens' role in learning and memory processes (Davoodi et al., 2009; Loureiro et al., 2012; Xu and Sudhof, 2013; Linley et al., 2016) I believe that the primary function of nucleus reuniens is the transfer of information between prefrontal and hippocampal networks during preferentially "online" states. Additionally, given the results of our study, and in light of the recent work of others (Mak-McCully et al., 2014; Lara-Vasquez et al., 2016) I do not believe that reuniens is causally involved in the coordination of K-complexes and ripples. Rather, it may be the case that reuniens is more involved in cortical upstate generation.

4.1 Concluding remarks and future directions

Unfortunately, given the lack of definitive proof that reuniens was effectively inactivated I cannot state with certainty that reuniens does not play some role coordinating

K-complexes and ripples. Though the work of others (Lara-Vasquez et al., 2016) would suggest that reuniens is selectively inhibited during the ripple and likely not causally involved in the coordination of KC's and SPWR's. Future studies investigating reuniens' role in coordinating KC's and SPWR's should utilize a combination of optogenetic neuronal silencing and electrophysiology to verify effective inactivation, and concisely answer the question. Nevertheless an important, and as of yet, unanswered question remains:

Is nucleus reuniens involved in memory consolidation?

In light of recent evidence (Xu and Sudhof, 2013; McNamara et al., 2014; Zimmerman et al., 2016) I propose an amended limbic circuit underpinning learning and memory which considers the role of information saliency as a possible explanation to reuniens' supposed role in memory formation.

Originally, Wei Xu and Thomas Sudhof suggested a limbic circuit for memory specificity and generalization including the medial prefrontal cortex, both prelimbic and infralimbic cortices, the thalamic nucleus reuniens, and CA1 of the hippocampus with a postulated VTA dopaminergic input to hippocampal neurons (Xu and Sudhof, 2013). I propose an

110

amendment to this original circuit description to include the ventral subiculum (VSub), nucleus accumbens (NAc), and the ventral tegmental area (VTA).

In a very recent study (Zimmerman et al., 2016) it was demonstrated that infusions of NMDA into nucleus reuniens enhanced burst firing in VTA dopaminergic neurons. Presumably the infusions of NMDA induced tonic activity in reuniens neurons effectively shifting the nucleus from burst mode to tonic mode, which as previously outlined likely underpins the reliable transfer of a spike message to downstream targets (Sherman, 2001) and was demonstrated to underpin memory specificity in a contextual fear conditioning paradigm (Xu and Sudhof, 2013). Zimmerman proposed a circuit whereby excitatory projections from nucleus reuniens to the ventral subiculum (VSub) of the hippocampal formation activate nucleus accumbens (NAc) which induces bursting in dopaminergic neurons of the ventral tegmental area. Zimmerman also demonstrated that inhibition of infralimbic cortex had the same effect on VTA neurons (increased bursting) as exciting nucleus reuniens tonically with infusions of NMDA. It is important to note: these effects were observed only in infralimbic cortex not prelimbic. Furthermore, it has been demonstrated that

enhanced burst firing of dopaminergic neurons of the VTA via optogenetic stimulation induce greater hippocampal reactivation strength in dCA1 networks (McNamara et al., 2014); reviewed by Ewell and Leutgeb (2014). The enhanced reactivation strength observed by McNamara et al. (2014) was not correlated with increased SPWR activity but rather the accuracy of the reactivated ensemble pattern embedded in the SPWR was enhanced. McNamara et al. (2014) believed that this dopaminergic influence on reactivation strength to be important for assigning reward saliency to hippocampal memory traces.

I believe that reuniens plays an important role relaying saliency information from the prelimbic cortex of the mPFC to the hippocampus via a loop including the ventral subiculum, nucleus accumbens, and ventral tegmental area. The enhancement of hippocampal memory traces with respect to experience saliency could explain the original findings of Xu and Sudhof (2013), whereby tonic activation of nucleus reuniens induced fear-memory specificity through burst activity of dopaminergic VTA neurons. It is possible that the effect of tonic activation of nucleus reuniens is to relay the "saliency signal" to the hippocampus from prefrontal networks thereby indicating that a specific

experience is significant and worth consolidating in high

detail. The amended memory circuit is outlined in figure 33

below.
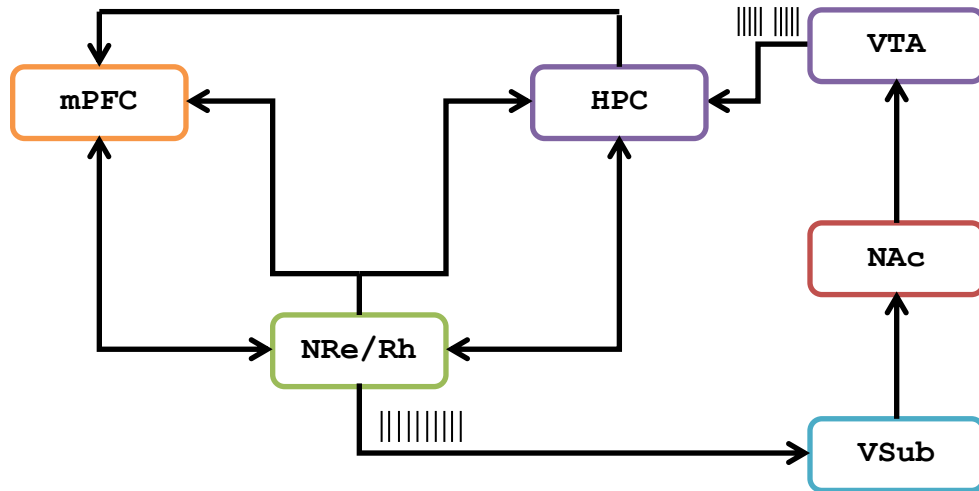
Figure 32. Circuit for memory saliency.

The above figure illustrates a hypothesized limbic circuit
whereby saliency information, encoded by prefrontal
networks, is integrated into hippocampal ensembles via
nucleus reuniens stimulated burst firing in VTA dopaminergic
neurons. This dopaminergic burst firing then attaches a
saliency "tag" to a particular memory trace, indicating its
significance.

Future studies would seek to investigate the role of nucleus

reuniens in modulating dopaminergic release in hippocampal

networks, and the degree to which nucleus reuniens lesions

and inactivation affect hippocampal reactivation strength.

References

Aggleton, J. P., & Brown, M. W. (1999). Episodic memory, amnesia, and the hippocampal-anterior thalamic axis. *Behavioral and brain sciences*, *22*(03), 425-444.

Amzica, F., & Steriade, M. (1997). The K-complex: its slow (< 1-Hz) rhythmicity and relation to delta waves. *Neurology*, *49*(4), 952-959.

Amzica, F., & Steriade, M. (2002). The functional significance of K-complexes. *Sleep medicine reviews*, *6*(2), 139-149.

Backus, A. R., Schoffelen, J. M., Szebényi, S., Hanslmayr, S., & Doeller, C. F. (2016). Hippocampal-prefrontal theta oscillations support memory integration. *Current Biology*, *26*(4), 450-457.

Bastien, C., Campbell, K. (1989). The evoked K-complex: all-or-non phenomenon? *Sleep, 15*(3), 235-245.

Bayer L, Eggermann E, Saint-Mleux B, Machard D, Jones BE, Muhlethaler M, Serafin M (2002) Selective action of orexin (hypocretin) on nonspecific thalamocortical projection neurons. *Journal of Neuroscience, 22*(18), 7835-7839.

Beh HC, Barratt PE. (1965). Discrimination and conditioning during sleep as indicated by the electroencephalogram. *Science*. 147, pp.1470-1471.

Ben-Ari, Y & Gho, M. (1988). Long-lasting modification of the synaptic properties of rat CA3 hippocampal neurones induced by kainic acid. *The Journal of physiology*, *404*, 365.

Benchenane, K., Peyrache, A., Khamassi, M., Tierney, P., Gioanni, Y., Battaglia, F. (2010). Coherent theta oscillations and reorganization of spike timing in the hippocampal-prefrontal network upon learning. *Neuron.* 66:6. pp. 921-936.

Bokor, H., Csaki, A., Kocsis, K., Kiss, K. (2002). Cellular architecture of the nucleus reuniens thalami and its putative aspartergic/glutamatergic projection to the hippocampus and medial septum in the rat. *European Journal of Neuroscience.* 16. pp. 1227-1239.

Braak, H., Braak, E. (1991). Alzheimer's disease affects limbic nuclei of the thalamus. *Acta Neuropathologica.* 81. pp. 261-268.

Buzsáki, G., Haas, H. L., & Anderson, E. G. (1987). Long-term potentiation induced by physiologically relevant stimulus patterns. *Brain research*, *435*(1-2), 331-333.

Buzsáki, G. (2006). *Rhythms of the brain*. Oxford University Press. New York, New York: Oxford University Press.

Cassel, J. C., De Vasconcelos, A. P., Loureiro, M., Cholvin, T., Dalrymple-Alford, J. C., & Vertes, R. P. (2013). The reuniens and rhomboid nuclei: neuroanatomy, electrophysiological characteristics and behavioral implications. *Progress in neurobiology*, *111*, 34-52.

Cavalcante JS, Costa MS, Santee UR, Britto LR. (2005). Retinal projections to the midline and intralaminar nuclei in the common marmoset (*Callithrix jacchus*). *Brain Research. 1043*(1-2), 42-47.

Cavdar, S., Onat, F. Y., Cakmak, Y. O., Yananli, H. R., Gulcebi, M., Aker, R. (2008). The pathways connecting the hippocampal formation, the thalamic reuniens nucleus and the thalamic reticular nucleus in the rat. *Journal of anatomy.* 212:3. pp. 249-256.

Clarke, P., Schwarz, R., Paul, S., Pert, C., Pert, A. (1985). Nicotinic binding in the rat brain: Autoradiographic comparison of [^{3}H]Acetylcholine, [^{3}H]Nictotine, and [^{125}I]-α-Bungarotoxin[1]. *The Journal of Neuroscience, 5*(5), 1307-1315.

Colrain, I.M. (2005). The K-complex: a 7 decade history. *Sleep.* 28(2), pp. 255-273.

Cox, R., Hofman, W. F., & Talamini, L. M. (2012). Involvement of spindles in memory consolidation is slow wave sleep-specific. *Learning & Memory*,*19*(7), 264-267.

Crick, F. (1984). Function of the thalamic reticular complex: the searchlight hypothesis. *Proceedings of the National Academy of Sciences of the United States of America*, *81*(14), 4586–4590.

Crochet, S., Onoe, H., Sakai, K. (2006). A potent non-monoaminergic paradoxical sleep inhibitory system: a reverse microdialysis and single-unit recording study. *European Journal of Neuroscience.* 24. pp. 1404-1412.

Crochet, S., Sakai, K. (1999). Effects of microdialysis application of monoamines on the EEG and behavioural states in the cat mesopontine tegmentum. *European Journal of Neuroscience.* 11. pp. 3738-3752.

Cruikshank, S., Ahmed, O., Stevens, T., Patrick, S., Gonzalez, A., Elmaleh, M., Connors, B. (2012). Thalamic control of layer 1 circuits in prefrontal cortex. *The Journal of Neuroscience.* 32:49. pp. 17813-17823.

Darvesh, A. S., Carroll, R. T., Geldenhuys, W. J., Gudelsky, G. A., Klein, J., Meshul, C. K., & Van der Schyf, C. J. (2011). In vivo brain microdialysis: advances in neuropsychopharmacology and drug discovery. *Expert opinion on drug discovery*, *6*(2), 109-127.

Davoodi, F. G., Motamedi, F., Akbari, E., Ghanbarian E., Jila, B. (2011). Effect of reversible inactivation of reuniens nucleus on memory processing in passive avoidance task. *Behavioural brain research.* 221:1. pp. 1-6.

Davoodi, F. G., Motamedi, F., Akbari, E., Nahdi, N., Akbari, E. (2009). Effect of reversible inactivation of reuniens nucleus on spatial learning and memory in rats using a Morris water maze. *Behavioural brain research, 198*(1), 130-135.

De Boer, E., & Kuyper, P. (1968). Triggered correlation. *IEEE Transactions on Biomedical Engineering*, (3), 169-179.

Di Prisco, G. V., Vertes, R. P. (2006). Excitatory actions of the ventral midline thalamus (rhomboid/reuniens) on the medial prefrontal cortex in the rat. *Synapse.* 60:1. pp. 45-55.

DiCiccio, Thomas J., Efron, Bradley (1996). *Bootstrap confidence intervals. Statistical Science, 11*(3), 189-228.

Diggle, P. (1990). *Time Series:* A biostatistical introduction. Oxford, New York: Oxford University Press.

Dolleman-van der Weel, M. J., Morris, R. G. M., Witter, M. P. (2008). Neurotoxic lesions of the thalamic reuniens or mediodorsal nucleus in rats affect non-mnemonic aspects of watermaze learning. *Brain structure and function.* 213:3. pp. 329-342

Dolleman-Van Der Weel, M. J., Witter, M. P. (1996). Projections from the nucleus reuniens thalami to the entorhinal cortex, hippocampal field CA1, and the subiculum in the rat arise from different populations of neurons. *Journal of comparative neurology.* 364:4. pp. 637-650.

Dolleman-van der Weel, M., Lopes da Silva, F., Witter, M. (1997). Nucleus reuniens thalami modulates activity in the hippocampal field CA1 through excitatory and inhibitory mechanisms. *The Journal of Neuroscience.* 17:14. pp. 5640-5650.

Dolleman-Van der Weel, M., Witter, P. (2000). Nucleus reuniens thalami innervates γ aminobutyric acid positive cells in hippocampal field CA1 of the rat. *Neuroscience Letters.* 278. pp. 145-148.

Drexel, M., Preidt, A., Kirchmair E., Sperk. (2011). Parvalbumin interneurons and calretinin fibers arising from thalamic nucleus reuniens degenerate in the subiculum after kainic acid-induced seizures. *Neuroscience.* 189. pp. 316-329.

Duan, A. R., Varela, C., Zhang, Y., Shen, Y., Xiong, L., Wilson, M. A., & Lisman, J. (2015). Delta frequency optogenetic stimulation of the thalamic nucleus reuniens is sufficient to produce working memory deficits: relevance to schizophrenia. *Biological psychiatry*, 77(12), 1098-1107.

Eichenbaum, H. (2000). A cortical-hippocampal system for declarative memory. *Nature Reviews Neuroscience.* 1, pp. 41-50.

Eleore, L., Lopez-Ramos, J., Guerra-Narbona, R., Delgado-Garcia, J. (2011). Role of reuniens nucleus projections to the medial prefrontal cortex and the hippocampal pyramidal CA1 area in associative learning. *PLoS One.* 6:8. pp. 1-11.

Eschenko, O., Ramadan, W., Mölle, M., Born, J., & Sara, S. J. (2008). Sustained increase in hippocampal sharp wave-ripple activity during slow-wave sleep after learning. *Learning & Memory*, *15*(4), 222–228.

Euston, D., Tatsuno, M., McNaughton, B. (2007). Fast-forward playback of recent memory sequences in prefrontal cortex during sleep. *Science.* 318:5853. pp. 1147-1150.

Evans, B. M. (2003). Sleep, consciousness and the spontaneous and evoked electrical activity of the brain. Is there a cortical integrating mechanism? *Neurophysiologie Clinique/Clinical Neurophysiology*, *33*(1), 1-10.

Ewell, L. A., & Leutgeb, S. (2014). Replay to remember: A boost from dopamine. *Nature neuroscience*, *17*(12), 1629-1631.

Fadel, J., Frederick-Duss, D. (2008). Orexin/hypocretin modulation of the basal forebrain cholinergic system: insights from in vivo microdialysis studies. *Pharmacology, Biochemistry and Behavior.* 90. pp. 156-162.

Forget, D., Morin, C. M., & Bastien, C. H. (2011). The Role of the Spontaneous and Evoked K-Complex in Good-Sleeper Controls and in Individuals with Insomnia. *Sleep*, *34*(9), 1251–1260.

Gasbarri, A. & Pompili, A. (2014). Serotonergic 5-HT7 receptors and cognition. *Reviews in the Neurosciences*, *25*(3), 311-323.

German, D., White III, C., Sparkman, D. (1987). Alzheimer's disease: neurofibrillary tangles in nuclei that project to the cerebral cortex. *Neuroscience.* 21:2. pp. 305-312.

Goaillard, J.-M., & Vincent, P. (2002). Serotonin suppresses the slow afterhyperpolarization in rat intralaminar and midline thalamic neurones by activating 5-HT$_7$ receptors. *The Journal of Physiology*, *541*(Pt 2), 453–465.

Guilding, C., Hughes, A. T. L., & Piggins, H. D. (2010). Circadian oscillators in the epithalamus. *Neuroscience*, *169*(4), 1630–1639.

Guseva, D., Wirth, A., & Ponimaskin, E. (2014). Cellular mechanisms of the 5-HT$_7$ receptor-mediated signaling. *Frontiers in Behavioral Neuroscience*. 8, 306.

Hallock, H., Wang, A., Griffin, A. (2016). Ventral midline thalamus is critical for hippocampal-prefrontal synchrony and spatial working memory. *The Journal of Neuroscience 36*(32), 8372-8389.

Hasselmo, M. E. (2006). The Role of Acetylcholine in Learning and Memory. *Current Opinion in Neurobiology*, *16*(6), 710–715.

Hay, Y.A., Andjelic, S., Badr, S., Bertrand, L. (2012). Orexin-dependent activation of layer IVb enhances cortical network activity and integration of non-specific thalamocortical inputs. *Brain Structure and Function. 220*(6), 3497-3512.

Hembrook, J., Mair, R. G. (2010). Lesions of reuniens and rhomboid thalamic nuclei impair radial maze win-shift performance. *Hippocampus.* 21:8. pp.815-826.

Hembrook, J., Onos, K., Mair, R. (2012). Inactivation of ventral midline thalamus produces selective spatial delayed conditional discrimination impairment in the rat. *Hippocampus.* 22. pp. 853-860.

Herkenham, M. (1978). The connections of the nucleus reuniens thalami: evidence for a direct thalamo-hippocampal pathway in the rat. *The Journal of Comparative Neurology.* 177. pp. 589-610.

Hirayasu, Y. and Wada, J. A. (1992), N-Methyl-D-Aspartate Injection Into the Massa Intermedia Facilitates Development of Limbic Kindling in Rats. *Epilepsia*, *33,* 965–970.

Hoover, W. B., & Vertes, R. P. (2007). Anatomical analysis of afferent projections to the medial prefrontal cortex in the rat. *Brain Structure and Function*, *212*(2), 149-179.

Hoover, W., Vertes, R. (2012). Collateral projections from nucleus reuniens of thalamus to hippocampus and medial prefrontal cortex in the rat: a single and double retrograde fluorescent labeling study. *Brain Structure and Function.* 217. pp. 191-209.

Hocht, C., Opezzo, J. A., & Taira, C. A. (2004). Microdialysis in drug discovery. *Current drug discovery technologies*, *1*(4), 269-285.

Höcht, C., Opezzo, J. A., & Taira, C. A. (2007). Applicability of reverse microdialysis in pharmacological and toxicological studies. *Journal of pharmacological and toxicological methods*, *55*(1), 3-15.

Ito, H. T., Zhang, S. J., Witter, M. P., Moser, E. I., & Moser, M. B. (2013). Trajectory-dependent firing in hippocampal place cells reflects nucleus reuniens-mediated input from the medial prefrontal cortex. In *Soc Neurosci Abstr* (Vol. 39, No. 769.11).

Jay, T. M. and Witter, M. P. (1991), Distribution of hippocampal CA1 and subicular efferents in the prefrontal cortex of the rat studied by means of anterograde transport of *Phaseolus vulgaris*-leucoagglutinin. *The Journal of Computational Neurology, 313*(4), 574–586.

Jay, T. M., Thierry, A.-M., Wiklund, L. and Glowinski, J. (1992), Excitatory Amino Acid Pathway from the Hippocampus to the Prefrontal Cortex. Contribution of AMPA Receptors in Hippocampo-prefrontal Cortex Transmission. *European Journal of Neuroscience*, 4: 1285–1295.

Jay, T. M., Burette, F. and Laroche, S. (1995), NMDA Receptor-dependent Long-term Potentiation in the Hippocampal Afferent Fibre System to the Prefrontal Cortex in the Rat. *European Journal of Neuroscience*, 7: 247–250.

Johnson, L., Euston, D., Tatsuno, M., & McNaughton, B. (2010). Stored-trace reactivation in rat prefrontal cortex is correlated with down-to-up state fluctuation density. *The Journal of Neuroscience: The Official Journal of the Society for Neuroscience*, *30*(7), 2650–2661.

Kim, U., & McCormick, D. A. (1998). The functional influence of burst and tonic firing mode on synaptic interactions in the thalamus. *The Journal of neuroscience*, *18*(22), 9500-9516.

King, C., Henze, D. A., Leinekugel, X., & Buzsáki, G. (1999). Hebbian modification of a hippocampal population pattern in the rat. *The Journal of Physiology*, *521*(1), 159-167.

Knezevic, A. (2008). Overlapping confidence intervals and statistical significance. *StatNews: Cornell University Statistical Consulting Unit*, *73*.

Kudrimoti H.S., Barnes C.A., McNaughton B.L. (1999). Reactivation of hippocampal cell assemblies: effects of behavioral state, experience, and EEG dynamics. *The Journal of Neuroscience, 19*(10), 4090-101.

Lara-Vásquez, A., Espinosa, N., Durán, E., Stockle, M., & Fuentealba, P. (2016). Midline thalamic neurons are differentially engaged during hippocampus network oscillations. *Scientific Reports*, *6*.

Linley, S., Gallo, M., Vertes, R. (2016). Lesions of the ventral midline thalamus produce deficits in reversal learning and attention on an odor texture set shifting task. *Brain Research, 16.*

Loureiro, M., Cholvin, T., Joelle, L., Merienne, N., Latreche, A., Cosquer, B., Geiger, K., Kelche, C., Cassel, J. C., de Vasconcelos, A. P. (2012). The ventral midline thalamus (reuniens and rhomboid nuclei) contributes to the persistence of spatial memory in rats. *Journal of neuroscience.* 32:29. pp. 9947-9959.

Mak-McCully, R. A., Deiss, S. R., Rosen, B. Q., Jung, K. Y., Sejnowski, T. J., Bastuji, H., ... & Halgren, E. (2014). Synchronization of isolated downstates (K-complexes) may be caused by cortically-induced disruption of thalamic spindling. *PLoS Comput Biol*, *10*(9), e1003855.

McDonald D, Schicht W, Frazier R, Shallenberger H, Edwards D. (1975). Studies of information processing in sleep. *Psychophysiology*. (12), pp. 624-9.

McKenna, J. T., Vertes, R. (2004). Afferent projections to nucleus reuniens of the thalamus. *Journal of comparative neurology.* 480:2. pp. 115-142.

McNamara, C. G., Tejero-Cantero, Á., Trouche, S., Campo-Urriza, N., & Dupret, D. (2014). Dopaminergic neurons promote hippocampal reactivation and spatial memory persistence. *Nature neuroscience*, *17*(12), 1658-1660.

Mehta, M. R. (2007). Cortico-hippocampal interaction during up-down states and memory consolidation. *Nature neuroscience*, *10*(1), 13-15.

Monti, M. M., Schnakers, C., Korb, A. S., Bystritsky, A., & Vespa, P. M. (2016). Non-invasive ultrasonic thalamic stimulation in disorders of consciousness after severe brain injury: a first-in-man report. *Brain stimulation*.

Morris, R. G. M., Garrud, P., Rawlins, J. N. P., & O'Keefe, J. (1982). Place navigation impaired in rats with hippocampal lesions. *Nature*, *297*(5868), 681-683.

Nieuwenhuys, R. (1998). Morphogenesis and general structure. In The Central Nervous System of Vertebrates, vol. 1 (ed. Nieuwenhuys Rten Donkelaar HJ, Nicholson C), pp. 158-228. Berlin: Springer.

Nicole, O., Hadzibegovic, S., Gajda, J., Bontempi, B., Bem, T., & Meyrand, P. (2016). Soluble amyloid beta oligomers block the learning-induced increase in hippocampal sharp wave-ripple rate and impair spatial memory formation. *Scientific Reports*, *6*(22728), 1-12.

O'keefe, J., & Nadel, L. (1978). *The hippocampus as a cognitive map*. New York, New York: Oxford University Press.

Oswald, I., Taylor, A., Treisman, M. (1960). Discriminative responses to stimulation during human sleep. *Brain*, *83*(3), 440-453.

Parent, M. A., Wang, L., Su, J., Netoff, T., & Yuan, L.-L. (2010). Identification of the Hippocampal Input to Medial Prefrontal Cortex In Vitro. *Cerebral Cortex (New York, NY)*, *20*(2), 393–403.

Peyrache, A., Battaglia, F. P., & Destexhe, A. (2011). Inhibition recruitment in prefrontal cortex during sleep spindles and gating of hippocampal inputs. *Proceedings of the National Academy of Sciences of the United States of America*, *108*(41), 17207–17212.

Portis, C., Bjorvatn, B., Ursin, R. (2000). Serotonin and the sleep/wake cycle: special emphasis on microdialysis studies. *Progress in Neurobiology.* 60. pp. 13-35.

Prasad, J. A., MacGregor E. M., Chdasama, Y. (2012). Lesions of the thalamic reuniens cause impulsive but not compulsive responses. *Brain structure and function.* 218:1. pp. 85-96.

Quinn, J., Ma QD, Tinsley, M., Koch, C., Fanselow, M. (2008). *Learning and Memory*, *15*(5), 368-72.

Reinhart, A. (2015). *Statistics done wrong:* The woefully complete guide. San Francisco, CA: No Starch Press.

Saalmann, Y. B. (2014). Intralaminar and medial thalamic influence on cortical synchrony, information transmission and cognition. *Frontiers in systems neuroscience*, *8*, 83.

Schwartz, J. R ., & Roth, T. (2008). Neurophysiology of Sleep and Wakefulness: Basic Science and Clinical Implications. *Current Neuropharmacology*, *6*(4), 367–378.

Sherman, S. (2001). Tonic and burst firing: dual modes of thalamocortical relay. *Trends in Neuroscience, 24*(2), 122-126.

Sherman, S. M. (2007). The thalamus is more than just a relay. *Current Opinions in Neurobiology*, *17*(4), 417–422.

Siapas, A. G., & Wilson, M. A. (1998). Coordinated interactions between hippocampal ripples and cortical spindles during slow-wave sleep. *Neuron*,*21*(5), 1123-1128.

Sloan, D., Zhang, D., Bertram III, E. (2011). Increased GABA-ergic inbibition in the midline thalamus affects signaling and seizure spread in the hippocampus-prefrontal cortex pathway. *Epilepsia.* 52:3. pp. 523-530.

Steenland, H.W., Zhuo, M. (2009). Neck electromyography is an effective measure of fear behavior. *Journal of Neuroscience Methods, 15*(177), 355-360.

Steriade, M., McCormick, D., Sejnowski, T. (1993). Thalamocortical oscillations in the sleeping and aroused brain. *Science, 262*(5134), 679-685.

Sutherland, G. R., & McNaughton, B. (2000). Memory trace reactivation in hippocampal and neocortical neuronal ensembles. *Current opinion in neurobiology*, *10*(2), 180-186.

Van Duuren, E., Van der Plasse, G., Van der Blom, R., Joosten, R., Mulder, A., Pennartz, C., Feenstra, M. (2007). Pharmacological manipulation of neuronal ensemble activity by reverse microdialysis in freely moving rats: a comparative study of the effects of tetrodotoxin, lidocaine, and muscimol. *Journal of Pharmacology and Experimental Therapeutics, 323*(1), 61-9.

Varela, C., Kumar, S., Yang, J., Wilson, M. (2013). Anatomical substrate for direct interactions between hippocampus, medial prefrontal cortex, and the thalamic nucleus reuniens. *Brain Structure and Function.*

Varela, C. (2014). Thalamic neuromodulation and its implications for executive networks. *Frontiers in neural circuits*, *8*, 69.

Vertes, R. (2002). Analysis of Projections From the Medial Prefrontal Cortex to the Thalamus in the Rat, With Emphasis on Nucleus Reuniens. *Journal of comparative neurology.* 442:2. pp. 163-187.

Vertes, R. (2006). Interactions among the medial prefrontal cortex, hippocampus and midline thalamus in emotional and cognitive processing in the rat. *Neuroscience.* 142:1. pp. 1-20.

Vertes, R. P., Hoover, W. B., Do Valle, A. C., Sherman, A., Rodriguez, J. J. (2006). Efferent projections of reuniens and rhomboid nuclei of the thalamus in the rat. *Journal of comparative neurology.* 499:5. pp. 768-796.

Vertes, R. P., Hoover, W. B., Szigeti-Buck, K., & Leranth, C. (2007). Nucleus reuniens of the midline thalamus: link between the medial prefrontal cortex and the hippocampus. *Brain research bulletin*, *71*(6), 601-609.

Wilson, M., McNaughton, B. (1994). Reactivation of hippocampal ensemble memories during sleep. *Science.* 265:5172. pp. 676-679.

Wilson, MA., Ji, D. (2007). Coordinated memory replay in the visual cortex and hippocampus during sleep.

Xu, W., Sudhof, T. (2013). A neural circuit for memory specificity and generalization. *Science.* 339, 1290-1295.

Zhang, Y., Yoshida, T., Katz, D., Lisman, J. (2012). NMDAR antagonist action in thalamus imposes delta oscillations on the hippocampus. *Journal of Neurophysiology.* 107, 3181-3189.

Zimmerman, E. C., & Grace, A. A. (2016). The nucleus reuniens of the midline thalamus gates prefrontal-hippocampal modulation of ventral tegmental area dopamine neuron activity. *Journal of Neuroscience*, *36*(34), 8977-8984.

Zola-Morgan, S., Squire, L. R., & Amaral, D. G. (1986). Human amnesia and the medial temporal region: enduring memory impairment following a bilateral lesion limited to field CA1 of the hippocampus. *The Journal of Neuroscience*, *6*(10), 2950-2967.3

Appendix

K-complex vs. Sharp wave-ripple cross-correlation summary.
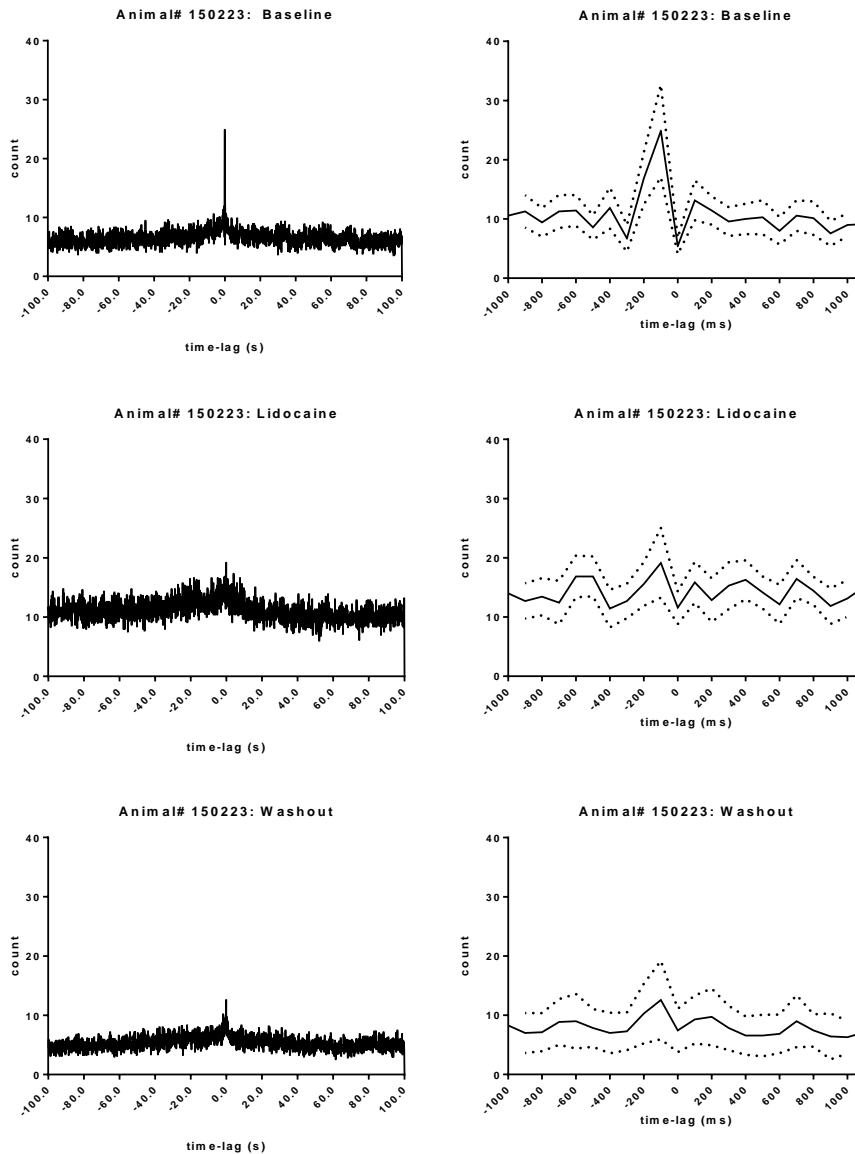
Figure S1. Animal# 150223 KC vs. SPWR cross-correlogram summary. The above figure illustrates the summmary of the KC vs. SPWR cross-correlation for animal# 150223. Note, the correlation decreases from baseline to lidocaine and finally to washout trials. N=7 trials.
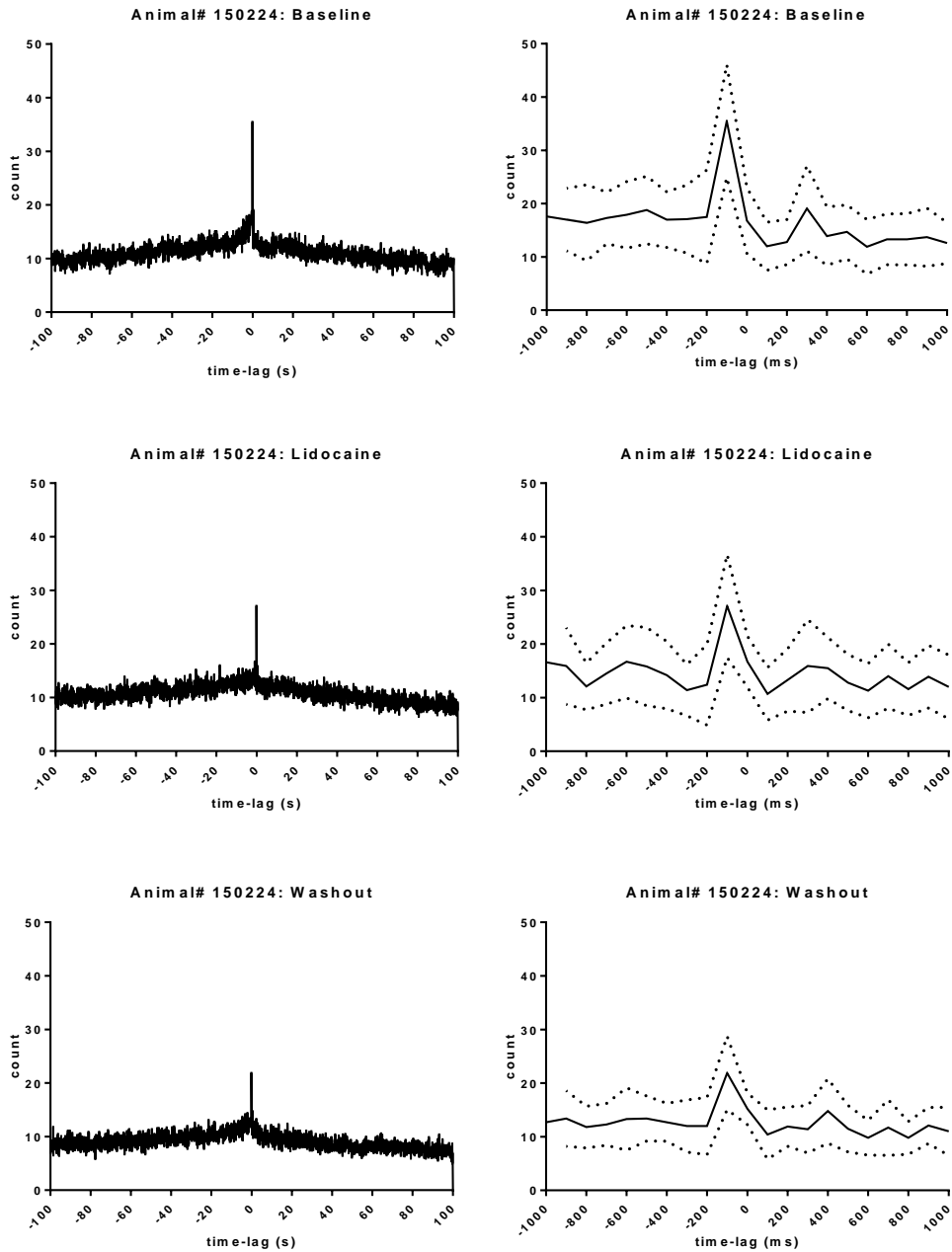
Figure S2. Animal# 150224 KC vs. SPWR cross-correlogram summary. The above figure illustrates the summmary of the KC vs. SPWR cross-correlation for animal# 150224. Note, the correlation decreases from baseline to lidocaine and finally to washout trials. N=10 trials.
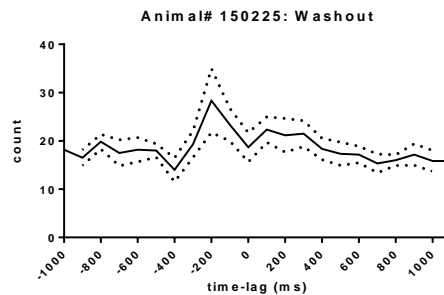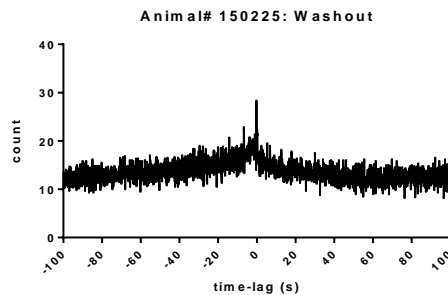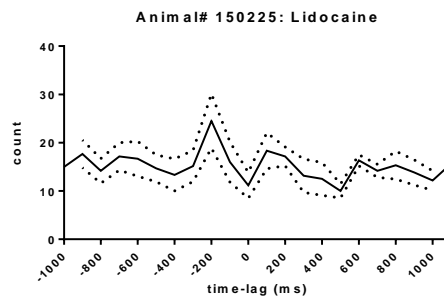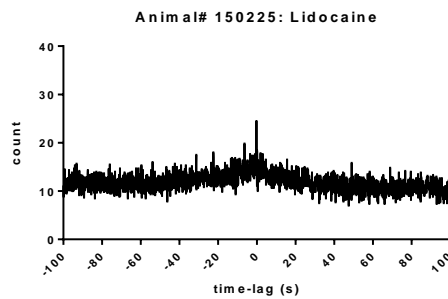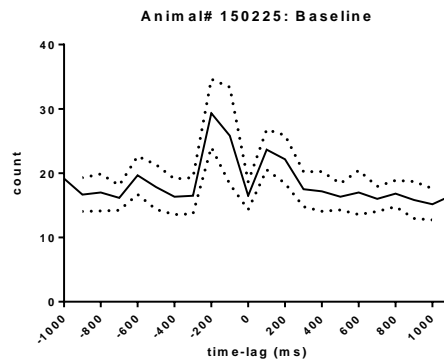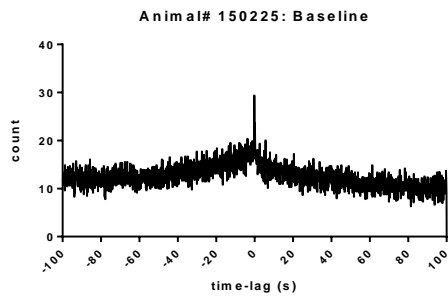
Figure S3. Animal# 150225 KC vs. SPWR cross-correlogram summary. The above figure illustrates the summmary of the KC vs. SPWR cross-correlation for animal# 150225. Note, the correlation decreases from baseline to lidocaine and finally to washout trials. N=6 trials.
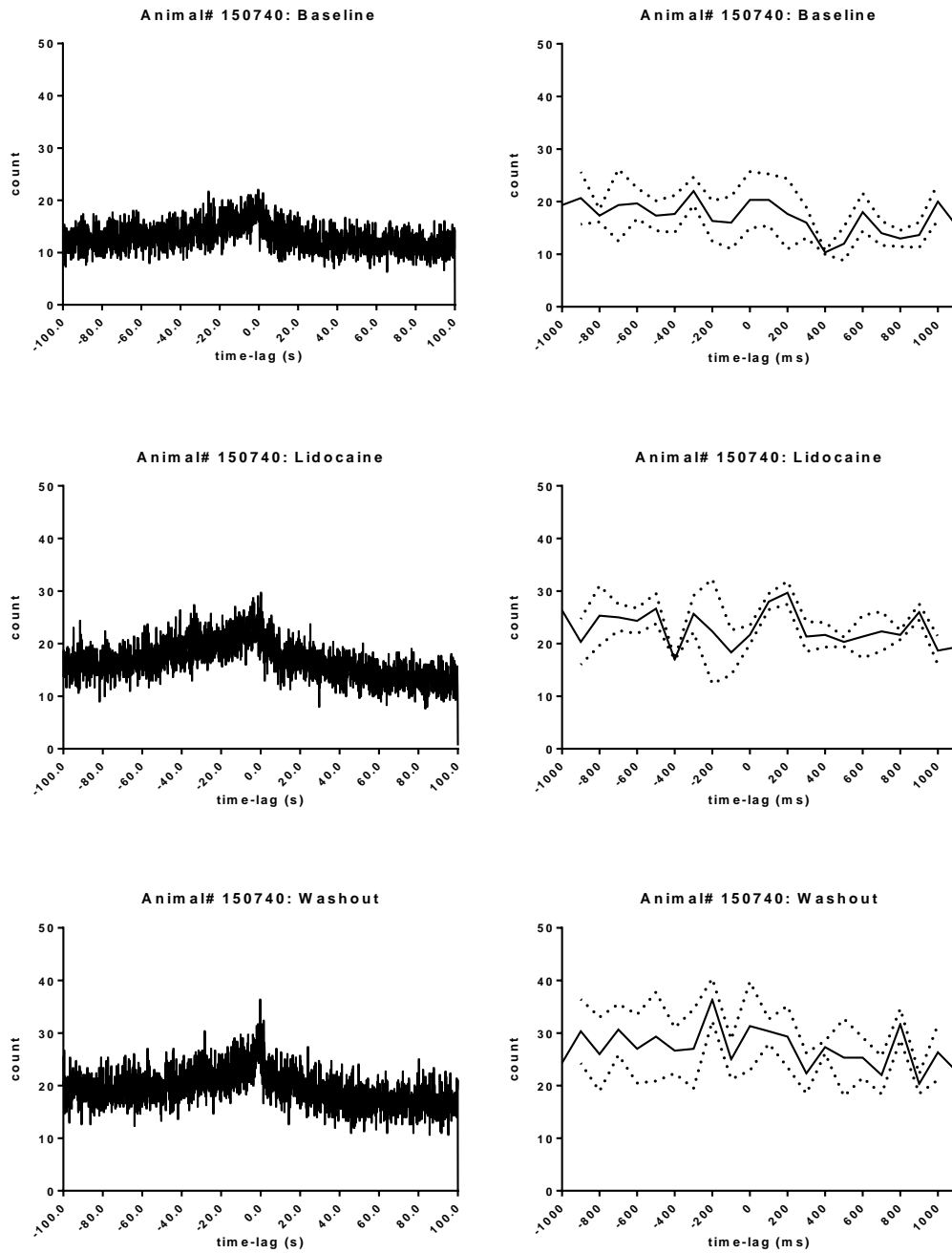
Figure S4. Animal# 150740 KC vs. SPWR cross-correlogram summary. The above figure illustrates the summmary of the KC vs. SPWR cross-correlation for animal# 150740. Note, the correlation decreases from baseline to lidocaine and finally to washout trials. N=3 trials.

Histology:
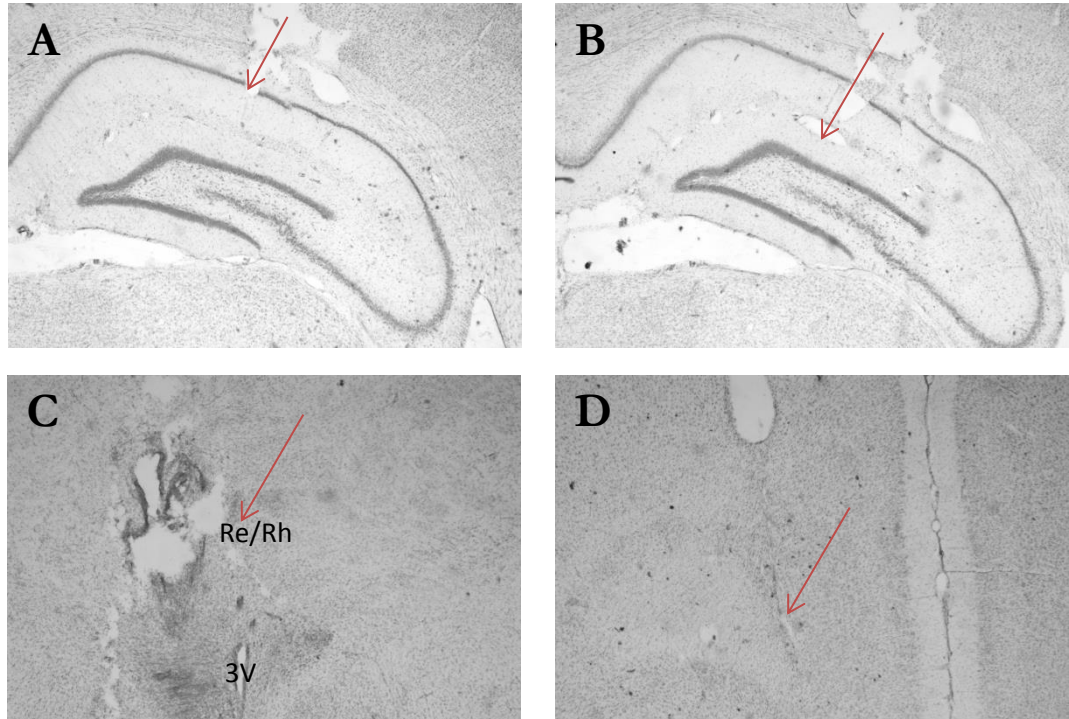
Figure S5. Animal #150225 Lesion marks and electrode tracks. (A) And (B) represent the approximate locations of hippocampal electrodes. We targeted the CA1 pyramidal cell layer as depicted by the lesion in (A), as well as the SLM as depicted by a lesion in (B). (C) Represents the location of the microdialysis probe. It is situated in the right-half of nucleus reuniens and rhomboid nucleus as indicated by the red arrow. (D) Depicts the track for the mPFC local field potential electrode with a small lesion mark indicated by the red arrow
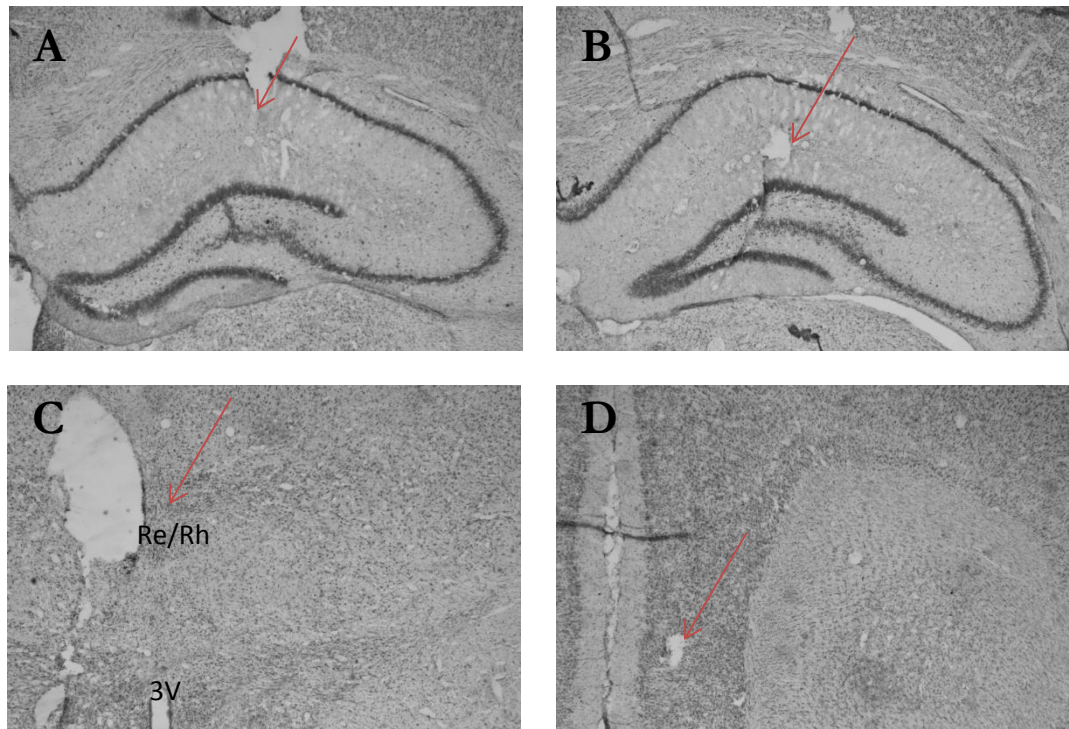
Figure S6. Animal #150223 Lesion marks and electrode tracks. (A) And (B) represent approximate locations of hippocampal electrodes. We targeted the CA1 pyramidal cell layer as depicted by the lesion in (A), as well as the SLM as depicted by a lesion in (B). (C) Represents the location of the microdialysis probe. It is situated in the right-half of nucleus reuniens and rhomboid nucleus as indicated by the red arrow. (D) Depicts the track for the mPFC local field potential electrode with a small lesion mark indicated by the red arrow.
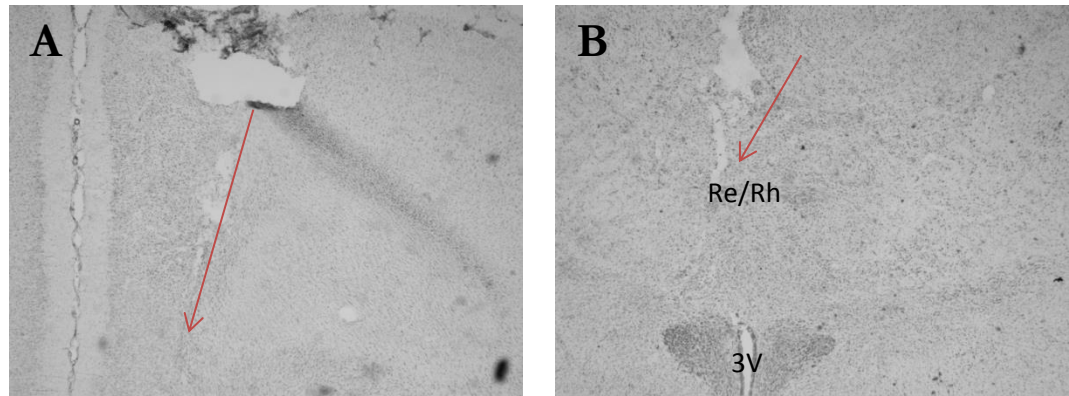
Figure S7. Animal #150224 Lesion marks and electrode tracks. (A) Depicts the track for the mPFC local field potential electrode with a small lesion mark indicated by the red arrow. (B) Represents the location of the microdialysis probe. Note, some sections were lost during histological processing and so better depictions of lesion sites are unavailable.
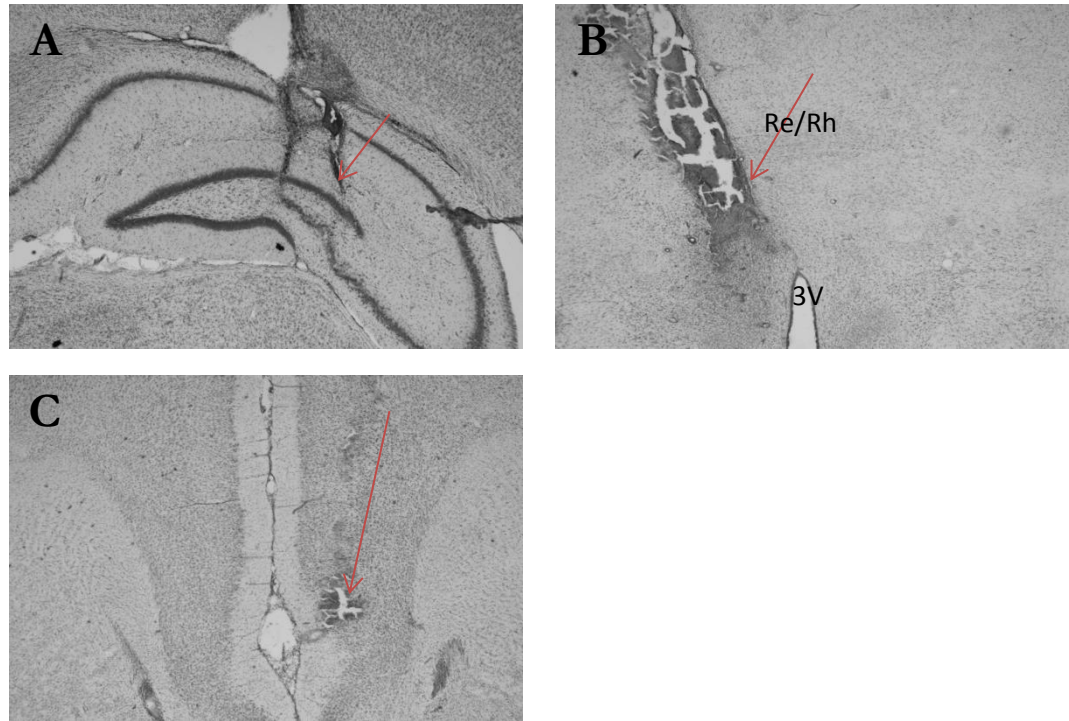
Figure S8. Animal #150740 Lesion marks and electrode tracks. (A) Depicts the track for the hippocampal local field potential electrode as indicated by the red arrow. (B) Represents the location of the microdialysis probe as indicated by the red arrow. (C) Depicts the track for the mPFC local field potential electrode with a small lesion mark indicated by the red arrow.